Łódź University of Technology
Department of Automation, Biomechanics and Mechatronics
May 16, 2023

Regular and chaotic dynamics of nonlinear systems

Larysa P. Dzyubak

Department of Applied Mathematics, National Technical University "Kharkiv Polytechnic Institute", Ukraine

Outline

I

- **2-dof nonlinear dynamics of the rotor suspended in a magneto-hydrodynamic field in the case of soft and rigid magnetic materials**

- Equations of motion

- Soft magnetic materials. System analysis by means of the method of multiple scales
  - Non-resonant case
  - Primary resonance. The cases of no internal resonance and the internal resonance

- Rigid magnetic materials. Conditions for chaotic vibrations of the rotor in various control parameter planes

The cross-section diagram of the rotor symmetrically supported on the magneto-hydrodynamic bearing

F_k is electromagnetic control force produced by the k-th opposed pair of electromagnet coils.

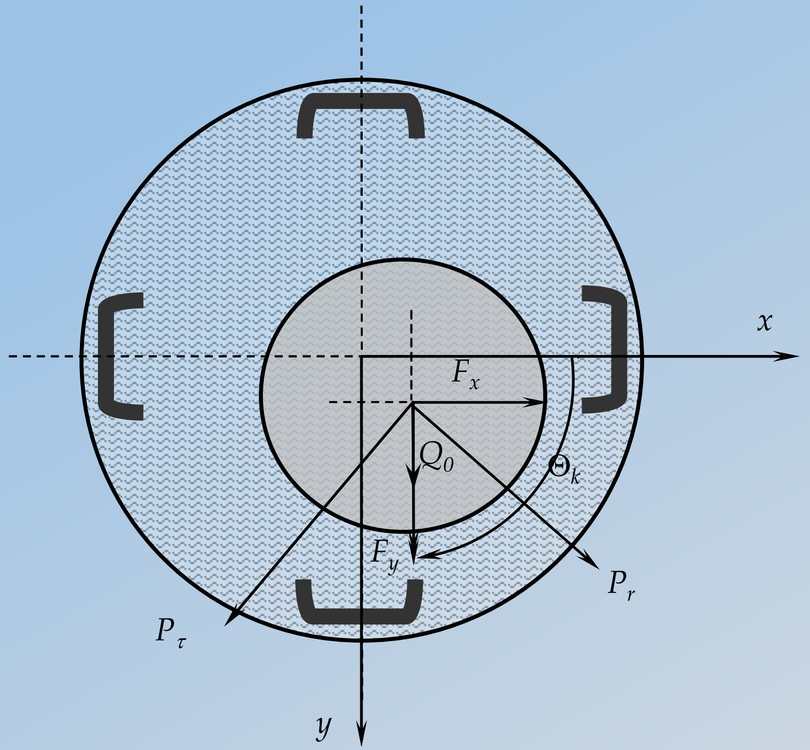

$$F_k = -\frac{2\mu_0 A N^2 i_0}{\left(2\delta + l/\mu^*\right)^2}\Delta i_k, \qquad i_k = i_0 \pm \Delta i_k$$

i_0 denotes bias current in the actuators electric circuits,

μ_0 is the magnetic permeability of vacuum,

A is core cross-section area,

N is number of windings of the electromagnet,

δ is the air gap in the central position of the rotor with reference to the bearing sleeve,

l is the total length of the magnetic path,

$\mu^* = B_s/(\mu_0 H_s)$ denotes the magnetic permeability of the core material (the constant value);

B_s , H_s are the values of the magnetic induction and magnetizing force (they define the magnetic saturation level);

θ_k is the angle between axis x and the k-th magnetic actuator;

(P_r, P_τ) are the radial and tangential components of the dynamic oil-film action,

Q_0 is the vertical rotor load identified with its weight

Equations of motion

$$m^*\ddot{x}^* = P_r^*\left(\rho,\dot{\rho}^*,\dot{\phi}^*\right)\cos\phi - P_\tau^*\left(\rho,\dot{\phi}^*\right)\sin\phi + \sum_{k=1}^{K} F_k^*\cos\theta_k + Q_x^*(t),$$

$$m^*\ddot{y}^* = P_r^*\left(\rho,\dot{\rho}^*,\dot{\phi}^*\right)\sin\phi + P_\tau^*\left(\rho,\dot{\phi}^*\right)\cos\phi + \sum_{k=1}^{K} F_k^*\sin\theta_k + Q_0^* + Q_y^*(t),$$

$$P_r^*\left(\rho,\dot{\rho}^*,\dot{\phi}^*\right) = -2C^*\left\{\frac{\rho^2\left(\omega^*-2\dot{\phi}^*\right)}{p(\rho)q(\rho)} + \frac{\rho\dot{\rho}^*}{p(\rho)} + \frac{2\dot{\rho}^*}{\sqrt{p(\rho)}}\, arctg\sqrt{\frac{1+\rho}{1-\rho}}\right\},$$

$$P_\tau^*\left(\rho,\dot{\phi}^*\right) = \pi C^*\frac{\rho\left(\omega^*-2\dot{\phi}^*\right)}{q(\rho)\sqrt{p(\rho)}},\quad p(\rho)=1-\rho^2,\quad q(\rho)=2+\rho^2,\quad C^*=\frac{6\mu_s R_c L_c}{\delta_s^{\,2}},$$

$$Q_x^*(t)=0,\qquad Q_y^*(t)=Q^*\sin\Omega^* t^*$$

m^* denotes rigid rotor mass,

(x^*, y^*) are Cartesian coordinates of the rotor center;

$Q_x^*(t)$, $Q_y^*(t)$ are an external excitation characterizing bearing housing movements. We are considering vibrations of the rotor excited by harmonic movements of the bearing foundation in the vertical direction;

μ_s, δ_s, R_c, L_c denote oil viscosity, relative bearing clearance, journal radius, total bearing length respectively;

(ρ, ϕ) are polar coordinates

To represent the equations of motion in dimensionless form the following changes of variables and parameters are introduced

$$t = \omega^* t^*, \quad \dot{\phi} = \frac{\dot{\phi}^*}{\omega^*}, \quad \dot{\rho} = \frac{\dot{\rho}^*}{\omega^*}, \quad x = \frac{x^*}{c^*}, \quad \dot{x} = \frac{\dot{x}^*}{\omega^* c^*},$$

$$\ddot{x} = \frac{\ddot{x}^*}{\omega^{*2} c^*}, \quad y = \frac{y^*}{c^*}, \quad \dot{y} = \frac{\dot{y}^*}{\omega^* c^*}, \quad \ddot{y} = \frac{\ddot{y}^*}{\omega^{*2} c^*}, \quad C = \frac{C^*}{m^* \omega^* c^*},$$

$$\Omega = \frac{\Omega^*}{\omega^*}, \quad Q = \frac{Q^*}{m^* \omega^{*2} c^*}, \quad Q_0 = \frac{Q_0^*}{m^* \omega^{*2} c^*}, \quad F_k = \frac{F_k^*}{m^* \omega^{*2} c^*},$$

$$P_r = \frac{P_r^*}{m^* \omega^{*2} c^*}, \quad P_\tau = \frac{P_\tau^*}{m^* \omega^{*2} c^*}$$

ω^* is rotation speed; c^* is bearing clearance

Dimensionless equations of motion

$$\ddot{x} = P_r(\rho, \dot{\rho}, \dot{\phi})\cos\phi - P_\tau(\rho, \dot{\phi})\sin\phi + F_x,$$

$$\ddot{y} = P_r(\rho, \dot{\rho}, \dot{\phi})\sin\phi + P_\tau(\rho, \dot{\phi})\cos\phi + F_y + Q_0 + Q\sin\Omega t,$$

$$P_r(\rho, \dot{\rho}, \dot{\phi}) = -2C\left\{\frac{\rho^2(1-2\dot{\phi})}{p(\rho)q(\rho)} + \frac{\rho\dot{\rho}}{p(\rho)} + \frac{2\dot{\rho}}{\sqrt{p(\rho)}}\,arctg\sqrt{\frac{1+\rho}{1-\rho}}\right\},$$

$$P_\tau(\rho, \dot{\phi}) = \pi C\frac{\rho(1-2\dot{\phi})}{q(\rho)\sqrt{p(\rho)}}, \qquad p(\rho) = 1-\rho^2, \qquad q(\rho) = 2+\rho^2,$$

$$F_x = -\gamma\dot{x} - \lambda(x - x_0), \qquad F_y = -\gamma\dot{y} - \lambda(y - y_0),$$

$$x = \rho\cos\phi, \qquad y = \rho\sin\phi, \qquad \dot{\phi} = \frac{\dot{y}x - \dot{x}y}{\rho^2}, \qquad \dot{\rho} = \frac{x\dot{x} + y\dot{y}}{\rho},$$

$$\rho = \sqrt{x^2 + y^2}, \qquad \cos\phi = \frac{x}{\sqrt{x^2+y^2}}, \qquad \sin\phi = \frac{y}{\sqrt{x^2+y^2}}.$$

F_x, F_y are the magnetic control forces,
(x_0, y_0) are coordinates of the rotor static equilibrium,
γ, λ are control parameters

Soft magnetic materials

The non-resonant case

The right hand side of the equations have been expanded in the Taylor's series as well as the origin have been shifted to the location of the static equilibrium for the convenience of the investigation . The linear and quadratic terms have been kept. So, the transformed equations of motion are cast into the following form

$$\ddot{x} + \alpha x - \beta \dot{y} = -2\hat{\mu}_1 \dot{x} + \alpha_1 x^2 + \alpha_2 y^2 + \alpha_3 x\dot{x} + \alpha_4 xy + \alpha_5 x\dot{y} + \alpha_6 \dot{x} y + \alpha_7 y\dot{y},$$

$$\ddot{y} + \alpha y + \beta \dot{x} = -2\hat{\mu}_2 \dot{x} + \beta_1 x^2 + \beta_2 y^2 + \beta_3 x\dot{x} + \beta_4 xy + \beta_5 x\dot{y} + \beta_6 \dot{x} y + \beta_7 y\dot{y} + F\cos(\Omega t + \tau). \qquad (1)$$

We seek a first-order solution for small but finite amplitudes in the form

$$x = \varepsilon x_1(T_0, T_1) + \varepsilon^2 x_2(T_0, T_1) + \dots,$$
$$y = \varepsilon y_1(T_0, T_1) + \varepsilon^2 y_2(T_0, T_1) + \dots,$$

where ε is a small, dimensionless parameter related to the amplitudes and $T_n = \varepsilon^n t.$

It follows that the derivatives with respect to t become expansions in terms of the partial derivatives with respect to T_n according to

$$\frac{d}{dt} = \frac{\partial}{\partial T_0}\frac{\partial T_0}{\partial t} + \frac{\partial}{\partial T_1}\frac{\partial T_1}{\partial t} + \frac{\partial}{\partial T_2}\frac{\partial T_2}{\partial t} + \dots = D_0 + \varepsilon D_1 + \varepsilon^2 D_2 + \dots,$$

$$\frac{d^2}{dt^2} = \left(D_0 + \varepsilon D_1 + \varepsilon^2 D_2 + \dots\right)^2 = D_0^2 + 2\varepsilon D_0 D_1 + \varepsilon^2\left(D_1^2 + 2D_0 D_2\right) + \dots,$$

where $$D_k = \frac{\partial}{\partial T_k}$$

The forcing term is introduced so that it appears at order ε, i.e. we take $F = \varepsilon f$, $\hat{\mu}_n = \varepsilon \mu_n$
Equating coefficients standing by the same powers of ε we obtain

Order ε

$$D_0^2 x_1 + \alpha x_1 - \beta D_0 y_1 = 0$$
$$D_0^2 y_1 + \alpha y_1 + \beta D_0 x_1 = f \cos\left(\Omega T_0 + \tau\right) \qquad (2)$$

Order ε^2

$$D_0^2 x_2 + \alpha x_2 - \beta D_0 y_2 = -2D_0\left(D_1 x_1 + \mu_1 x_1\right) + \beta D_1 y_1 + \alpha_1 x_1^2 + \alpha_2 y_1^2$$
$$+ \alpha_3 x_1 D_0 x_1 + \alpha_4 x_1 y_1 + \alpha_5 x_1 D_0 y_1 + \alpha_6 y_1 D_0 x_1 + \alpha_7 y_1 D_0 y_1 \qquad (3)$$
$$D_0^2 y_2 + \alpha y_2 + \beta D_0 x_2 = -2D_0\left(D_1 y_1 + \mu_2 y_1\right) - \beta D_1 x_1 + \beta_1 x_1^2 + \beta_2 y_1^2$$
$$+ \beta_3 x_1 D_0 x_1 + \beta_4 x_1 y_1 + \beta_5 x_1 D_0 y_1 + \beta_6 y_1 D_0 x_1 + \beta_7 y_1 D_0 y_1$$

The solution of equations (1) is expressed in the following form

$$x_1 = A_1(T_1)\exp(i\omega_1 T_0) + A_2(T_1)\exp(i\omega_2 T_0) + \Phi_1 \exp[i(\Omega T_0 + \tau)] + CC,$$
$$y_1 = \Lambda_1 A_1(T_1)\exp(i\omega_1 T_0) + \Lambda_2 A_2(T_1)\exp(i\omega_2 T_0) + \Phi_2 \exp[i(\Omega T_0 + \tau)] + CC, \qquad (4)$$

where

$$\Lambda_n = \frac{\omega_n^2 - \alpha}{\omega_n \beta} i, \qquad \Phi_1 = \frac{i}{2}\frac{\beta\Omega f}{(\alpha - \Omega^2)^2 - \beta^2\Omega^2}, \qquad \Phi_2 = \frac{1}{2}\frac{f(\alpha - \Omega^2)}{(\alpha - \Omega^2)^2 - \beta^2\Omega^2},$$

$\omega_n{}^2$ are roots of the algebraic equation $\omega_n^4 - (2\alpha + \beta^2)\omega_n^2 + \alpha^2 = 0.$

Substituting (4) into (3) yields

$$D_0^2 x_2 + \alpha x_2 - \beta D_0 y_2 = [-2i\omega_1(A_1' + \mu_1 A_1) + \beta\Lambda_1 A_1']\exp(i\omega_1 T_0) +$$
$$[-2i\omega_2(A_2' + \mu_1 A_2) + \beta\Lambda_2 A_2']\exp(i\omega_2 T_0) + \ldots + CC$$
$$D_0^2 y_2 + \alpha y_2 + \beta D_0 x_2 = [-2i\omega_1\Lambda_1(A_1' + \mu_2 A_1) - \beta A_1']\exp(i\omega_1 T_0) +$$
$$[-2i\omega_2\Lambda_2(A_2' + \mu_2 A_2) - \beta A_2']\exp(i\omega_2 T_0) + \ldots + CC$$

The solvability conditions are

$$\begin{vmatrix} R_{1n} & -i\beta\omega_n \\ R_{2n} & \left(\alpha-\omega_n^2\right) \end{vmatrix} = 0,$$

where

$$R_{11} = -2i\omega_1\left(A_1' + \mu_1 A_1\right) + \beta\Lambda_1 A_1', \quad R_{12} = -2i\omega_2\left(A_2' + \mu_1 A_2\right) + \beta\Lambda_2 A_2',$$
$$R_{21} = -2i\omega_1\Lambda_1\left(A_1' + \mu_2 A_1\right) - \beta A_1', \quad R_{22} = -2i\omega_2\Lambda_2\left(A_2' + \mu_2 A_2\right) - \beta A_2',$$

and hence $$R_{1n} = \frac{R_{2n}}{\overline{\Lambda}_n}.$$

Finally, the equations for A_1 and A_2 are the following ones

$$\left(\beta\Lambda_1 - 2i\omega_1 + \frac{2i\omega_1\Lambda_1 + \beta}{\overline{\Lambda}_1}\right)A_1' + \left(\frac{2i\omega_1\Lambda_1\mu_2}{\overline{\Lambda}_1} - 2i\omega_1\mu_1\right)A_1 = 0,$$
$$\left(\beta\Lambda_2 - 2i\omega_2 + \frac{2i\omega_2\Lambda_2 + \beta}{\overline{\Lambda}_2}\right)A_2' + \left(\frac{2i\omega_2\Lambda_2\mu_2}{\overline{\Lambda}_2} - 2i\omega_2\mu_1\right)A_2 = 0.$$

Therefore, the complex form solutions are as follows

$$x=\varepsilon\left[\exp(-\varepsilon\nu_1 t)a_1\exp(i\omega_1 t)+\exp(-\varepsilon\nu_2 t)a_2\exp(i\omega_2 t)\right.$$
$$\left.+\Phi_1\exp[i(\Omega t+\tau)]+CC\right]+O(\varepsilon^2),$$
$$y=\varepsilon\left[\Lambda_1\exp(-\varepsilon\nu_1 t)a_1\exp(i\omega_1 t)+\Lambda_2\exp(-\varepsilon\nu_2 t)a_2\exp(i\omega_2 t)\right.$$
$$\left.+\Phi_2\exp[i(\Omega t+\tau)]+CC\right]+O(\varepsilon^2).$$

On the other hand, the real solutions are following

$$x=\varepsilon\left[\exp(-\varepsilon\nu_1 t)a_1\cos(\omega_1 t+\Theta_1)+\exp(-\varepsilon\nu_2 t)a_2\cos(\omega_2 t+\Theta_2)\right.$$
$$\left.+2\operatorname{Im}\Phi_1\sin(\Omega t+\tau)\right]+O(\varepsilon^2),$$
$$y=\varepsilon\left[\Lambda_1\exp(-\varepsilon\nu_1 t)a_1\sin(\omega_1 t+\Theta_1)+\Lambda_2\exp(-\varepsilon\nu_2 t)a_2\sin(\omega_2 t+\Theta_2)\right.$$
$$\left.+2\Phi_2\cos(\Omega t+\tau)\right]+O(\varepsilon^2),$$

where $$\nu_n=\frac{2\omega_n(\mu_1+\mu_2)}{4\omega_n-\beta\left(\operatorname{Im}\Lambda_n+\dfrac{1}{\operatorname{Im}\Lambda_n}\right)},$$ a_n and Θ_n are real constants.

Comparison of the numerical integration of (1) and the perturbation solutions in the case of non-resonant undamped vibrations

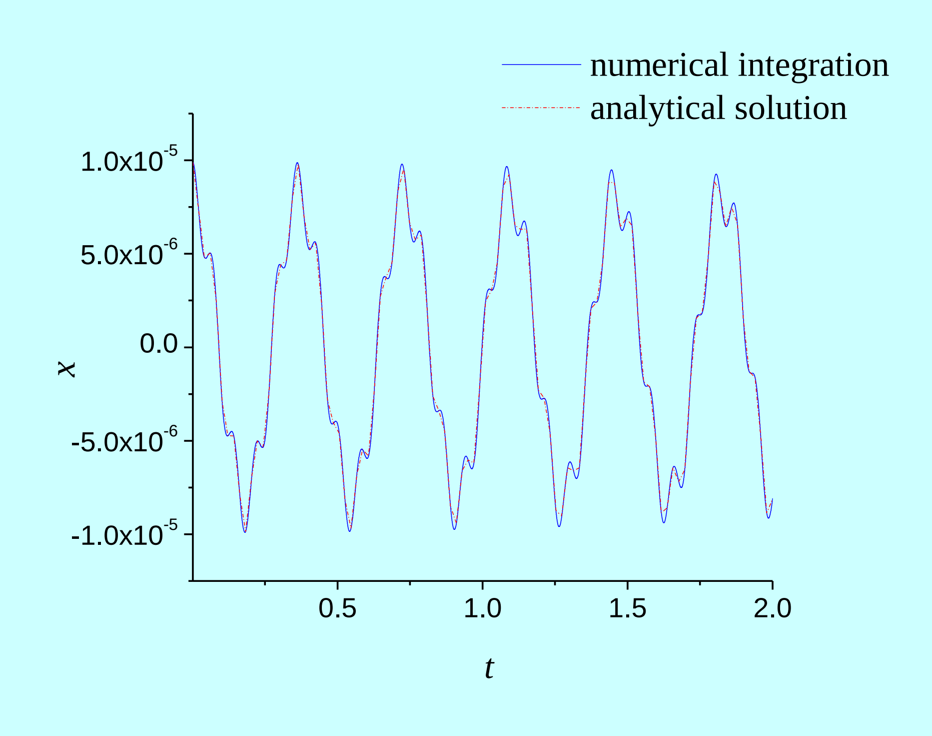

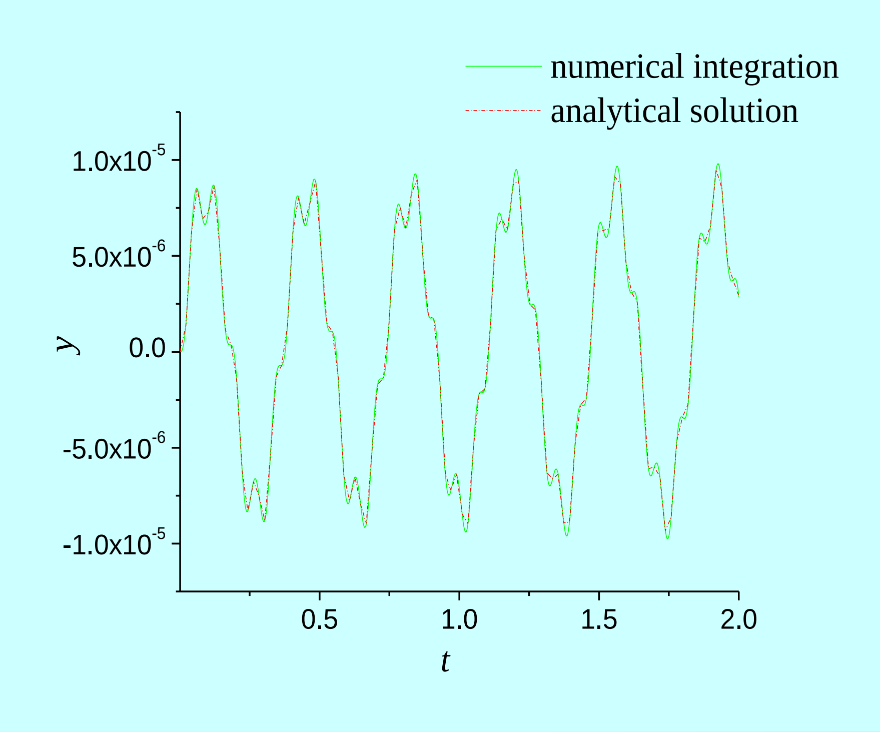

Comparison of the numerical integration of (1) and the perturbation solutions in the case of non-resonant damped vibrations

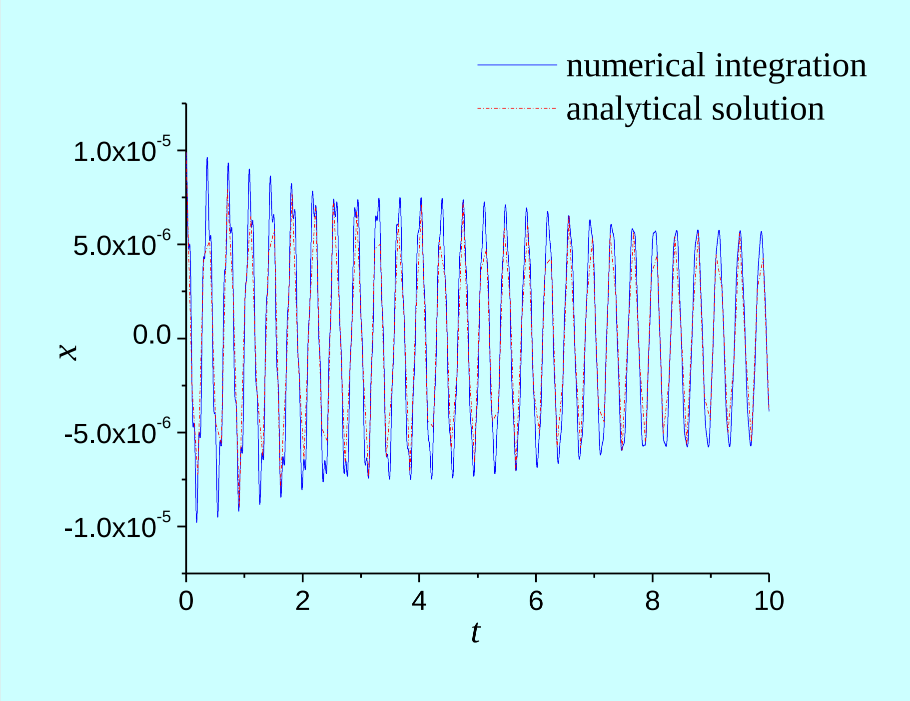

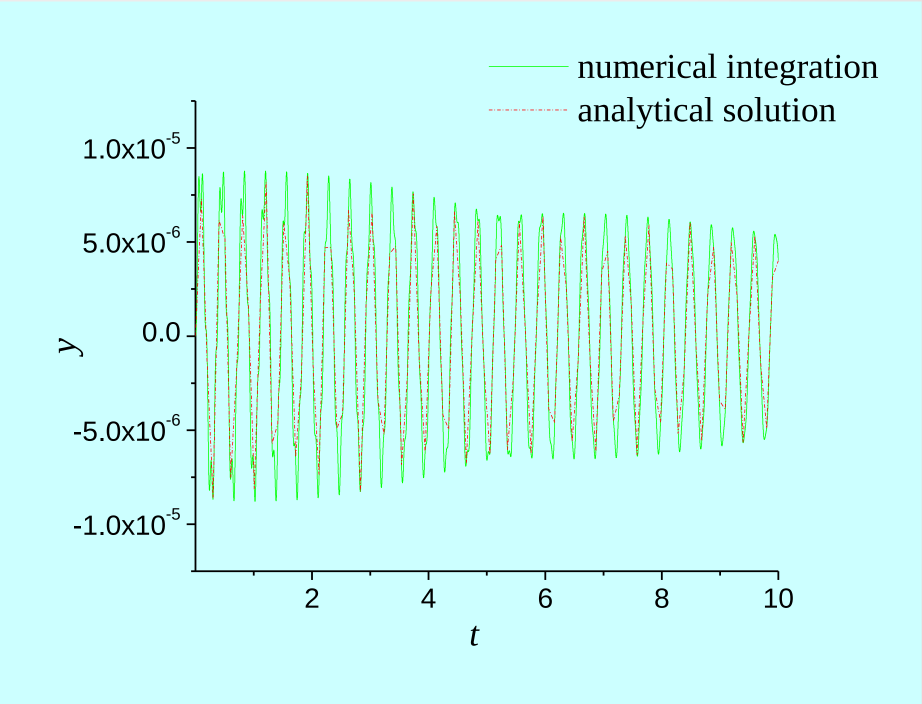

Comparison of the numerical integration of (1) and the perturbation solutions in the case of non-resonant forced damped vibrations

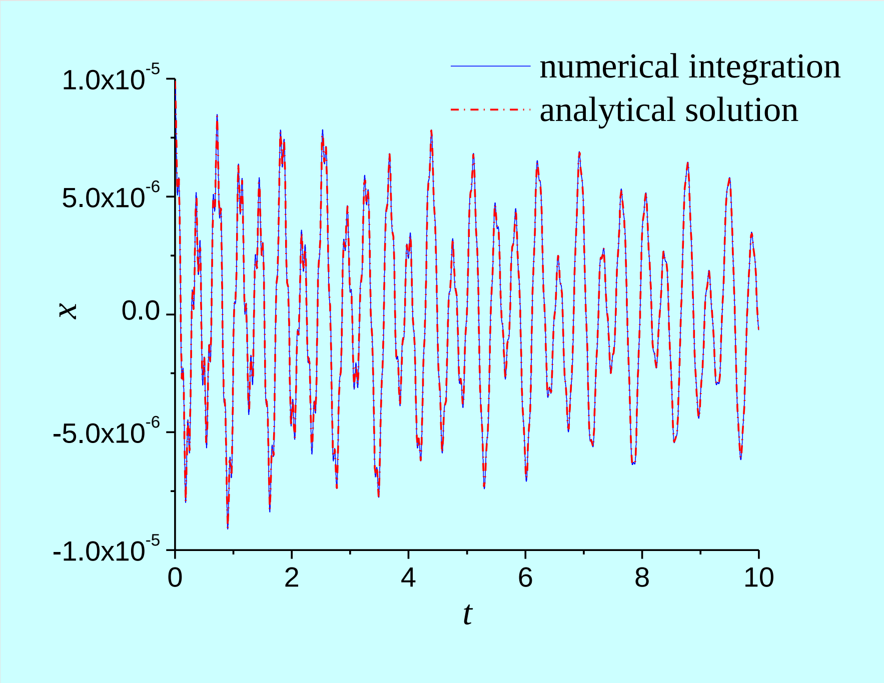

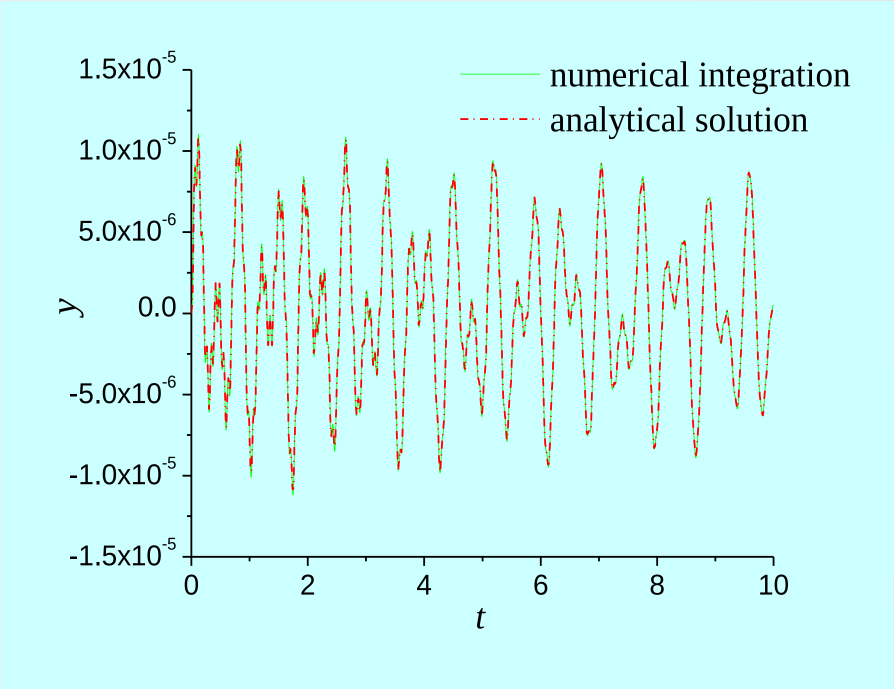

Primary resonance
The cases of no internal resonance and an internal resonance

Analyzing primary resonances the forcing term is ordered so that it appears at order ε^2 ($F = \varepsilon^2 f$, $\hat{\mu}_n = \varepsilon \mu_n$).

Consider the case $\Omega \approx \omega_2$.

Let us introduce the detuning parameter σ_1 in the following way $\Omega = \omega_2 + \varepsilon \sigma_1$.

Equating coefficients of the same powers of ε we obtain

Order ε^1

$$D_0^2 x_1 + \alpha x_1 - \beta D_0 y_1 = 0,$$
$$D_0^2 y_1 + \alpha y_1 + \beta D_0 x_1 = 0. \tag{5}$$

Order ε^2

$$D_0^2 x_2 + \alpha x_2 - \beta D_0 y_2 = -2 D_0 \left(D_1 x_1 + \mu_1 x_1 \right) + \beta D_1 y_1 + \alpha_1 x_1^2 + \alpha_2 y_1^2$$
$$+ \alpha_3 x_1 D_0 x_1 + \alpha_4 x_1 y_1 + \alpha_5 x_1 D_0 y_1 + \alpha_6 y_1 D_0 x_1 + \alpha_7 y_1 D_0 y_1, \tag{6}$$
$$D_0^2 y_2 + \alpha y_2 + \beta D_0 x_2 = -2 D_0 \left(D_1 y_1 + \mu_2 y_1 \right) - \beta D_1 x_1 + \beta_1 x_1^2 + \beta_2 y_1^2$$
$$+ \beta_3 x_1 D_0 x_1 + \beta_4 x_1 y_1 + \beta_5 x_1 D_0 y_1 + \beta_6 y_1 D_0 x_1 + \beta_7 y_1 D_0 y_1 + f \cos\left(\Omega t + \tau \right).$$

The solution of (5) is expressed in the form

$$\begin{aligned} x_1 &= A_1(T_1)\exp(i\omega_1 T_0) + A_2(T_1)\exp(i\omega_2 T_0) + CC, \\ y_1 &= \Lambda_1 A_1(T_1)\exp(i\omega_1 T_0) + \Lambda_2 A_2(T_1)\exp(i\omega_2 T_0) + CC, \end{aligned} \tag{7}$$

where $\Lambda_n = \dfrac{\omega_n^2 - \alpha}{\omega_n \beta} i.$

Then, the second approximation reads

$$\begin{aligned} D_0^2 x_2 + \alpha x_2 - \beta D_0 y_2 &= \left[-2i\omega_1(A_1' + \mu_1 A_1) + \beta\Lambda_1 A_1'\right]\exp(i\omega_1 T_0) + \\ &\left[-2i\omega_2(A_2' + \mu_1 A_2) + \beta\Lambda_2 A_2'\right]\exp(i\omega_2 T_0) + \\ &A_1^2\left[\alpha_1 + \Lambda_1^2\alpha_2 + i\omega_1\alpha_3 + \Lambda_1\alpha_4 + i\omega_1\Lambda_1\alpha_5 + i\omega_1\Lambda_1\alpha_6 + i\omega_1\Lambda_1^2\alpha_7\right]\exp(2i\omega_1 T_0) \\ &+ A_2^2\left[\alpha_1 + \Lambda_2^2\alpha_2 + i\omega_2\alpha_3 + \Lambda_2\alpha_4 + i\omega_2\Lambda_2\alpha_5 + i\omega_2\Lambda_2\alpha_6 + i\omega_2\Lambda_2^2\alpha_7\right]\exp(2i\omega_2 T_0) \\ &+ A_1 A_2\left[2\alpha_1 + 2\Lambda_1\Lambda_2\alpha_2 + (i\omega_1 + i\omega_2)\alpha_3 + (\Lambda_1 + \Lambda_2)\alpha_4 + (i\omega_2\Lambda_2 - i\omega_1\Lambda_1)\alpha_5\right. \\ &\left.+ (i\omega_2\Lambda_1 + i\omega_1\Lambda_2)\alpha_6 + (i\omega_1 + i\omega_2)\Lambda_1\Lambda_2\alpha_7\right]\exp(i(\omega_1 + \omega_2)T_0) \\ &+ \bar{A}_1 A_2\left[2\alpha_1 + 2\bar{\Lambda}_1\Lambda_2\alpha_2 + (i\omega_2 - i\omega_1)\alpha_3 + (\Lambda_2 + \bar{\Lambda}_1)\alpha_4 + (i\omega_2\Lambda_2 - i\omega_1\bar{\Lambda}_1)\alpha_5\right. \\ &\left.+ (i\omega_2\bar{\Lambda}_1 - i\omega_1\Lambda_2)\alpha_6 + (i\omega_2 - i\omega_1)\bar{\Lambda}_1\Lambda_2\alpha_7\right]\exp(i(\omega_2 - \omega_1)T_0) \\ &+ A_1\bar{A}_1\left(\alpha_1 + \Lambda_1\left(\bar{\Lambda}_1\alpha_2 + \alpha_4 + i\omega_1(\alpha_5 - \alpha_6)\right)\right) + A_2\bar{A}_2\left(\alpha_1 + \Lambda_2\left(\bar{\Lambda}_2\alpha_2 + \alpha_4 + i\omega_2(\alpha_5 - \alpha_6)\right)\right) + CC \end{aligned}$$

and

$$
\begin{aligned}
&D_0^2 y_2 + \alpha y_2 + \beta D_0 x_2 = \left[-2i\omega_1\Lambda_1\left(A_1' + \mu_2 A_1\right) - \beta A_1'\right]\exp\left(i\omega_1 T_0\right) + \\
&\left[-2i\omega_2\Lambda_2\left(A_2' + \mu_2 A_2\right) - \beta A_2'\right]\exp\left(i\omega_2 T_0\right) + \\
&A_1^2\left[\beta_1 + \Lambda_1^2\beta_2 + i\omega_1\beta_3 + \Lambda_1\beta_4 + i\omega_1\Lambda_1\beta_5 + i\omega_1\Lambda_1\beta_6 + i\omega_1\Lambda_1^2\beta_7\right]\exp\left(2i\omega_1 T_0\right) \\
&+ A_2^2\left[\beta_1 + \Lambda_2^2\beta_2 + i\omega_2\beta_3 + \Lambda_2\beta_4 + i\omega_2\Lambda_2\beta_5 + i\omega_2\Lambda_2\beta_6 + i\omega_2\Lambda_2^2\beta_7\right]\exp\left(2i\omega_2 T_0\right) \\
&+ A_1 A_2\left[2\beta_1 + 2\Lambda_1\Lambda_2\beta_2 + \left(i\omega_1 + i\omega_2\right)\beta_3 + \left(\Lambda_1 + \Lambda_2\right)\beta_4 + \left(i\omega_2\Lambda_2 - i\omega_1\Lambda_1\right)\beta_5\right. \\
&\left.+ \left(i\omega_2\Lambda_1 + i\omega_1\Lambda_2\right)\beta_6 + \left(i\omega_1 + i\omega_2\right)\Lambda_1\Lambda_2\beta_7\right]\exp\left(i\left(\omega_1 + \omega_2\right)T_0\right) \\
&+ \bar{A}_1 A_2\left[2\beta_1 + 2\bar{\Lambda}_1\Lambda_2\beta_2 + \left(i\omega_2 - i\omega_1\right)\beta_3 + \left(\Lambda_2 + \bar{\Lambda}_1\right)\beta_4 + \left(i\omega_2\Lambda_2 - i\omega_1\bar{\Lambda}_1\right)\beta_5\right. \\
&\left.+ \left(i\omega_2\bar{\Lambda}_1 - i\omega_1\Lambda_2\right)\beta_6 + \left(i\omega_2 - i\omega_1\right)\bar{\Lambda}_1\Lambda_2\beta_7\right]\exp\left(i\left(\omega_2 - \omega_1\right)T_0\right) \\
&+ A_1\bar{A}_1\left(\beta_1 + \Lambda_1\left(\bar{\Lambda}_1\beta_2 + \beta_4 + i\omega_1\left(\beta_5 - \beta_6\right)\right)\right) + A_2\bar{A}_2\left(\beta_1 + \Lambda_2\left(\bar{\Lambda}_2\beta_2 + \beta_4 + i\omega_2\left(\beta_5 - \beta_6\right)\right)\right) \\
&+ \frac{1}{2} f \exp\left(i\left(\omega_2 T_0 + \sigma_1 T_1 + \tau\right)\right) + CC
\end{aligned}
$$

The case of no internal resonance
(ω_2 *is away from* $2\omega_1$)

The solvability conditions are

$$q_{\omega_1} + \frac{1}{\Lambda_1} p_{\omega_1} = 0,$$

$$q_{\omega_2} + \frac{1}{\Lambda_2} p_{\omega_2} + \frac{1}{2\Lambda_2} f \exp\left(i\left(\sigma_1 T_1 + \tau\right)\right) = 0,$$

where $$q_{\omega_1} = -2i\omega_1\left(A_1' + \mu_1 A_1\right) + \beta\Lambda_1 A_1', \quad q_{\omega_2} = 2i\omega_2\left(A_2' + \mu_1 A_2\right) + \beta\Lambda_2 A_2',$$

$$p_{\omega_1} = -2i\omega_1\Lambda_1\left(A_1' + \mu_2 A_1\right) - \beta A_1', \quad p_{\omega_2} = -2i\omega_2\Lambda_2\left(A_2' + \mu_2 A_2\right) - \beta A_2'$$

The first approximation is not influenced by the nonlinear terms. It is essentially the solution of the corresponding linear problem.

$$A_1(T_1) = \frac{1}{2} a_1 \exp\left(-\nu_1 T_1 + i\Theta_1\right),$$

$$A_2(T_1) = \frac{1}{2} a_2 \exp\left(-\nu_2 T_1 + i\Theta_2\right) + \frac{f\left(\nu_2 - i\sigma_1\right)}{2\,\mathrm{Im}\,\Lambda_2\,\mathrm{Im}\,\kappa_2\left(\nu_2^2 + \sigma_1^2\right)} \exp\left[i\left(\sigma_1 T_1 + \tau\right)\right],$$

where $$\nu_n = \frac{2\omega_n\left(\mu_1 + \mu_2\right)}{4\omega_n - \beta\left(\mathrm{Im}\,\Lambda_n + \dfrac{1}{\mathrm{Im}\,\Lambda_n}\right)}, \qquad \kappa_2 = -4\omega_2 i + \beta\left(\mathrm{Im}\,\Lambda_2 + \frac{1}{\mathrm{Im}\,\Lambda_2}\right) i.$$

As $t \to \infty$, $T_1 \to \infty$

$$A_1 \to 0, \qquad A_2 \to \frac{f(\nu_2 - i\sigma_1)}{2\,\mathrm{Im}\,\Lambda_2\,\mathrm{Im}\,\kappa_2(\nu_2^2+\sigma_1^2)}\exp[i(\sigma_1 T_1+\tau)]$$

Therefore, the real solutions are

$$x = \frac{F}{\varepsilon}\frac{1}{\mathrm{Im}\,\Lambda_2\,\mathrm{Im}\,\kappa_2(\nu_2^2+\sigma_1^2)^{1/2}}\sin(\Omega t+\tau+\tilde{\gamma}_1)+O(\varepsilon^2),$$

$$y = \frac{F}{\varepsilon}\frac{1}{\mathrm{Im}\,\kappa_2(\nu_2^2+\sigma_1^2)^{1/2}}\sin(\Omega t+\tau+\tilde{\gamma}_2)+O(\varepsilon^2),$$

where $\quad \tilde{\gamma}_1 = arctg(\nu_2/\sigma_1), \qquad \tilde{\gamma}_2 = -arctg(\sigma_1/\nu_2).$

The case when the internal resonance exists

$$\omega_2 \approx 2\omega_1$$

Let us introduce detuning parameter σ_2 in the following way $\quad \omega_2 = 2\omega_1 - \varepsilon\sigma_2$

The solvability conditions for this case become

$$q_{\omega_1} + \frac{1}{\Lambda_1} p_{\omega_1} + \left(q_{\omega_2-\omega_1} + \frac{1}{\Lambda_1} p_{\omega_2-\omega_1} \right) \overline{A}_1 A_2 \exp(-i\sigma_2 T_1) = 0,$$

$$q_{\omega_2} + \frac{1}{\Lambda_2} p_{\omega_2} + \left(q_{2\omega_1} + \frac{1}{\Lambda_2} p_{2\omega_1} \right) A_1^2 \exp(i\sigma_2 T_1) + \frac{1}{2\Lambda_2} f \exp(i(\sigma_1 T_1 + \tau)) = 0,$$

where

$$q_{\omega_1} = -2i\omega_1 (A_1' + \mu_1 A_1) + \beta\Lambda_1 A_1', \quad q_{\omega_2} = 2i\omega_2 (A_2' + \mu_1 A_2) + \beta\Lambda_2 A_2',$$

$$q_{2\omega_1} = \alpha_1 + \Lambda_1^2 \alpha_2 + i\omega_1\alpha_3 + \Lambda_1\alpha_4 + i\omega_1\Lambda_1\alpha_5 + i\omega_1\Lambda_1\alpha_6 + i\omega_1\Lambda_1^2\alpha_7,$$

$$q_{\omega_2-\omega_1} = 2\alpha_1 + 2\overline{\Lambda}_1\Lambda_2\alpha_2 + (i\omega_2 - i\omega_1)\alpha_3 + (\Lambda_2 + \overline{\Lambda}_1)\alpha_4 + (i\omega_2\Lambda_2 - i\omega_1\overline{\Lambda}_1)\alpha_5$$
$$+ (i\omega_2\overline{\Lambda}_1 - i\omega_1\Lambda_2)\alpha_6 + (i\omega_2 - i\omega_1)\overline{\Lambda}_1\Lambda_2\alpha_7,$$

$$p_{\omega_1} = -2i\omega_1\Lambda_1 (A_1' + \mu_2 A_1) - \beta A_1', \quad p_{\omega_2} = -2i\omega_2\Lambda_2 (A_2' + \mu_2 A_2) - \beta A_2',$$

$$p_{2\omega_1} = \beta_1 + \Lambda_1^2\beta_2 + i\omega_1\beta_3 + \Lambda_1\beta_4 + i\omega_1\Lambda_1\beta_5 + i\omega_1\Lambda_1\beta_6 + i\omega_1\Lambda_1^2\beta_7,$$

$$p_{\omega_2-\omega_1} = 2\beta_1 + 2\overline{\Lambda}_1\Lambda_2\beta_2 + (i\omega_2 - i\omega_1)\beta_3 + (\Lambda_2 + \overline{\Lambda}_1)\beta_4 + (i\omega_2\Lambda_2 - i\omega_1\overline{\Lambda}_1)\beta_5$$
$$+ (i\omega_2\overline{\Lambda}_1 - i\omega_1\Lambda_2)\beta_6 + (i\omega_2 - i\omega_1)\overline{\Lambda}_1\Lambda_2\beta_7.$$

For the convenience let us introduce the polar notation

$$A_m = \frac{1}{2} a_m \exp(i\Theta_m), \quad m = 1, 2,$$

where a_m and Θ_m are real functions of T_1. Then the solvability conditions can be written in the form

$$(a_1' + i a_1 \Theta_1') + \nu_1 a_1 + \frac{1}{2\kappa_1} a_1 a_2 [\varphi + i\psi] \exp(i\gamma_2) = 0,$$

$$(a_2' + i a_2 \Theta_2') + \nu_2 a_2 + \frac{1}{2\kappa_2} a_1^{\,2} [\zeta + i\eta] \exp(-i\gamma_2) + \frac{f}{\kappa_2 \Lambda_2} \exp(i\gamma_1) = 0,$$

where

$$\varphi = \mathrm{Re}\left(q_{\omega_2 - \omega_1} + \frac{1}{\Lambda_1} p_{\omega_2 - \omega_1} \right), \qquad \psi = \mathrm{Im}\left(q_{\omega_2 - \omega_1} + \frac{1}{\Lambda_1} p_{\omega_2 - \omega_1} \right),$$

$$\zeta = \mathrm{Re}\left(q_{2\omega_1} + \frac{1}{\Lambda_2} p_{2\omega_1} \right), \qquad \eta = \mathrm{Im}\left(q_{2\omega_1} + \frac{1}{\Lambda_2} p_{2\omega_1} \right),$$

$$\gamma_1 = \sigma_1 T_1 + \tau - \Theta_2, \quad \gamma_2 = \Theta_2 - 2\Theta_1 - \sigma_2 T_1,$$

$$\kappa_n = -4\omega_n i + \beta \left(\mathrm{Im}\,\Lambda_n + \frac{1}{\mathrm{Im}\,\Lambda_n} \right) i, \quad n = 1,2.$$

Separating the previous equations into real and imaginary parts, we obtain

$$a_1' = -\nu_1 a_1 - \frac{a_1 a_2}{2\,\mathrm{Im}\,\kappa_1}\left(\psi\cos\gamma_2 + \varphi\sin\gamma_2\right),$$

$$a_1\Theta_1' = \frac{a_1 a_2}{2\,\mathrm{Im}\,\kappa_1}\left(\varphi\cos\gamma_2 - \psi\sin\gamma_2\right),$$

$$a_2' = -\nu_2 a_2 - \frac{a_1^2}{2\,\mathrm{Im}\,\kappa_2}\left(\eta\cos\gamma_2 - \zeta\sin\gamma_2\right) + \frac{f}{\mathrm{Im}\,\kappa_2\,\mathrm{Im}\,\Lambda_2}\cos\gamma_1,$$

$$a_2\Theta_2{}' = \frac{a_1^2}{2\,\mathrm{Im}\,\kappa_2}\left(\zeta\cos\gamma_2 + \eta\sin\gamma_2\right) + \frac{f}{\mathrm{Im}\,\kappa_2\,\mathrm{Im}\,\Lambda_2}\sin\gamma_1.$$

Finally, we obtain the expressions for a_1 and a_2

$$a_1 = \left[-\frac{p}{2} \pm \left(\left(\frac{p}{2} \right)^2 - q \right)^{\frac{1}{2}} \right]^{\frac{1}{2}}, \qquad a_2 = \left(\frac{16\omega_1^2 (\mu_1 + \mu_2)^2 + \operatorname{Im} \kappa_1^2 \left((\sigma_1 - \sigma_2)^2 \right)}{\varphi^2 + \psi^2} \right)^{1/2},$$

where
$$p = \frac{4a_2}{\zeta^2 + \eta^2} \left[-2\omega_2 (\mu_1 + \mu_2)(\eta \cos \gamma_2 - \zeta \sin \gamma_2) - \operatorname{Im} \kappa_2 \sigma_1 (\zeta \cos \gamma_2 + \eta \sin \gamma_2) \right],$$

$$q = \frac{1}{\zeta^2 + \eta^2} \left\{ 4a_2^2 \left[4\omega_2^2 (\mu_1 + \mu_2)^2 + \operatorname{Im} \kappa_2^2 \sigma_1^2 \right] - \frac{4 f^2}{(\operatorname{Im} \Lambda_2)^2} \right\}.$$

Then, the real solutions follow

$$x = \varepsilon \left\{ a_1 \cos \left[\frac{1}{2} (\Omega t + \tau - \gamma_1 - \gamma_2) \right] + a_2 \cos(\Omega t + \tau - \gamma_1) \right\} + O(\varepsilon^2),$$

$$y = -\varepsilon \left\{ a_1 \operatorname{Im} \Lambda_1 \sin \left[\frac{1}{2} (\Omega t + \tau - \gamma_1 - \gamma_2) \right] + a_2 \operatorname{Im} \Lambda_2 \sin(\Omega t + \tau - \gamma_1) \right\} + O(\varepsilon^2).$$

Frequency-response curves; $\sigma_2=0$, $\Omega\approx\omega_2$

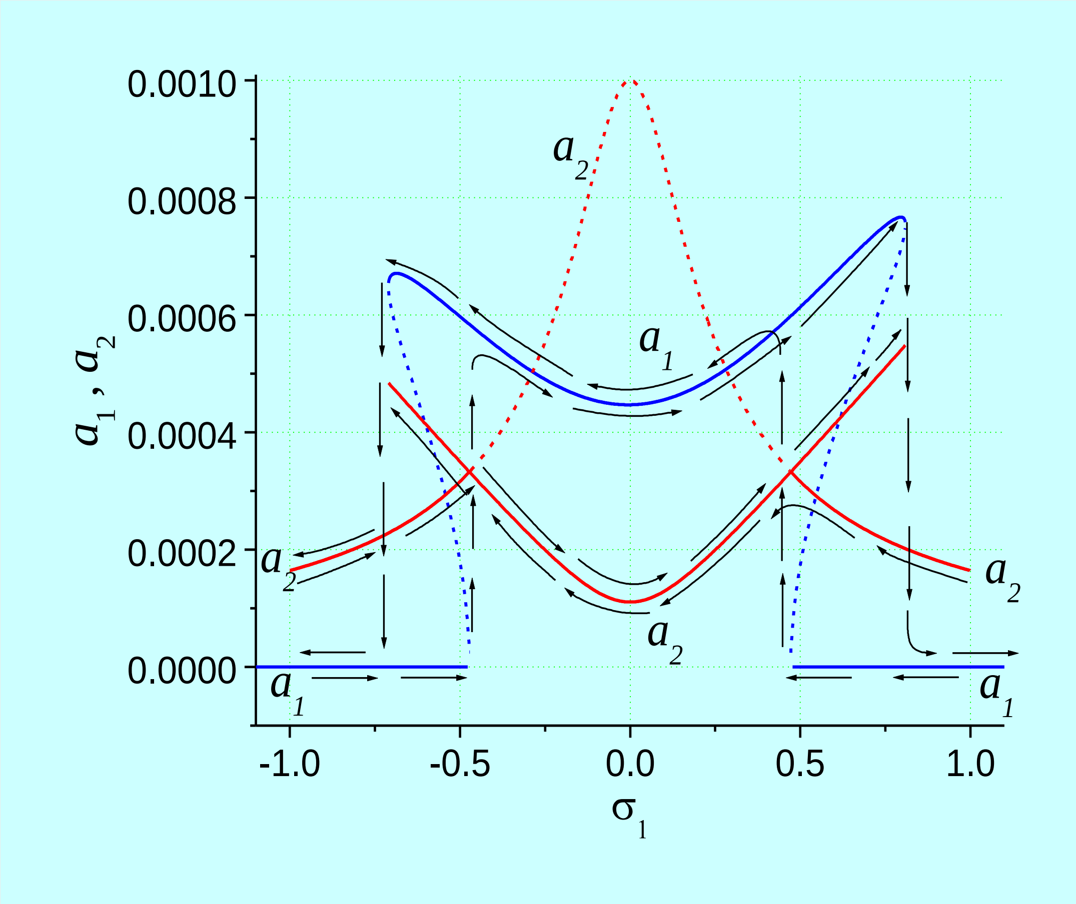

Comparison of the analytical results presented on the frequency response curves with the numerical integration of (1)

(a) Ω=19 (σ_1= –1, σ_2= 0), f=0.01

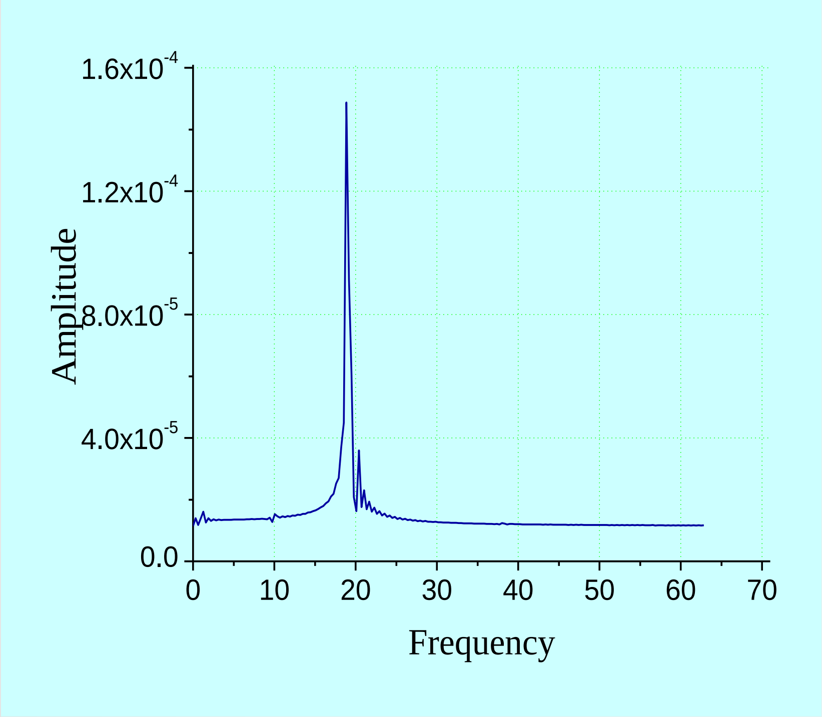

(b) Ω=20 (σ_1=0, σ_2= 0), f=0.01

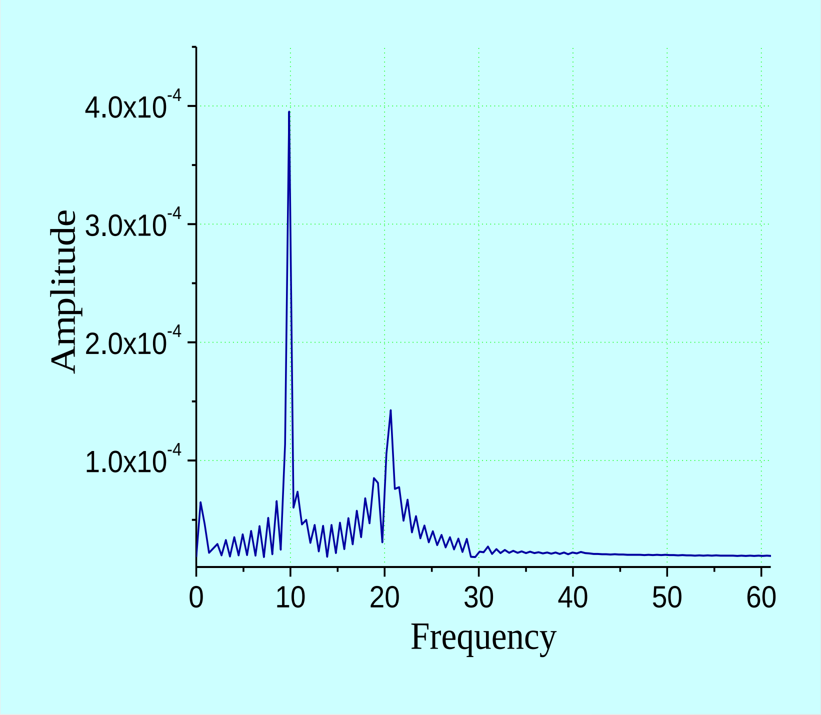

Amplitudes a_1, a_2 versus the amplitude of the external excitation f ;
$\Omega \approx \omega_2$, $\sigma_1 = -0.5$, $\sigma_2 = 0$

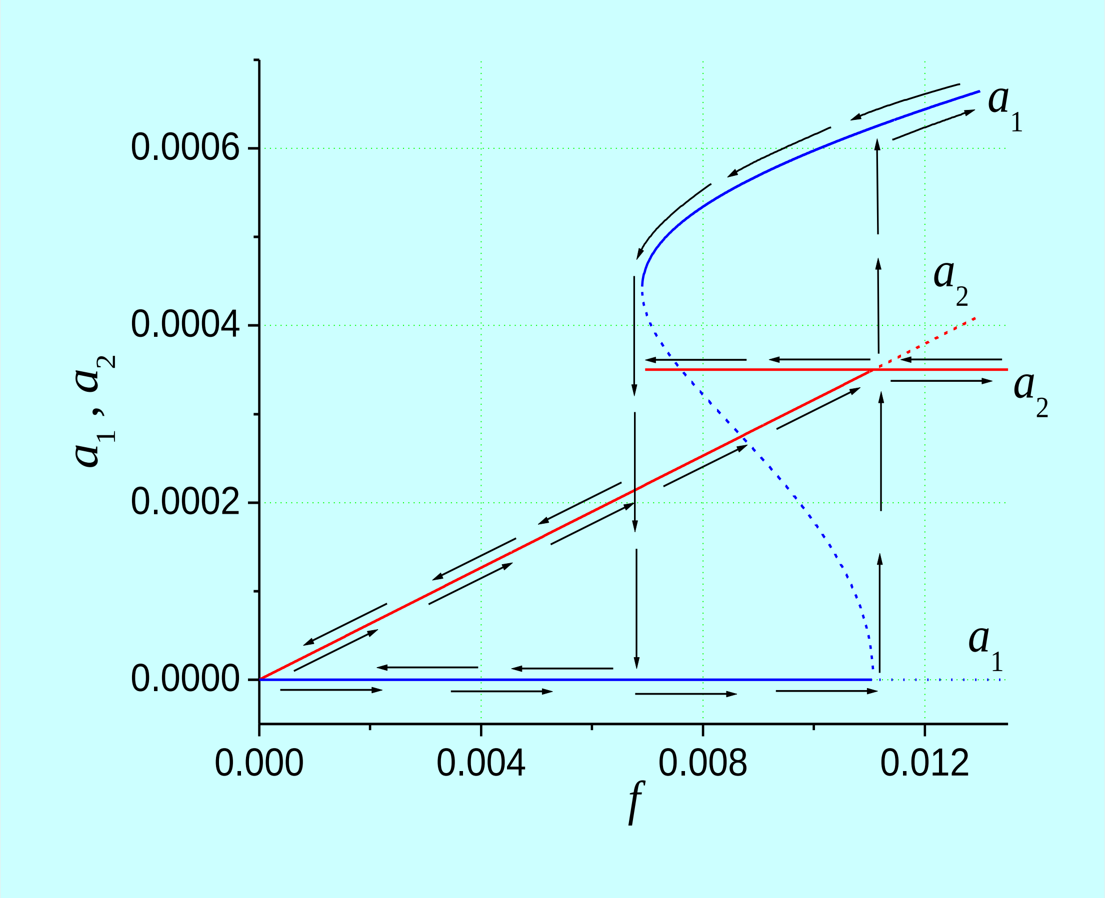

Comparison of the analytical results presented on the previous picture curves with the numerical integration of (1)

(a) Ω=19.5 (σ_1= –0.5, σ_2= 0), f=0.0065

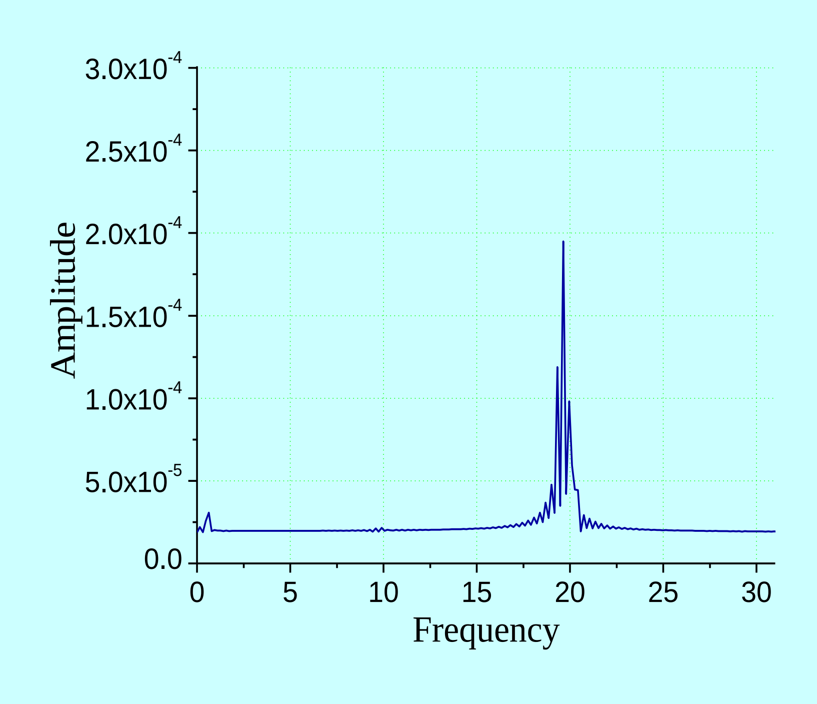

(b) Ω=19.5 (σ_1= –0.5, σ_2= 0), f=0.01

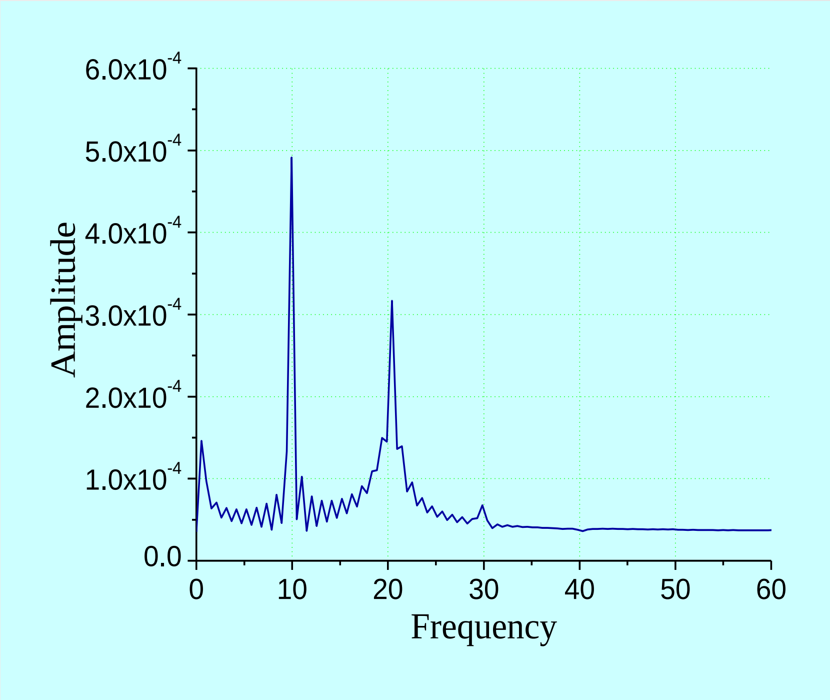

Amplitudes a_1, a_2 versus the amplitude of the external excitation f;
$\Omega \approx \omega_2$, $\sigma_1 = \sigma_2 = 0$

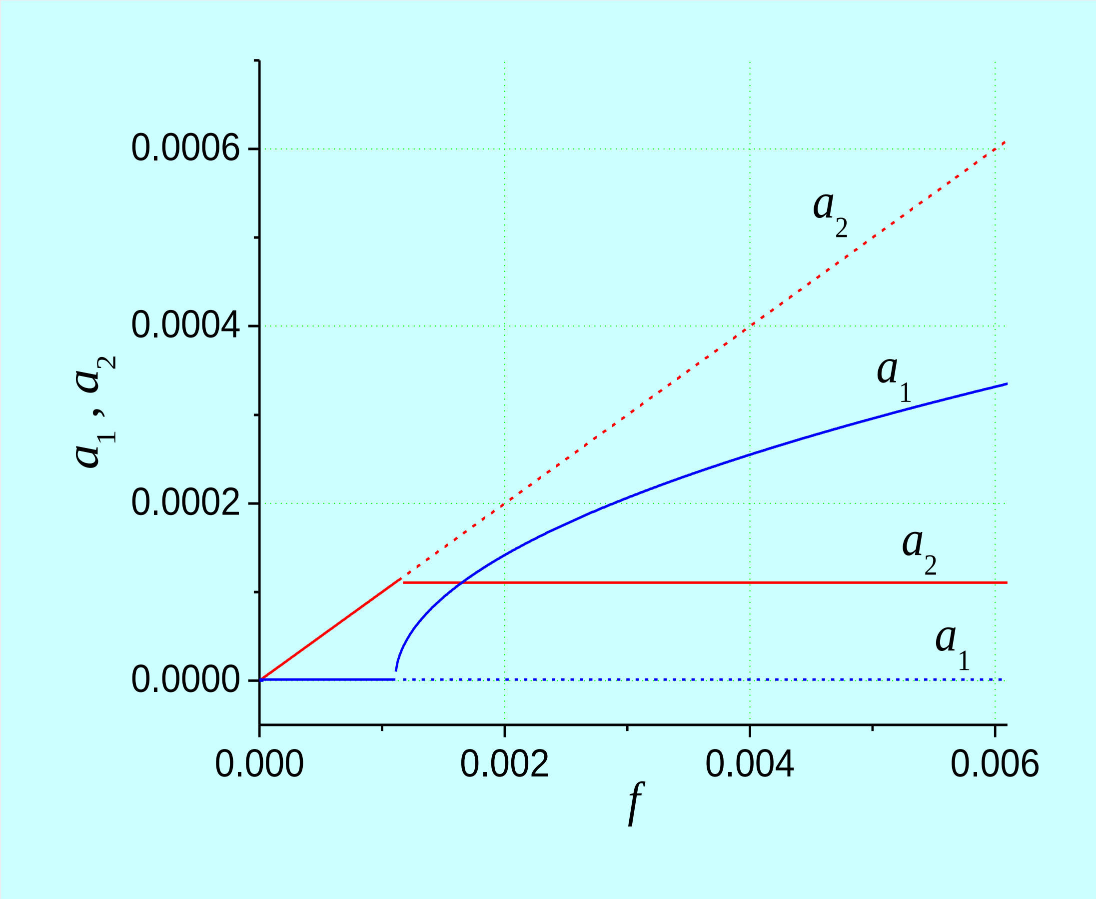

Comparison of the analytical results presented on the previous picture curves with the numerical integration of (1)

(a) Ω=20 (σ_1= σ_2= 0), f=0.0006

(b) Ω=20 (σ_1= σ_2= 0), f=0.003

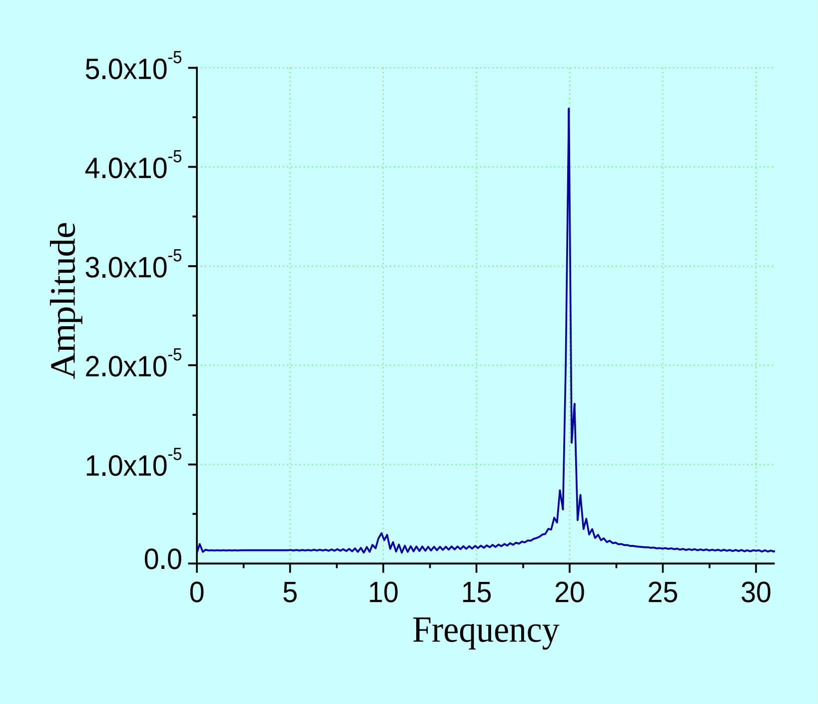

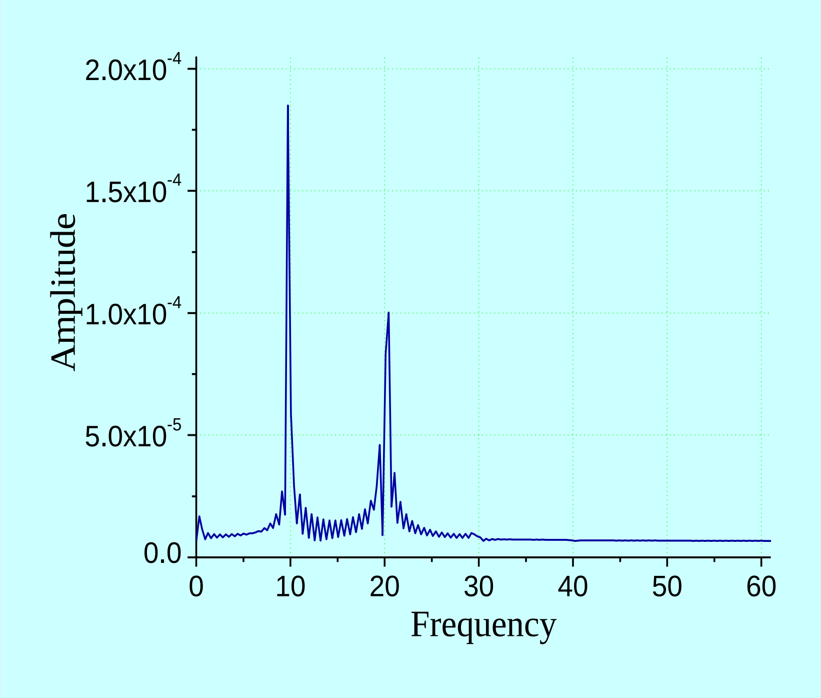

Rigid magnetic materials. Hysteretic close-loop control

The hysteretic properties of the system (1) can be taken into consideration by means of Bouc-Wen hysteretic model

$$\begin{aligned} \ddot{x} &= P_r(\rho,\dot{\rho},\dot{\phi})\cos\phi - P_\tau(\rho,\dot{\phi})\sin\phi - \gamma_m\dot{x} - \lambda_m[\delta(x-x_0)+(1-\delta)z_1], \\ \ddot{y} &= P_r(\rho,\dot{\rho},\dot{\phi})\sin\phi + P_\tau(\rho,\dot{\phi})\cos\phi - \gamma_m\dot{y} - \lambda_m[\delta(y-y_0)+(1-\delta)z_2] \\ &\quad + Q_0 + Q\sin\Omega t, \\ \dot{z}_1 &= \left\lfloor k_z - (\gamma + \beta\,\mathrm{sgn}(\dot{x})\,\mathrm{sgn}(z_1))|z_1|^n \right\rfloor \dot{x}, \\ \dot{z}_2 &= \left\lfloor k_z - (\gamma + \beta\,\mathrm{sgn}(\dot{y})\,\mathrm{sgn}(z_2))|z_2|^n \right\rfloor \dot{y}. \end{aligned} \tag{8}$$

Here z_1 and z_2 are hysteretic forces. The case δ=0 corresponds to maximal hysteretic dissipation and δ=1 corresponds to absence of hysteretic forces in the system, the parameters $(k_z, \beta, n) \in R+$ and $\gamma \in R$ govern the shape of the hysteresis loop

The influence of hysteretic dissipation δ on chaos occurring in horizontal (a), (c) and vertical (b), (d) vibrations of the rotor (8) in the case of rigid magnetic materials.

(a)

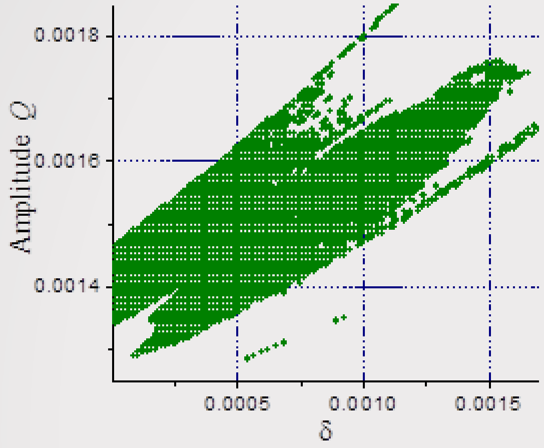

(b)

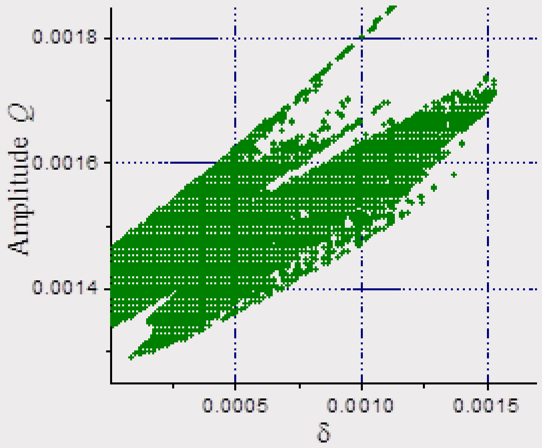

C=0.03, γ_m=0.001, λ_m=450

(c)

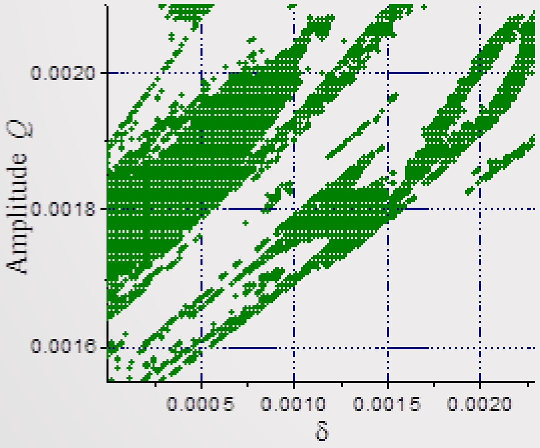

(d)

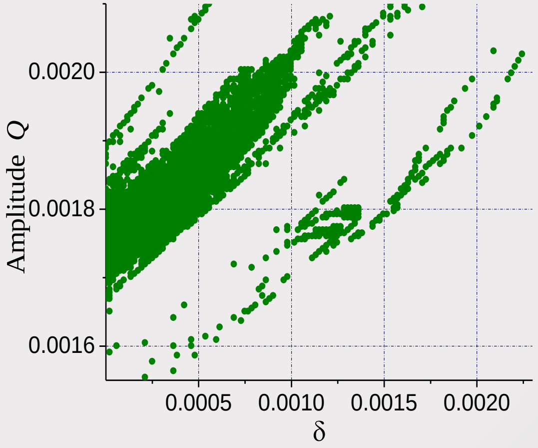

C=0.2, γ_m=0, λ_m=500

Parameters k_z=0.000055, γ=15, β=0.25, n=1.0, Ω=0.87 are fixed

Chaotic regions for the horizontal (a), (c) and vertical (b), (d) vibrations of the rotor (8) in the (Ω, Q) parametric plane with decreasing of the hysteretic dissipation value δ

(a)

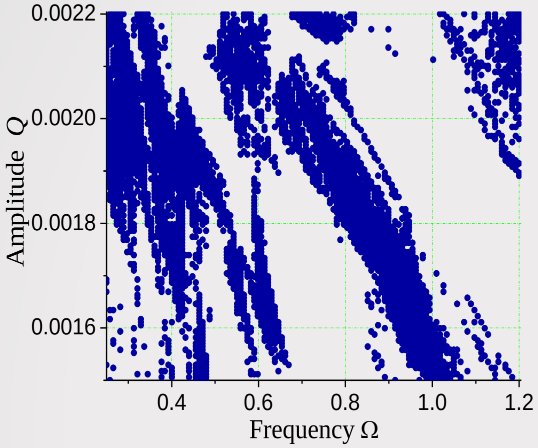

(b)

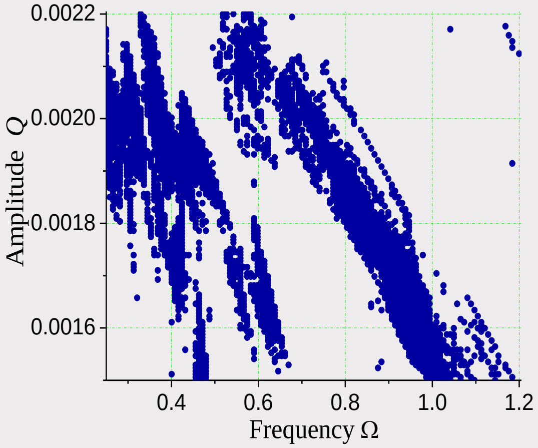

δ=0.0001

(c)

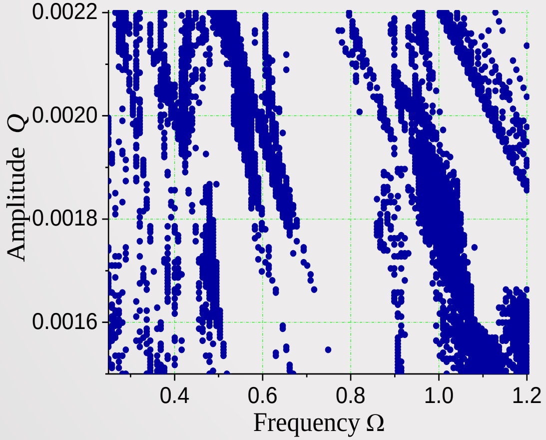

(d)

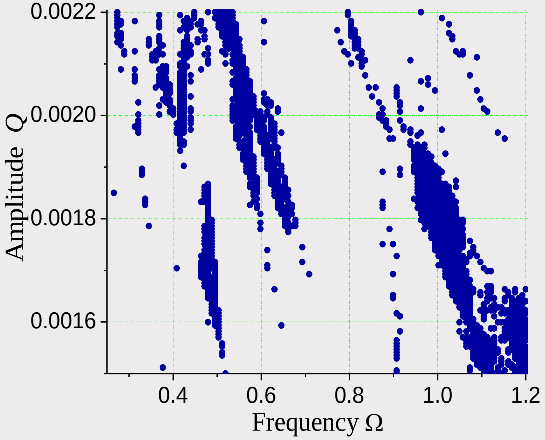

δ=0.0013

Parameters of the system C=0.2, γ_m=0, λ_m=500, k_z=0.000055, γ=15, β=0.25, n=1.0 are fixed

Phase portraits and hysteresis loops of the rotor motion that agree with the chaotic regions in the (Ω, Q) plane

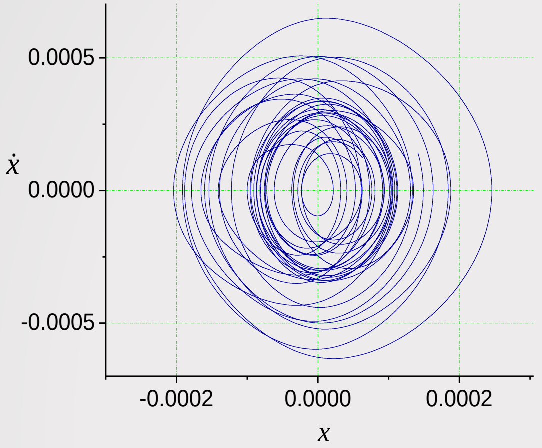

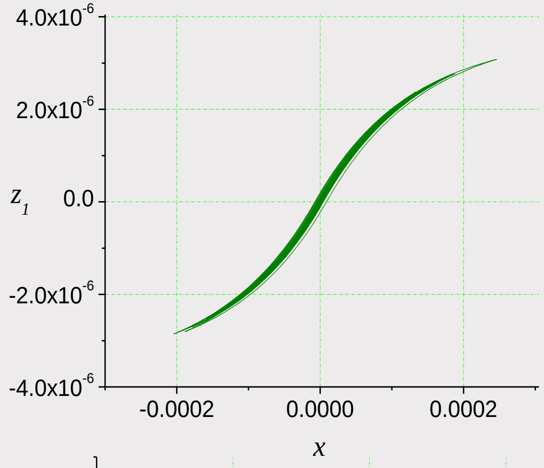

horizontal vibrations of the rotor

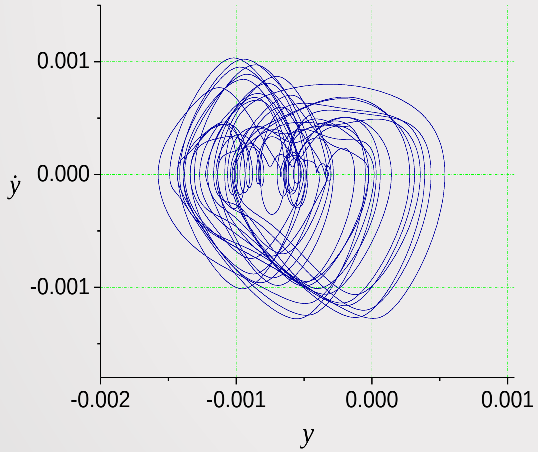

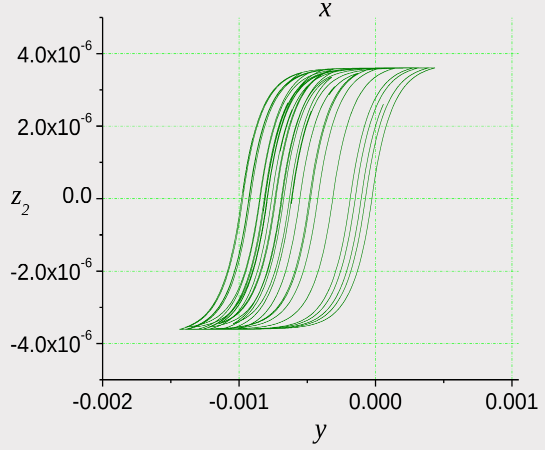

vertical vibrations of the rotor

The parameters Ω=0.87, Q=0.00177, δ=0.0001, C=0.2, γ_m=0, λ_m=500, k_z=0.000055, γ=15, β=0.25, n=1.0 are fixed

Phase portraits and hysteresis loops of the periodic rotor motion that agree with the regions of regular motion in the (Ω, Q) plane

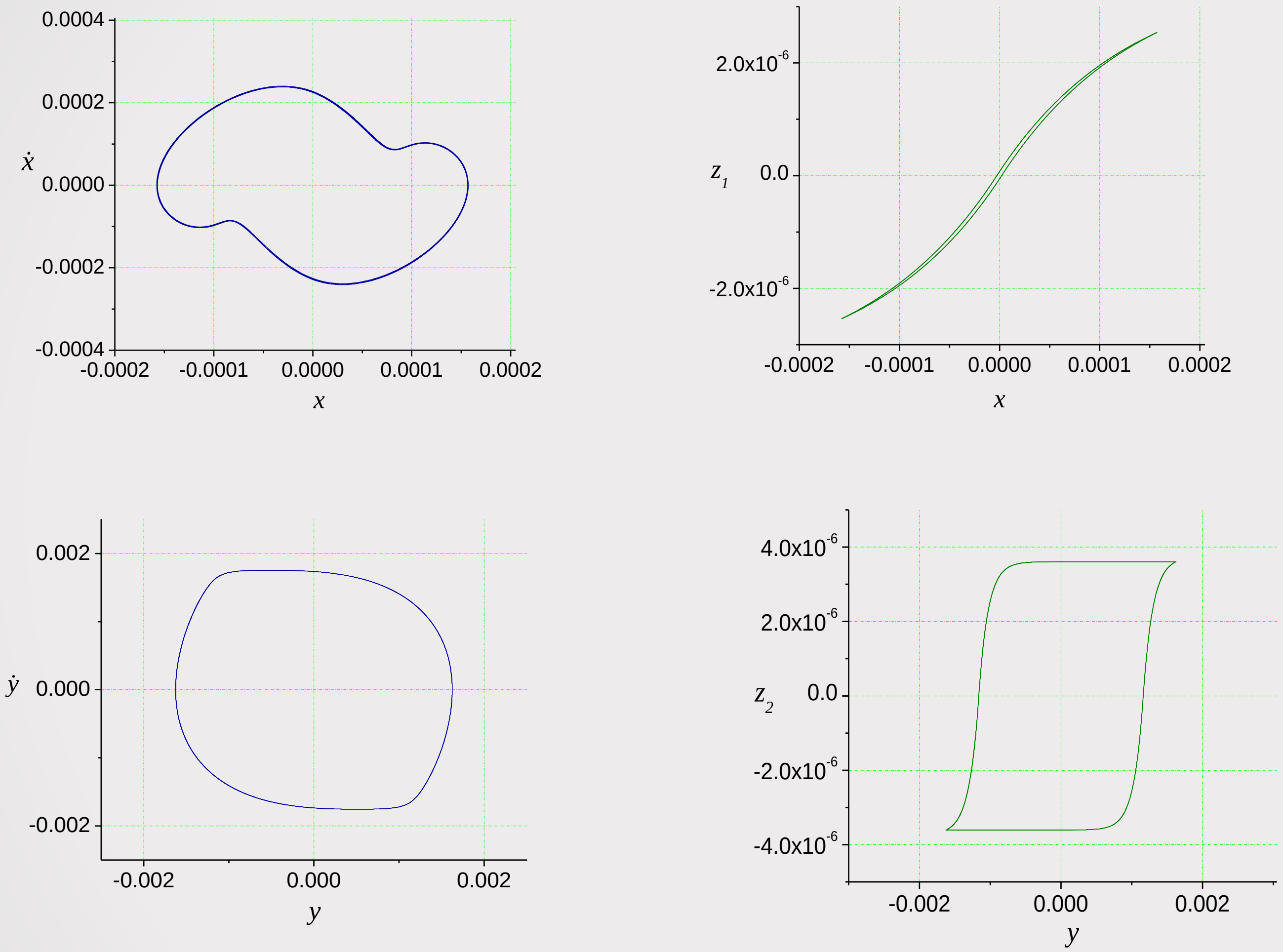

horizontal vibrations of the rotor

vertical vibrations of the rotor

Parameters Ω=1.2, Q=0.0017, δ=0.0001, C=0.2, γ_m=0, λ_m=500, k_z=0.000055, γ=15, β=0.25, n=1.0 are fixed

The influence of the dynamic oil-film action characteristics on chaos occurring in horizontal (a), (c) and vertical (b), (d) vibrations of the rotor (8) in the case of rigid magnetic materials.

(a)

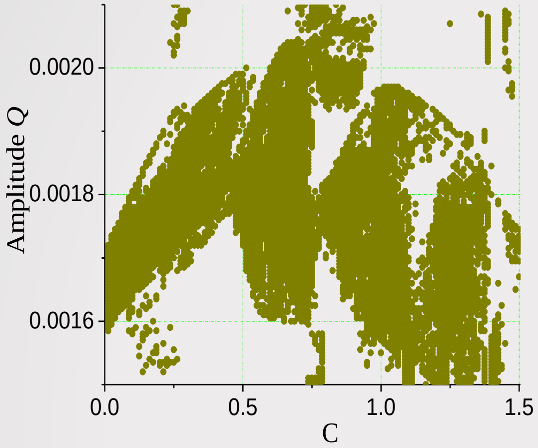

(b)

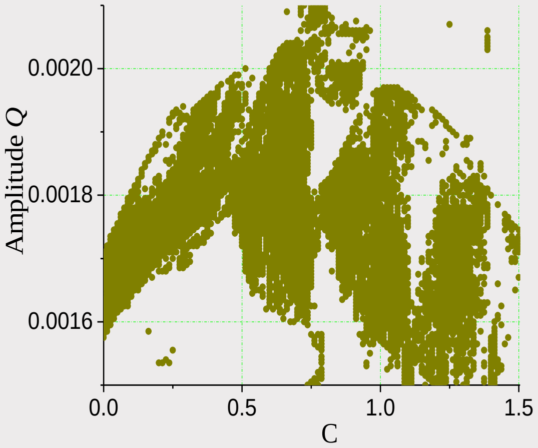

δ=0.000001, γ_m=0

(c)

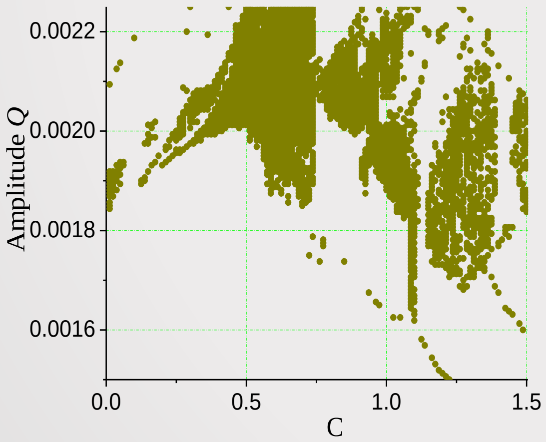

(d)

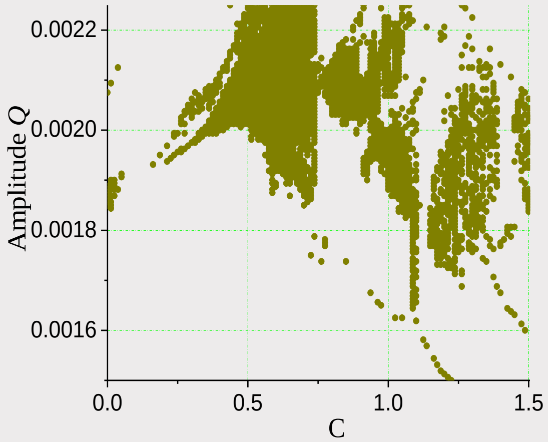

δ=0.001, γ_m=0.03

Parameters of the system λ_m=500, k_z=0.000055, γ=15, β=0.25, n=1.0, Ω=0.87

The influence of the magnetic control parameter γ_m on chaos occurring in horizontal (a), (c) and vertical (b), (d) vibrations of the rotor (8) in the case of rigid magnetic materials

(a)

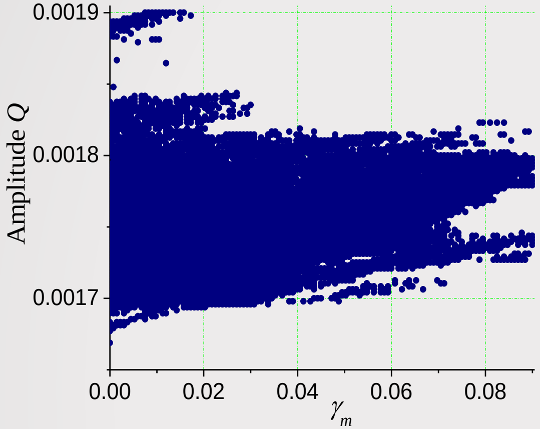

(b)

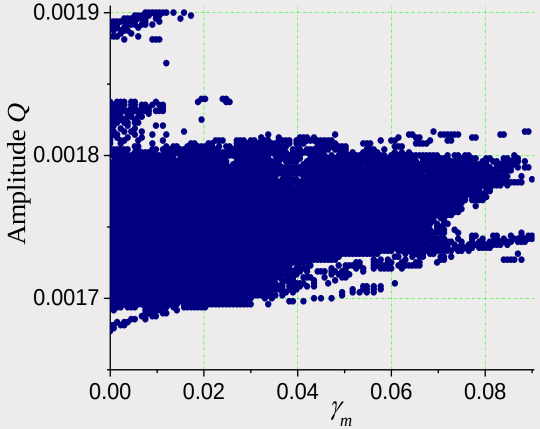

δ=0.000001, C=0.2

(c)

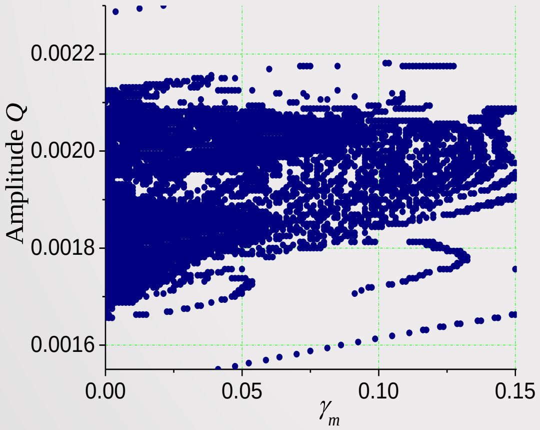

(d)

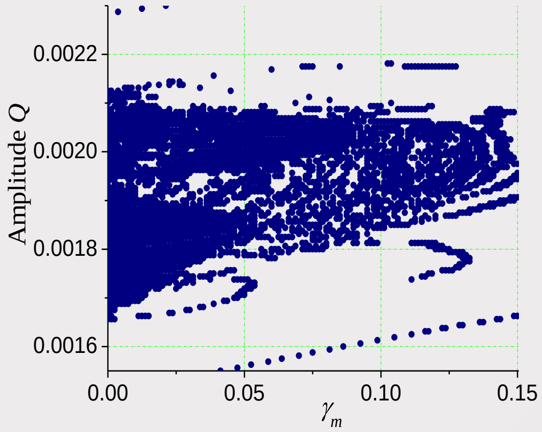

δ=0.0005, C=1

Parameters of the system λ_m=500, k_z=0.000055, γ=15, β=0.25, n=1.0, Ω=0.87 are fixed

The influence of the magnetic control parameter λ_m on chaos occurring in horizontal (a), (c) and vertical (b), (d) vibrations of the rotor (8) in the case of rigid magnetic materials.

(a)

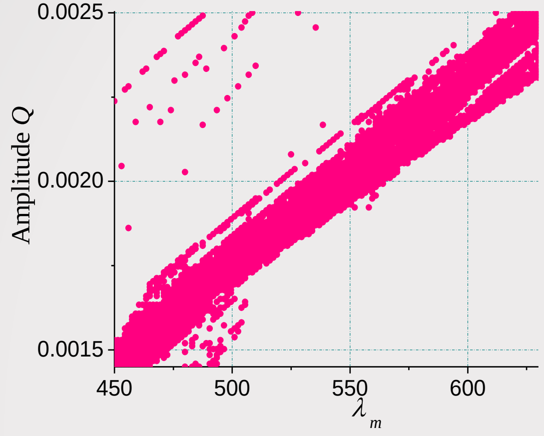

(b)

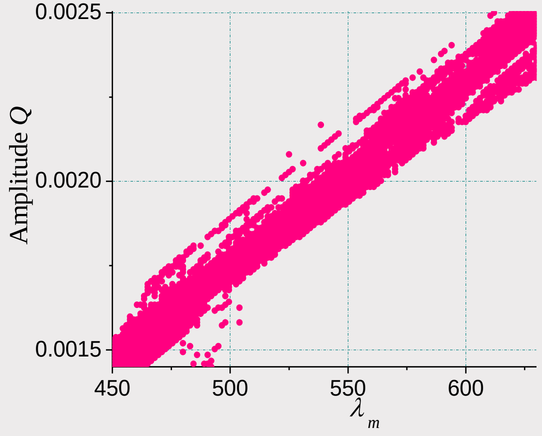

δ=0.000001, C=0.2, γ_m=0

(c)

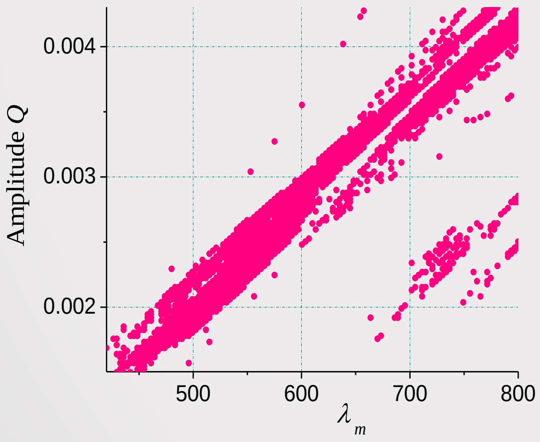

(d)

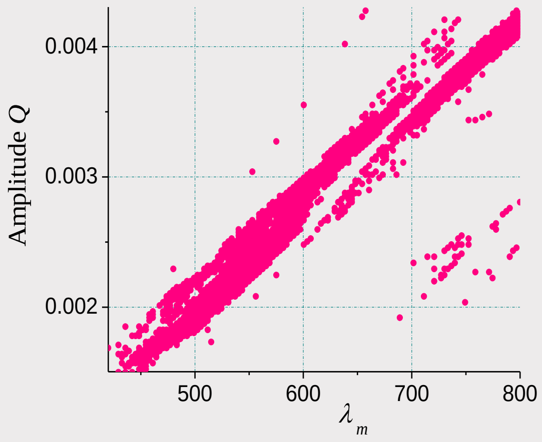

δ=0.001, C=1, γ_m=0.005

Parameters of the system k_z=0.000055, γ=15, β=0.25, n=1.0, Ω=0.87 are fixed

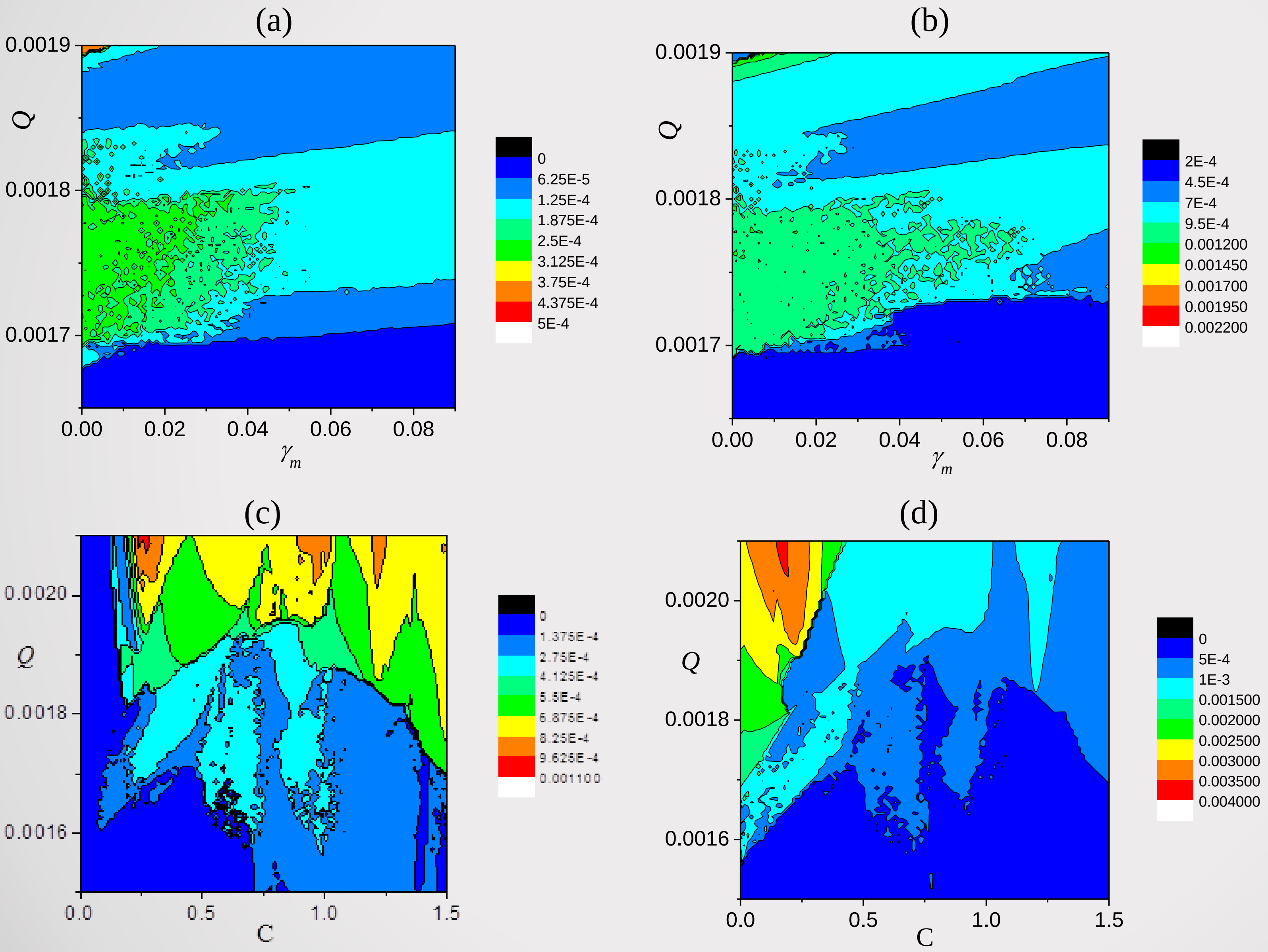

δ=0.000001, C=0.2, λ_m=500, k_z=0.000055, γ=15, β=0.25, n=1.0, Ω=0.87

δ=0.000001, γ_m=0, λ_m=500, k_z=0.000055, γ=15, β=0.25, n=1.0, Ω=0.87

Conclusions I

- 2-dof nonlinear dynamics of the rotor suspended in a magneto-hydrodynamic field has been considered;

- In the case of soft magnetic materials the analytical solutions have been obtained using the method of multiple scales:
  - in the non-resonant case the system exhibits linear properties; the perturbation solutions are in good agreement with the numerical solutions;
  - the cases of the primary resonances with and without the internal resonance have been investigated; frequency-response curves have been obtained; the saturation phenomenon has been demonstrated; the comparison of the analytical and numerical solutions has been carried out.

- In the case of rigid magnetic materials the hysteresis has been taken into account by means of the Bouc-Wen hysteretic model. Conditions for optimal control of the motion are based on the instability regions obtained in the 'frequency-amplitude' of external excitation parametric plane as well as on the amplitude level contours of vertical and horizontal vibrations of the rotor. When the hysteretic dissipation is increased, the amplitude level is decreased and resonance peaks correspond to regions with lower frequencies of the external excitation.

References

- [1] A. H. Nayfeh, D. T. Mook, *Nonlinear oscillations*. Wiley, 2004.
- [2] K. Dziedzic, W. Kurnik, Stability of a rotor with hybrid magnetohydrodynamic support. *Machine Dynamics Problems*, 26(4), 33-43, 2002.
- [3] W. Kurnik, Active magnetic antiwhirl control of a rigid rotor supported on hydrodynamic bearings. *Machine Dynamics Problems*, 10, 21-36, 1995.
- [4] Z. Osinski (Ed.), Damping of Vibrations, A.A. Balkema, Rotterdam, Brookfield, 1998.
- [6] J. Awrejcewicz, L. Dzyubak, Hysteresis modelling and chaos prediction in one- and two-dof hysteretic models, *Arch Appl Mech*, 77, 261-279, 2007.
- [7] J. Awrejcewicz and L.P. Dzyubak, Chaos caused by hysteresis and saturation phenomenon in 2-dof vibrations of the rotor supported by the magneto-hydrodynamic bearing, *International Journal of Bifurcation and Chaos* **15(6)** (2011) 2041-2055.

Outline

II

- **Hysteresis simulation and investigation of the control parameter planes**

- Hysteresis simulation by means of internal variables

- Analytical models of
  - hysteretic behaviour of magnetorheological/electrorheological fluids in a damper/absorber
  - hysteresis in shape-memory alloys (superelastic behaviour of an NiTi polycrystalline helix)
  - stress-strain hysteresis with transient processes

- Evolution of chaotic behaviour regions in various control parameter planes of the Masing and Bouc-Wen hysteretic oscillators. Conditions for pinched hysteresis
  - restraining and generating effect of the hysteretic dissipation on chaos occurring
  - substantial influence of a hysteretic dissipation value on form and location of the chaotic regions

HYSTERESIS SIMULATION AND INVESTIGATION OF THE CONTROL PARAMETER PLANES

Mechanical system with elastic-plastic properties for hysteresis modelling (the Masing model)

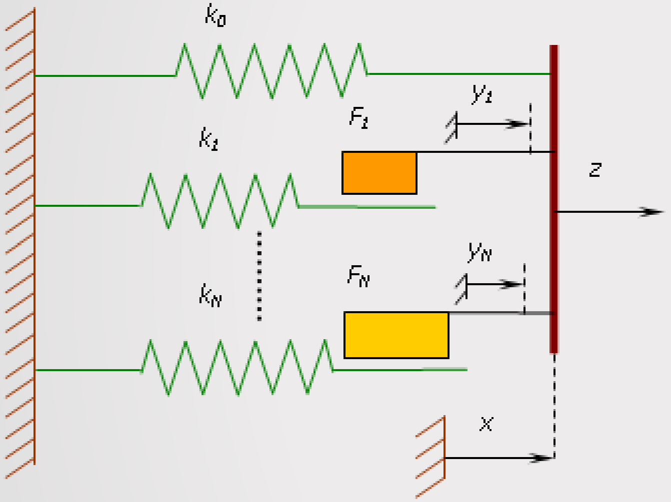

x, z are input and output signals of the system

$y_1, y_2, \ldots, y_N$. are internal variables

$$\dot{y}_i = k_i \dot{x} \frac{1}{2}\left(1 - \mathbf{sgn}\left(y_i^2 - F_i^2\right) - \mathbf{sgn}\left(\dot{x} y_i\right)\left[1 + \mathbf{sgn}\left(y_i^2 - F_i^2\right)\right]\right)$$

i.e.

$$\dot{y}_i = k_i \dot{x} \quad \text{for } |y_i| < F_i \vee \left(|y_i| = F_i \wedge \mathbf{sgn}(\dot{x} y_i) \le 0\right)$$

$$\dot{y}_i = 0 \qquad \textit{in all other cases}$$

$$\mathbf{sgn}\left(y_i^2 - F_i^2\right) \approx \left|\frac{y_i}{F_i}\right|^m - 1 \quad \text{for } y_i^2 \le F_i^2,\ m \in \Re^+ \wedge m \ge 1$$

$$\dot{y}_i = k_i \dot{x}\left(1 - \frac{1}{2}\left(1 + \mathbf{sgn}(\dot{x} y_i)\right)\left|\frac{y_i}{F_i}\right|^m\right)$$

The output (or response) of hysteretic system is $z(t)$:

$$z(t) = k_0(x) x(t) + \sum_{i=1}^{N} y_i(t)$$

$$\dot{y}_i = \left(A_i(x) - \left(\beta_i + \alpha_i\, \mathbf{sgn}(\dot{x})\, \mathbf{sgn}(y_i)\right)\left|\frac{y_i}{F_i(x)}\right|^m\right)\dot{x}$$

where $k_0(x)$, $A_i(x) \ge 0$, $F_i(x) > 0$, $x \in [x_{min}, x_{max}]$, α_i, $\beta_i \in \Re$;

$$z = p(x, y_1, y_2, \ldots, y_N),$$
$$\dot{y}_i = q(x, \dot{x}, y_i) \quad i = 1,2,\ldots, N.$$

The parameters of functions $p(x, y_1, y_2, \ldots, y_N)$ and $q(x, \dot{x}, y_i)$ (i=1, 2,…,N) are determined via a procedure minimizing the criterion function

$$\Phi(c_1,\ldots,c_j,\alpha_1,\ldots,\alpha_k,\ldots,\beta_1,\ldots,\beta_l) =$$
$$\sum_i \left(p\left(x(c_1,\ldots,c_j,t_i), y_1(\alpha_1,\ldots,\alpha_k,t_i),\ldots,y_N(\beta_1,\ldots,\beta_l,t_i)\right) - z_i\right)^2$$

which characterizes an error between the experimental curve and the calculated one. Here *zi* are responses of a hysteretic system, which are known from an experiment and the values are obtained as result of integration of the system, which is described by means of the analytical model.

To solve the optimization problem

$$\Phi(c_1,\dots,c_j,\alpha_1,\dots,\alpha_k,\dots,\beta_1,\dots,\beta_l)\to \boldsymbol{min}$$

the method of gradient descent is used. The step-by-step descent to the minimum of the criterion function realises in the opposite direction to the criterion function gradient

$$\mathbf{grad}\,\Phi=\left\{\frac{\partial\Phi}{\partial c_1},\dots,\frac{\partial\Phi}{\partial c_j},\frac{\partial\Phi}{\partial\alpha_1},\dots,\frac{\partial\Phi}{\partial\alpha_k},\frac{\partial\Phi}{\partial\beta_1},\dots,\frac{\partial\Phi}{\partial\beta_l}\right\}$$

$$\tilde{c}_i=c_i-h_{c_i}\left(\frac{\partial\Phi}{\partial c_i}\Big/\left|\mathbf{grad}\,\Phi\right|\right),\quad i=\overline{1,j}$$

$$\tilde{\alpha}_i=\alpha_i-h_{\alpha_i}\left(\frac{\partial\Phi}{\partial\alpha_i}\Big/\left|\mathbf{grad}\,\Phi\right|\right),\quad i=\overline{1,k}$$

....

$$\tilde{\beta}_i=\beta_i-h_{\beta_i}\left(\frac{\partial\Phi}{\partial\beta_i}\Big/\left|\mathbf{grad}\,\Phi\right|\right),\quad i=\overline{1,l}$$

Experimental (red/ ○ ○ ○) and simulated (blue/——) hysteresis loop
for the magnetorheological damper filled with MRF-132LD
(applied current 0.15 A, frequency 5 Hz)

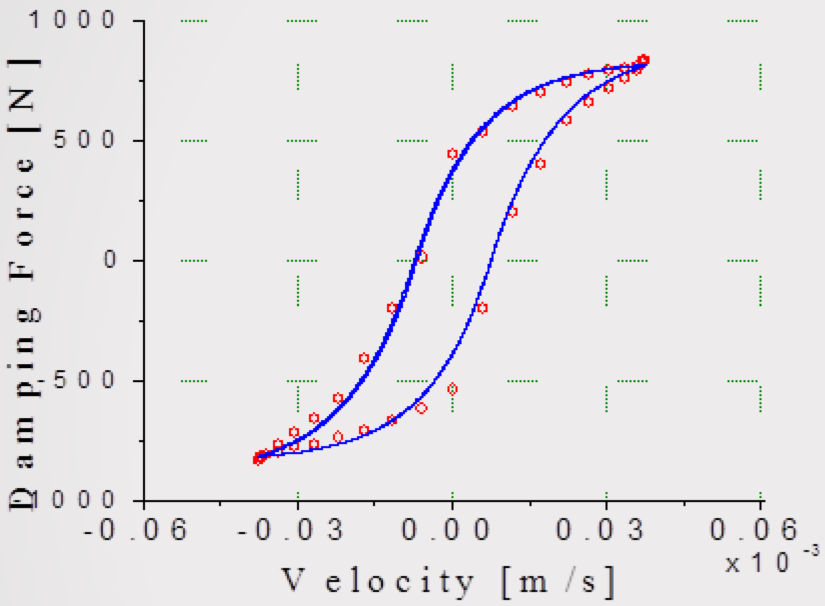

$$z(t) = y_1(t),$$

$$\dot{y}_1 = \left(c_1 - \left(c_2 + c_3\, \mathbf{sgn}(\dot{x})\, \mathbf{sgn}(y_1)\right)|y_1|\right)\dot{x}$$

Final values of the parameters used in the analytical model
for identification of the experimental data

c_1	c_2	c_3
70000	80.7208	3.002

Hysteresis in shape-memory alloys:
superelastic behaviour of an NiTi polycrystalline helix

Experimental/simulated hysteresis loop is red (∘ ∘ ∘)/blue (——)

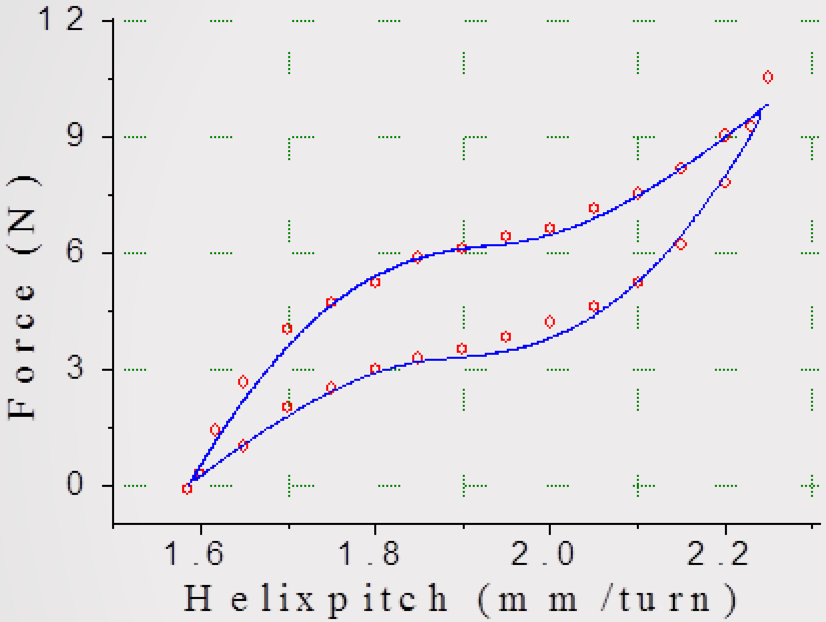

$$z(t) = c_4\left(x(t) - x_c\right) + c_5 + y_1(t),$$
$$\dot{y}_1 = \left(c_1 \,\boldsymbol{tanh}\left|x - x_c\right| - \left(c_2 + c_3\,\boldsymbol{sgn}(\dot{x})\,\boldsymbol{sgn}(y_1)\right)\left|y_1\right|\right)\dot{x}$$

Final values of the parameters used in the analytical model for identification of the experimental data

c_1	c_2	c_3	c_4	c_5
82.8007	0.926997	3.33899	6.17671	4.88777

Stress-strain hysteresis with transient processes
for the steel rope (stress (N) vs. strain (mm))
Experimental/simulated hysteresis loop is red (○ ○ ○)/blue (———)

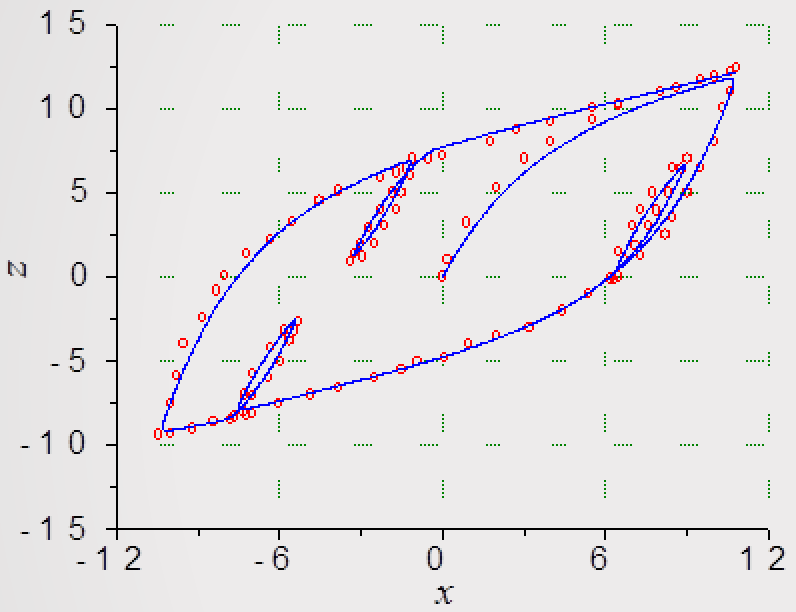

$$z(t) = c_4 x(t) + c_5 + y_1(t),$$
$$\dot{y}_1 = \left(c_1 - \left(c_2 + c_3\, \mathbf{sgn}(\dot{x})\, \mathbf{sgn}(y_1)\right)|y_1|\right)\dot{x}$$

$$z(t) = c_4 x(t) + c_5 + y_1(t),$$
$$\dot{y}_1 = \left(c_1 - \left(c_2 + c_3\, \mathbf{sgn}(\dot{x})\, \mathbf{sgn}(y_1 - z_e)\right)|y_1 - z_e|\right)\dot{x}$$

Final values of the parameters used in the analytical model
for identification of the experimental data

c_1	c_2	c_3	c_4	c_5
2.22254	0.0010226	0.338787	0.387749	1.45286

Scheme of Masing and Bouc-Wen hysteretic systems

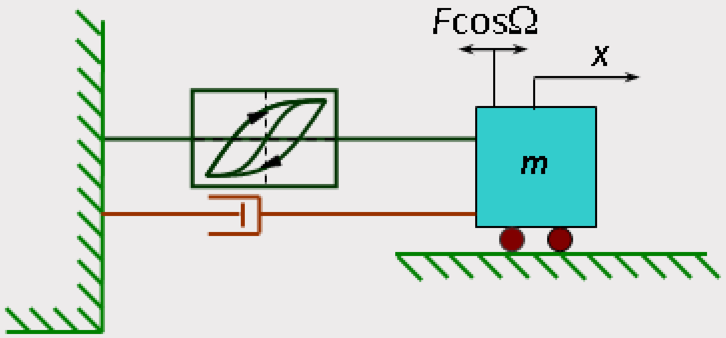

Masing oscillator

$$\dot{x} = y,$$
$$\dot{y} = -2\mu y - (1-\nu)g(x) - \nu z + F\cos\Omega t,$$
$$\dot{z} = g'\left(\frac{z - z_i}{2}\right)y,$$
$$g(x) = \frac{(1-\delta)x}{\left(1+|x|^n\right)^{\frac{1}{n}}} + \delta x$$

Bouc-Wen oscillator

$$\dot{x} = y,$$
$$\dot{y} = -2\mu y - \delta x - (1-\delta)z + F\cos\Omega t,$$
$$\dot{z} = \left[k_z - (\gamma + \beta\,\mathrm{sgn}(\dot{x})\,\mathrm{sgn}(z))\,|z|^n\right]y.$$

Total restoring force with elastic part and hysteretic one:

$$R=(1-\nu)g(x)+\nu z$$

$$R=\delta x + (1-\delta)\, z$$

The influence of hysteretic dissipation on chaos occurring

Masing hysteretic oscillator

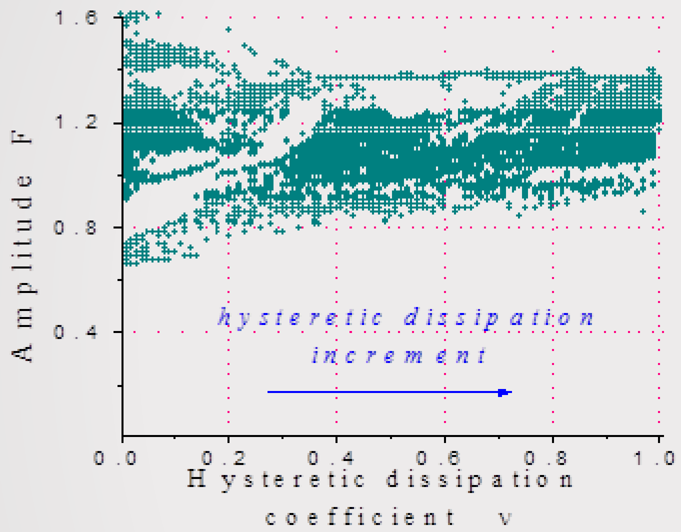

Ω=0.16, μ=0.0005, δ=0.05, n=10.0, $x(0)$=0.1, $\dot{x}(0)$=0.1, $z(0)$=0

Bouc-Wen hysteretic oscillator

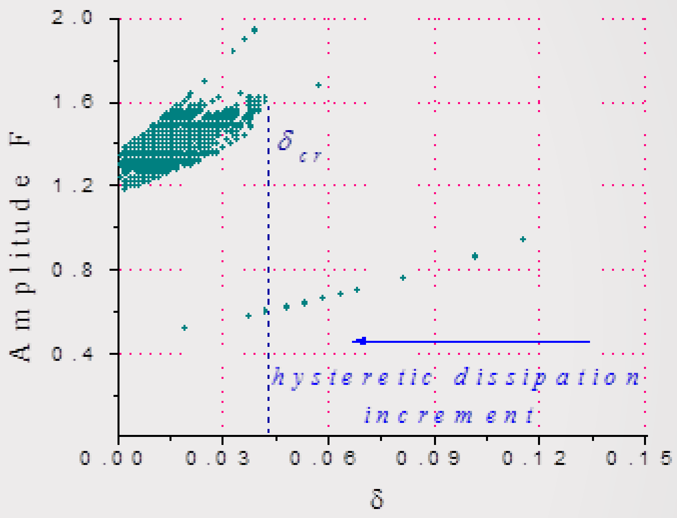

Ω=0.2, μ=0, k_z=0.5, γ=0.3, β=0.005, n=1.0, $x(0)$=0.1, $\dot{x}(0)$=0.1, $z(0)$=0

Evolution of the chaotic regions (olive) and the regions of pinched hysteresis (dark yellow – $\varepsilon_r/\varepsilon<1\%$), (yellow – $1\%<\varepsilon_r/\varepsilon<5\%$) for the Masing hysteresis model in the (Ω, F) plane with increasing of the hysteretic dissipation value $\nu=0 \rightarrow \nu=0.5 \rightarrow \nu=0.8$.

The parameters $\mu=0.0005$, $\delta=0.05$, $n=10.0$, $x(0)=0.1$, $\dot{x}(0)=0.1$, $z(0)=0$ are fixed for all cases

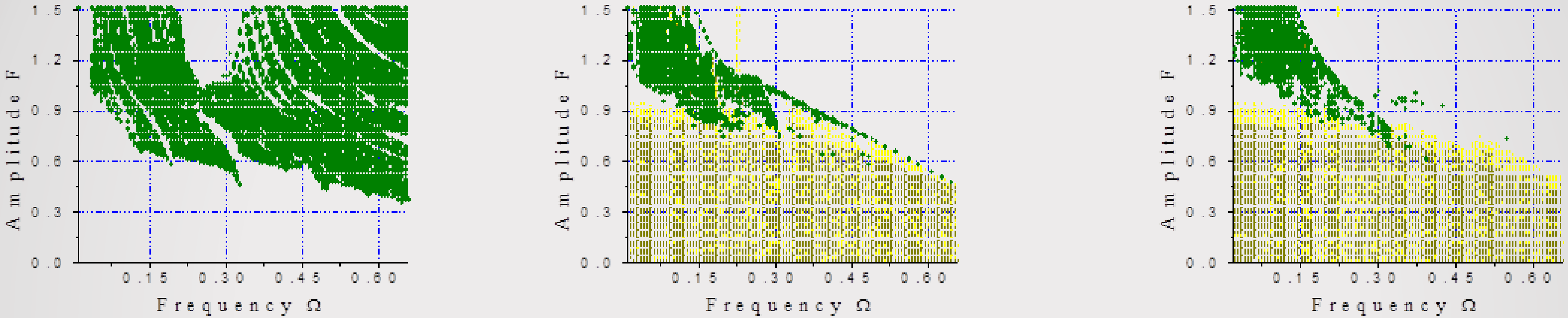

Evolution of the chaotic regions (blue) and the regions of pinched hysteresis (dark yellow – $\varepsilon_r/\varepsilon<1\%$), (yellow – $1\%<\varepsilon_r/\varepsilon<5\%$) for the Masing hysteresis model in the (μ, F) plane with increasing of the hysteretic dissipation value $\nu=0 \rightarrow \nu=0.5 \rightarrow \nu=0.8$.

The parameters $\Omega=0.12$, $\delta=0.05$, $n=10.0$, $x(0)=0.1$, $\dot{x}(0)=0.1$, $z(0)=0$ are fixed for all cases

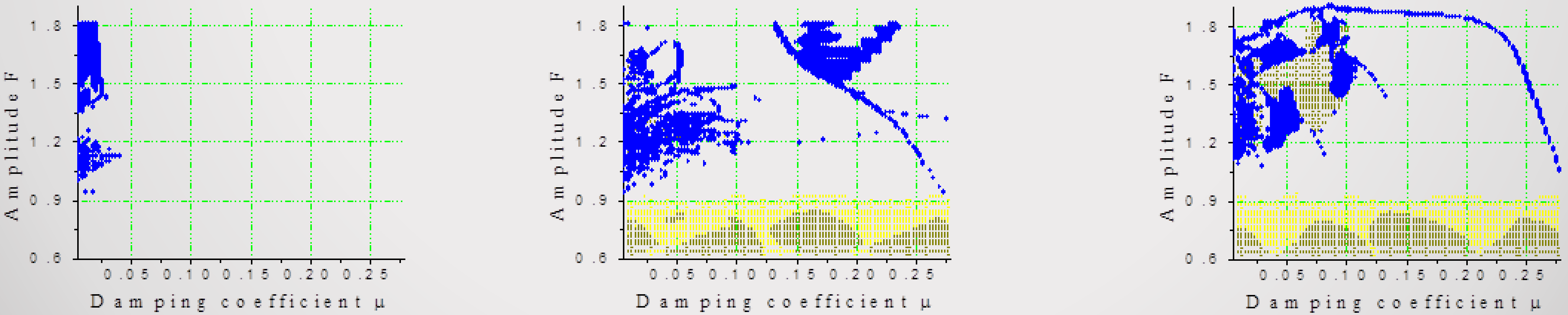

Phase portraits and hysteresis loops of the Masing hysteretic oscillator

in the case of chaotic response (Ω=0.12, F=1.27, μ=0.057, ν=0.5);

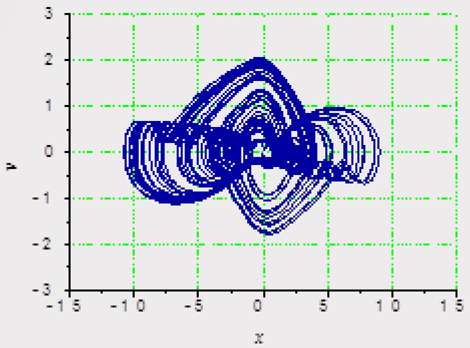

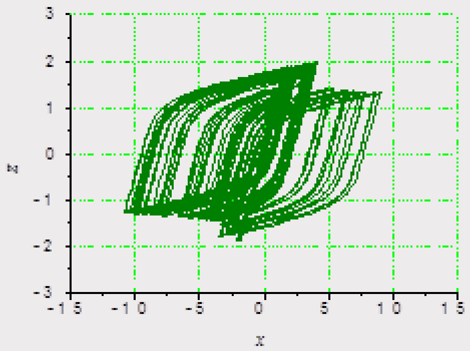

in the case of periodic response (Ω=0.6, F=0.9, μ=0.0005, ν=0.5).

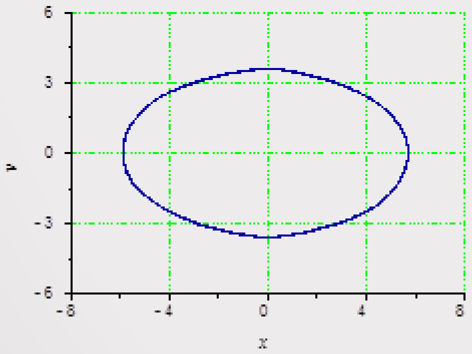

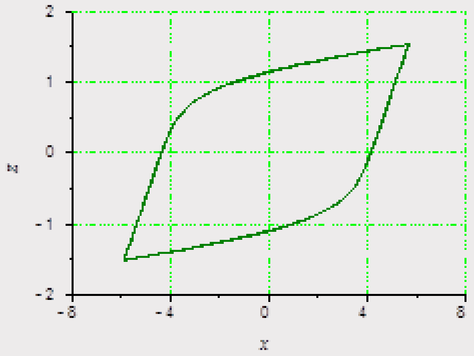

In all cases the parameters δ=0.05, n=10.0, $x(0)$=0.1, $\dot{x}(0)$=0.1, $z(0)$=0 are fixed.

Evolution of the chaotic regions (pink) and the regions of pinched hysteresis (dark yellow – $\varepsilon_r/\varepsilon<1\%$), (yellow – $1\%<\varepsilon_r/\varepsilon<5\%$) for the Bouc-Wen oscillator in the (Ω, F) plane with increasing of the hysteretic dissipation value $\delta=0.03 \to \delta=0.01 \to \delta=0.001$ at $k_z=0.5$, $\gamma=0.3$, $\beta=0.005$, $n=1.0$, $x(0)=0.1$, $\dot{x}(0)=0.1$, $z(0)=0$ and $\mu=0$.

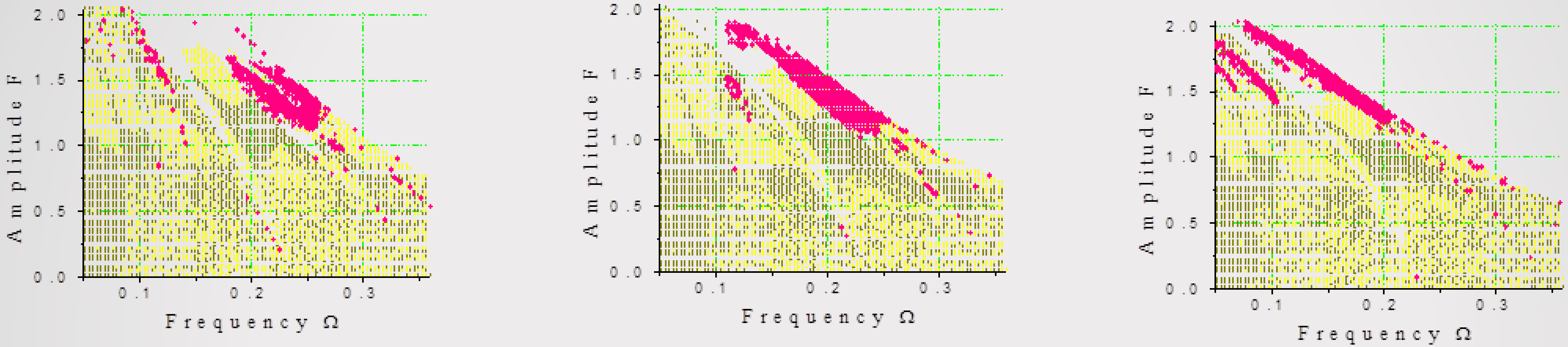

Evolution of the chaotic regions (dark blue) and the regions of pinched hysteresis (dark yellow – $\varepsilon_r/\varepsilon<1\%$), (yellow – $1\%<\varepsilon_r/\varepsilon<5\%$) for the Bouc-Wen oscillator in the (μ, F) plane with increasing of the hysteretic dissipation value $\delta=0.03 \to \delta=0.01 \to \delta=0.001$ at $k_z=0.5$, $\gamma=0.3$, $\beta=0.005$, $n=1.0$, $x(0)=0.1$, $\dot{x}(0)=0.1$, $z(0)=0$ and $\Omega=0.2$.

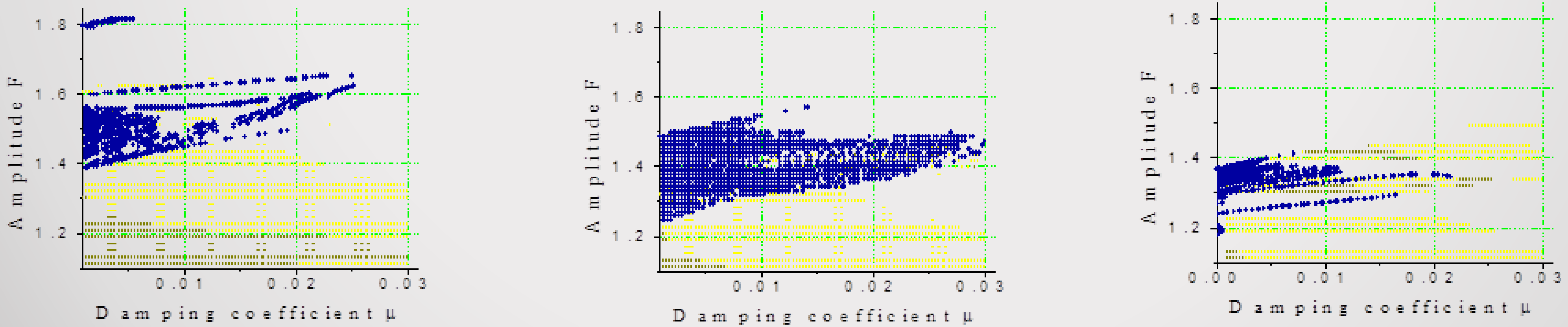

Phase portraits and hysteresis loops of the Bouc-Wen hysteretic oscillator

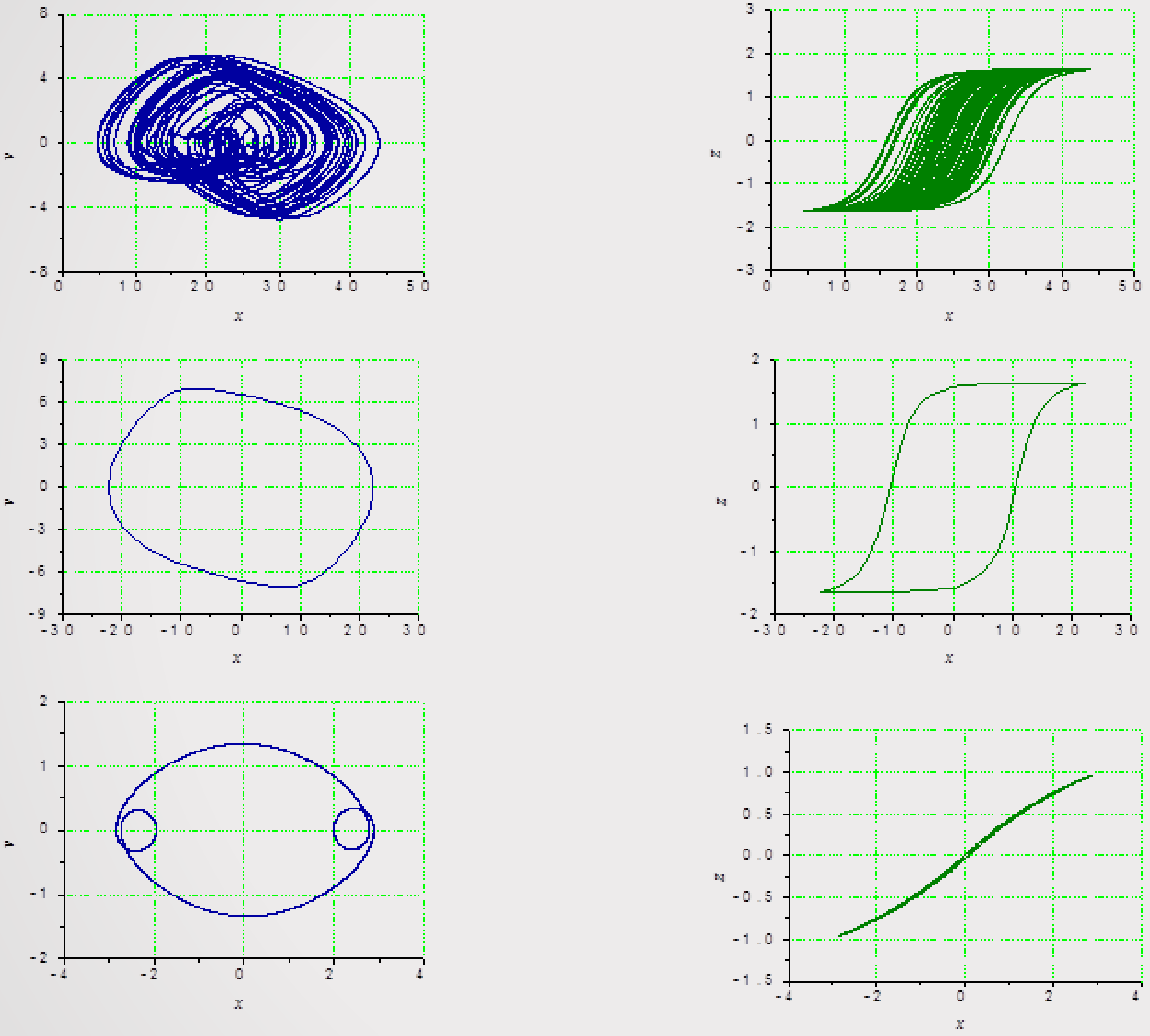

chaotic response
(Ω=0.2, F=1.38, μ=0.0022, δ=0.01)

periodic response
(Ω=0.3, F=1, μ=0.0, δ=0.001)

periodic response with pinched loop
(Ω=0.2, F=1, μ=0.0, δ=0.03)

- In all cases the parameters k_z=0.5, γ=0.3, β=0.005, n=1.0, $x(0)$=0.1, $\dot{x}(0)$=0.1, $z(0)$=0 are fixed.

Conclusions II

- hysteretic loops of various form are simulated by means of internal variables;
- the behaviour of magnetorheological/electrorheological fluids in a damper/absorber is simulated as well as hysteresis in shape-memory alloys (superelastic behaviour of an NiTi polycrystalline helix) and stress-strain hysteresis with transient processes;
- the developed models are effective, enable to produce minor loops, present fast numerical convergence and provide a high degree of correspondence with experimental data;
- highly non-linear Masing and Bouc-Wen hysteretic models with discontinuous right-hand sides are investigated using effective approach based on analysis of the wandering trajectories. This algorithm of quantifying regular and chaotic dynamics is more simple and faster from a computational point of view comparing with standard procedures and allows sufficiently accurate to trace regular/unregular responses of the hysteretic systems;
- the evolution of chaotic behaviour regions of oscillators with hysteresis is presented in various control parameter spaces: in the damping coefficient – amplitude and in the frequency – amplitude of external periodic excitation planes;
- substantial influence of a hysteretic dissipation value on possibility of chaotic behaviour occurring in the systems with hysteresis is shown;
- the restraining and generating effect of the hysteretic dissipation on chaotic behaviour occurring are ascertained;
- the regions of pinched hysteresis with various dissipation properties are presented

References

- [1] Lacarbonara W, Vestroni F. Nonclassical responses of oscillators with hysteresis. *Nonlinear Dyn* 2004.
- [2] Sapinski B. Dynamic characteristics of an experimental MR fluid. *Eng Trans* 2003;51(4):399–418.
- [3] Ortin J, Delaey L. Hysteresis in shape-memory alloys. *Int J Non-Linear Mech* 2002;37:1275–81.
- [4] J. Awrejcewicz, L. Dzyubak, Hysteresis modelling and chaos prediction in one- and two-dof hysteretic models, *Arch Appl Mech*, 77, 261-279, 2007.
- [5] J. Awrejcewicz, L. Dzyubak, C.-H. Lamarque, Modelling of hysteresis using Masing–Bouc-Wen's framework and search of conditions for the chaotic responses, *Communications in Nonlinear Science and Numerical Simulation* 13, 2008, 939-958.

Outline

III

- **Quantifying smooth and non-smooth regular and chaotic dynamics based on analysis of the wandering trajectories**
- Analysis of the wandering trajectories
- Comparison with other approaches
- Chaos in the “smooth” test models
  – Duffing equation
  – Lorenz system
  – three-well potential oscillator
- Chaos in the “non-smooth” models
  – stick-slip chaotic oscillations in a quasi-autonomous mechanical system with Coulomb and viscous friction
  – Regular and chaotic behavior exhibited by coupled oscillators with friction
  – Conditions for chaos occurring in self-excited 2-DOF Masing/Bouc-Wen/hybrid hysteretic systems with friction

- Conclusions
- References

Quantifying smooth and non-smooth regular and chaotic dynamics based on the analysis of wandering trajectories

$$\dot{\mathbf{x}} = f(t, \mathbf{x}) \qquad \mathbf{x} \in R^n$$

$$\mathbf{x}^{(0)} = \mathbf{x}(t_0) \qquad D(f) = R \times R^n$$

$$\forall \mathbf{x}^{(0)}, \tilde{\mathbf{x}}^{(0)} \in R^n, \quad \forall T > 0, \quad \forall \varepsilon > 0 \quad \exists \delta > 0 \ : \quad \left(\rho\left(\mathbf{x}^{(0)}, \tilde{\mathbf{x}}^{(0)}\right) < \delta \wedge |t| \le T\right) \Rightarrow \rho(\mathbf{x}(t), \tilde{\mathbf{x}}(t)) < \varepsilon .$$

$$\exists C_i \in R : \max_t |x_i(t)| \le C_i \qquad (i=1,2 \ldots n).$$

$$A_i = \frac{1}{2}\left|\max_{t_1 \le t \le T} x_i(t) - \min_{t_1 \le t \le T} x_i(t)\right|, \quad [t_1, T] \subset [t_0, T] \qquad (i=1,2 \ldots n).$$

Embedding theorem: $S_\varepsilon(\mathbf{x}) = \{\tilde{\mathbf{x}} \in R^n : \rho(\mathbf{x}, \tilde{\mathbf{x}}) < \varepsilon\} \wedge P_{\varepsilon_1, \varepsilon_2, \ldots, \varepsilon_n}(\mathbf{x}) = \{\tilde{\mathbf{x}} \in R^n : |x_i - \tilde{x}_i| < \varepsilon_i\}$

$$\Downarrow$$

$$\forall \varepsilon > 0 \quad \exists P_{\varepsilon_1, \varepsilon_2, \ldots, \varepsilon_n}(\mathbf{x}) \ : \quad P_{\varepsilon_1, \varepsilon_2, \ldots, \varepsilon_n}(\mathbf{x}) \subset S_\varepsilon(\mathbf{x}).$$

And conversely, $\forall P_{\varepsilon_1,\varepsilon_2,\ldots,\varepsilon_n}(\mathbf{x}) \quad \exists \varepsilon > 0 \; : S_\varepsilon(\mathbf{x}) \subset P_{\varepsilon_1,\varepsilon_2,\ldots,\varepsilon_n}(\mathbf{x}).$

$$\mathbf{x}^{(0)},\ \tilde{\mathbf{x}}^{(0)} \in P_{\delta_1,\delta_2,\ldots,\delta_n}\left(\mathbf{x}^{(0)}\right),$$

$$\left|x_i^{(0)} - \tilde{x}_i^{(0)}\right| < \delta_i \qquad \delta_i \ll A_i \quad (i=1,2\ \ldots\ n)\ .$$

chaotic motion (including transient and alternating chaos):

$$\exists t^* \in [t_1, T] : \left|x_i(t^*) - \tilde{x}_i(t^*)\right| > \alpha A_i\ ,\ 0<\alpha<1 \qquad (i=1, 2, \ldots n).$$

Domains of chaotic behavior for the Duffing equation:
(a) in the (ω, f) plane (γ=0.15, $x(0)$=0.1, $\dot{x}(0)$=0.01);
(b) in the (γ, f) plane (ω=1.7, $x(0)$=0.1, $\dot{x}(0)$=0.01).
The smooth threshold corresponds to the homoclinic trajectory criterion.

$$f > \frac{4}{3}\gamma\frac{ch(\pi\omega/2)}{\sqrt{2}\pi\omega}$$

$$\ddot{x} + \gamma\dot{x} - \frac{1}{2}x\left(1 - x^2\right) = f\cos\omega t$$

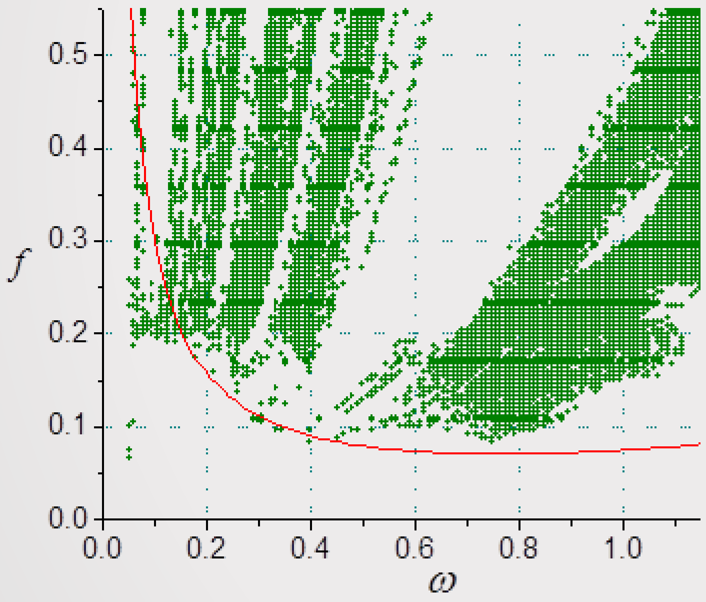

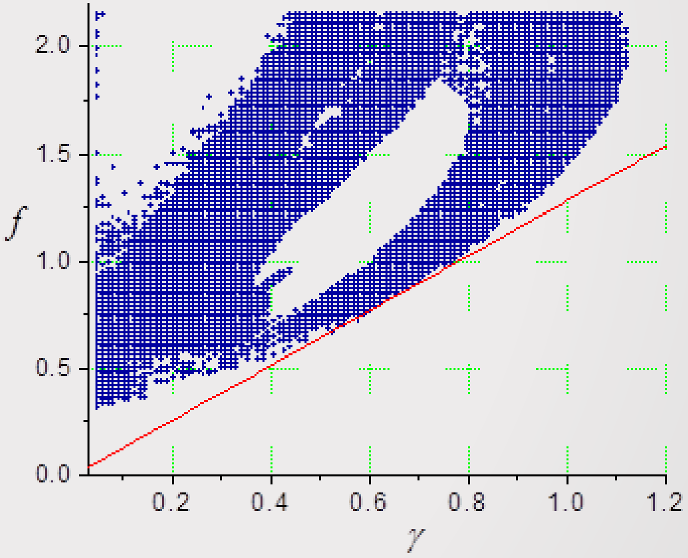

The initial conditions phase plane for the Duffing equation for different values of the amplitude of excitation (γ=0.15, ω=0.8): (a) f=0.08; (b) f=0.09.

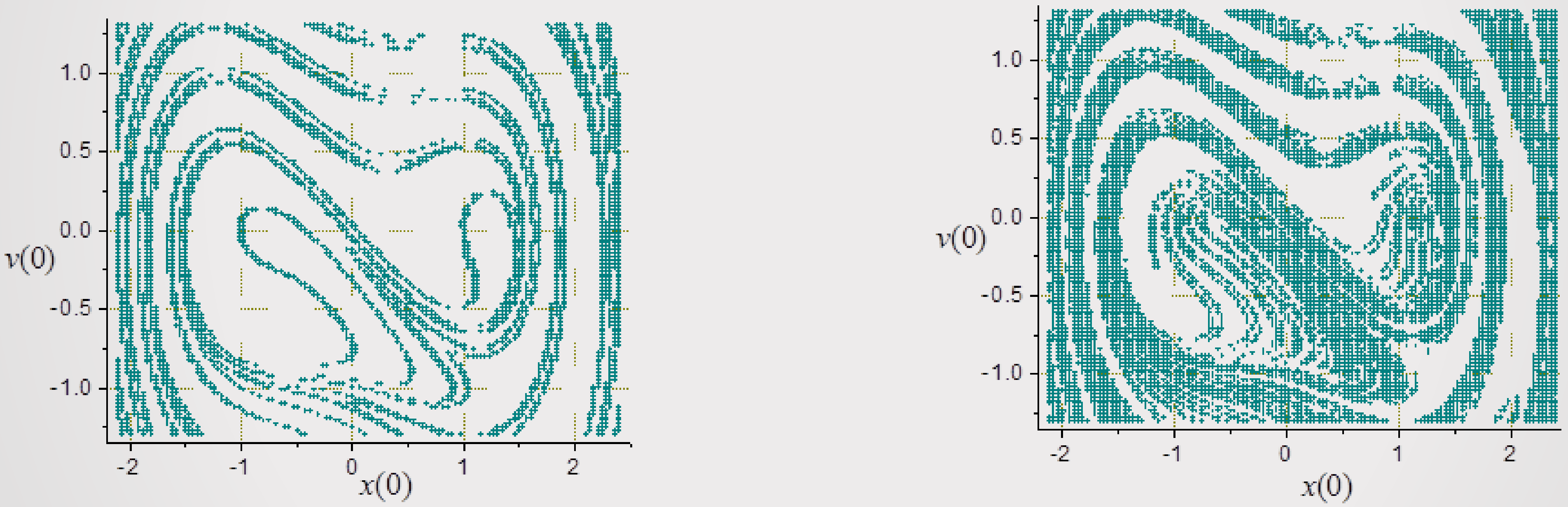

The domains of chaotic vibrations for the Lorenz equations

$$\begin{cases} \dot{x} = \sigma(y - x), \\ \dot{y} = \rho x - y - xz, \\ \dot{z} = xy - \beta z \end{cases}$$

in the (β, ρ) plane (σ=10, $x(0)$=5, $y(0)$=5, $z(0)$=10).

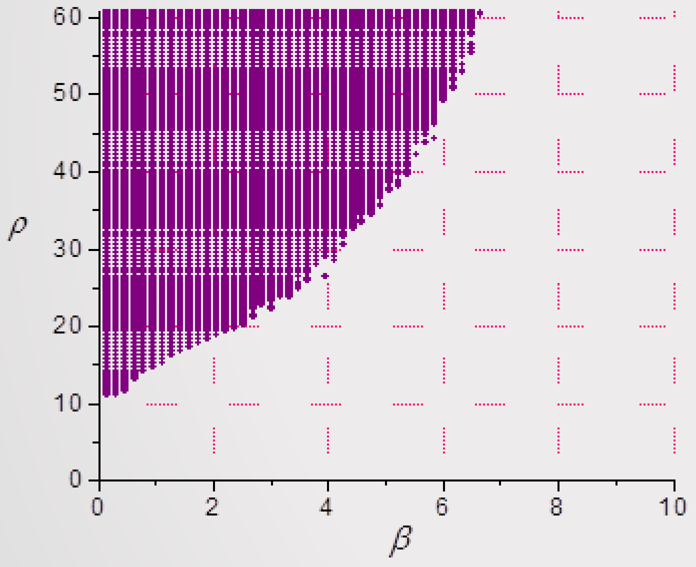

The phase space of the initial conditions (σ=10, β=8/3, ρ=16).

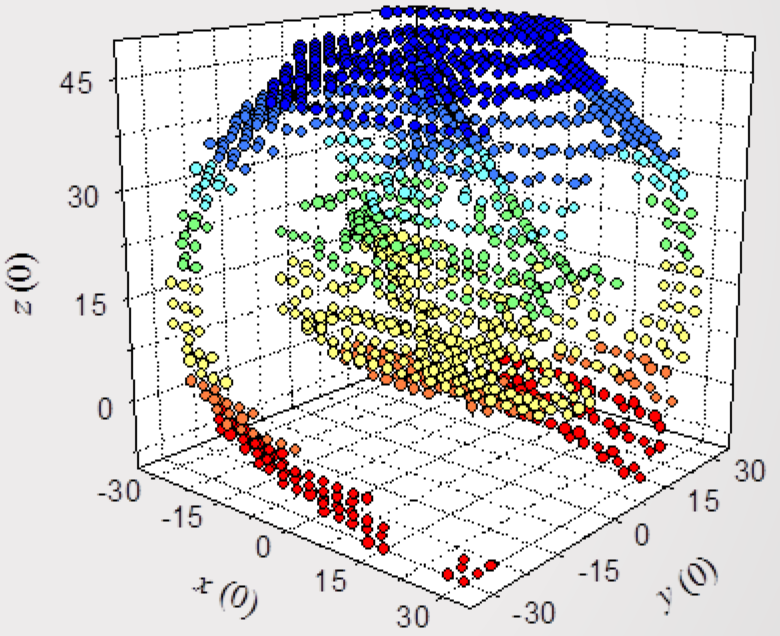

Domains of chaotic behavior for the three-well potential system

$$\ddot{x} + \gamma \dot{x} + x\left(x^2 - x_0^2\right)\left(x^2 - 1\right) = f \cos \omega t$$

in the (ω, f) plane (γ=0.1, $x(0)$=0.5, $\dot{x}(0)$=0.1).

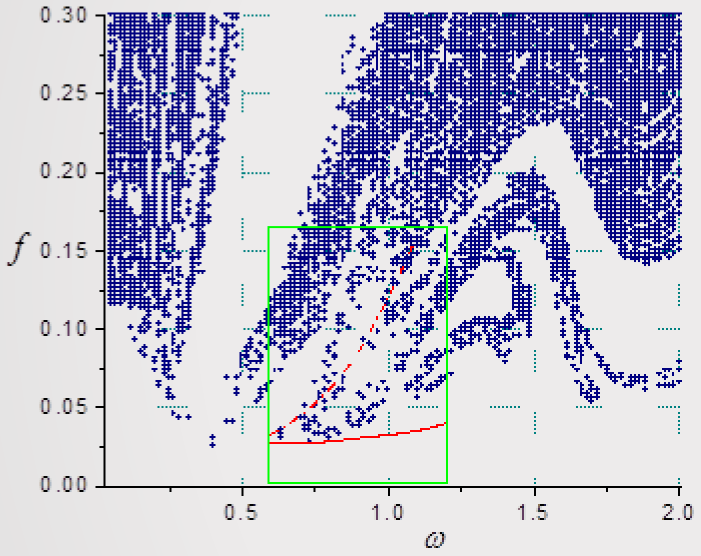

in the (γ, f) plane (ω=0.73, $x(0)$=0.5, $\dot{x}(0)$=0.1).

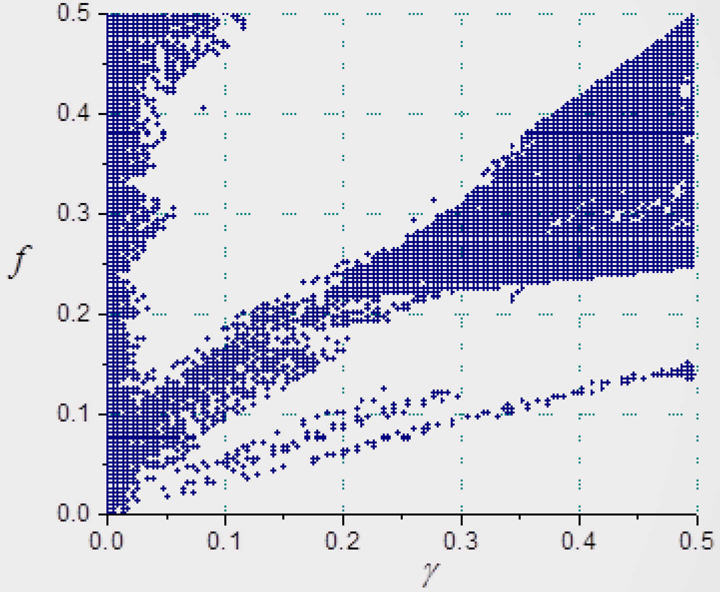

The part of (ω, f) plane investigated by Li and Moon [1990] is in rectangle bounded by lines (ω=0.6, ω=1.2, f=0, f=0.16). Solid line in this rectangle corresponds to the homoclinic bifurcation curve and dash line corresponds to the heteroclinic bifurcation curve. Li and Moon calculated also 100×100 Lyapunov exponents in this part of (ω, f) plane.

The phase plane of the initial conditions for the three-well potential system for the different values of the amplitude of excitation (γ=0.1, ω=0.714):

(a) f=0.04; (b) f=0.07.

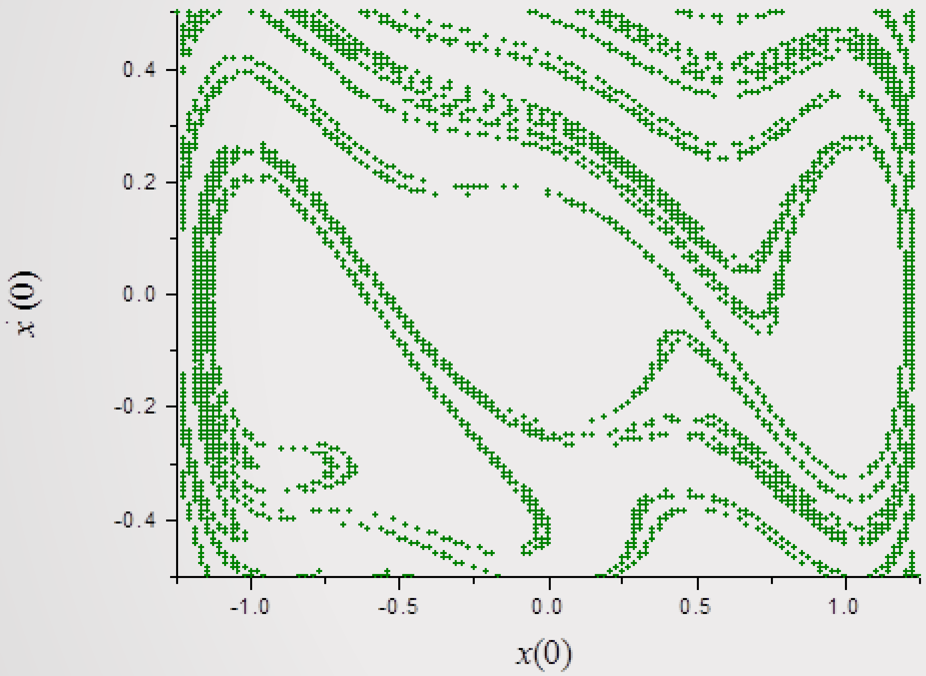

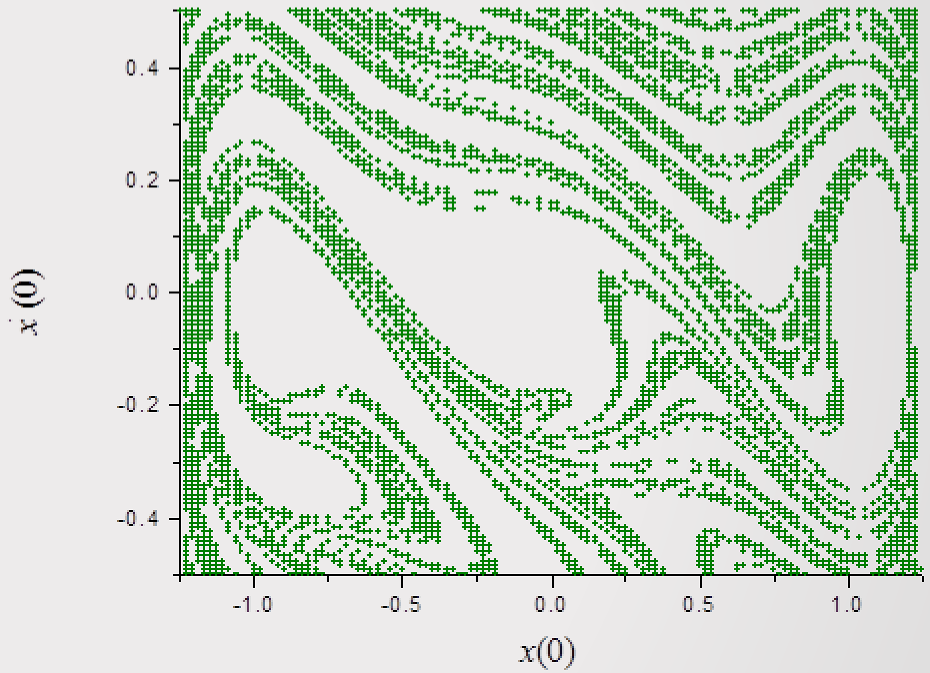

The one-degree-of-freedom mechanical system with stick-slip oscillations.

$$\ddot{x} - ax + bx^3 = \varepsilon[\gamma\cos\omega t - T(\dot{x} - v_*)]$$

$$T(\dot{x} - v_*) = T_0 \,\mathrm{sign}\,(\dot{x} - v_*) - \alpha(\dot{x} - v_*) + \beta(\dot{x} - v_*)^3$$

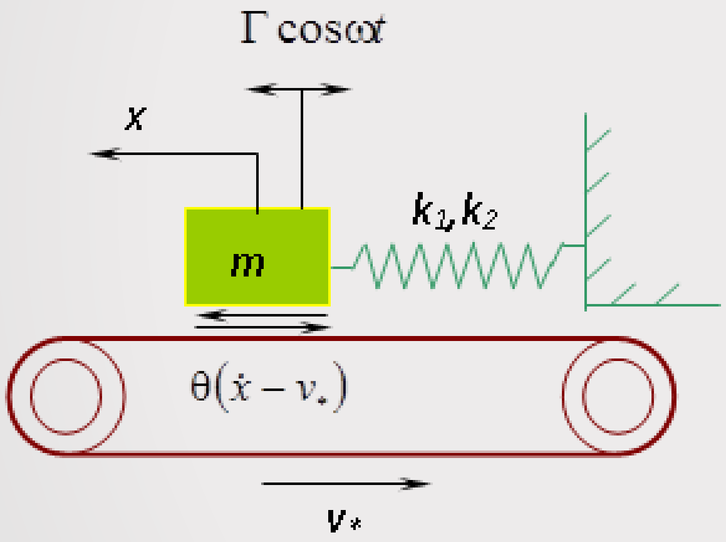

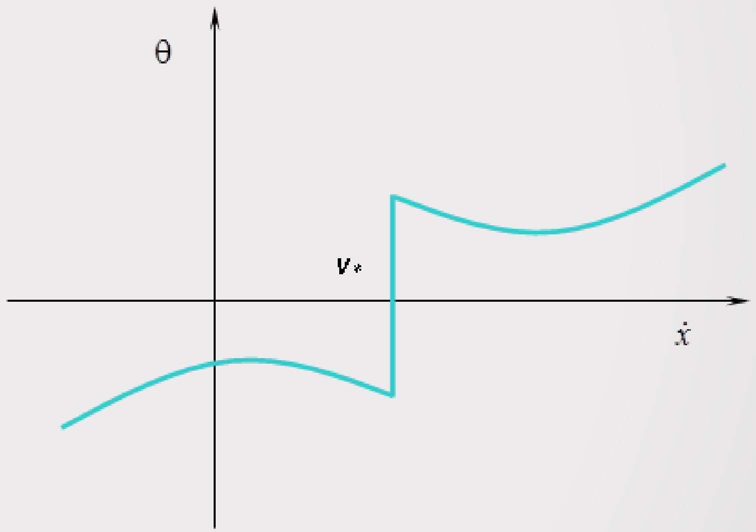

Domains of stick-slip chaos in the (v_*, γ) plane
($a = b = 1$, $\alpha = \beta = T_0 = 0.3$, $\omega = 2$, $x(0) = 1$, $v(0) = 0.4$).
The smooth chaotic threshold is obtained using Melnikov's technique.

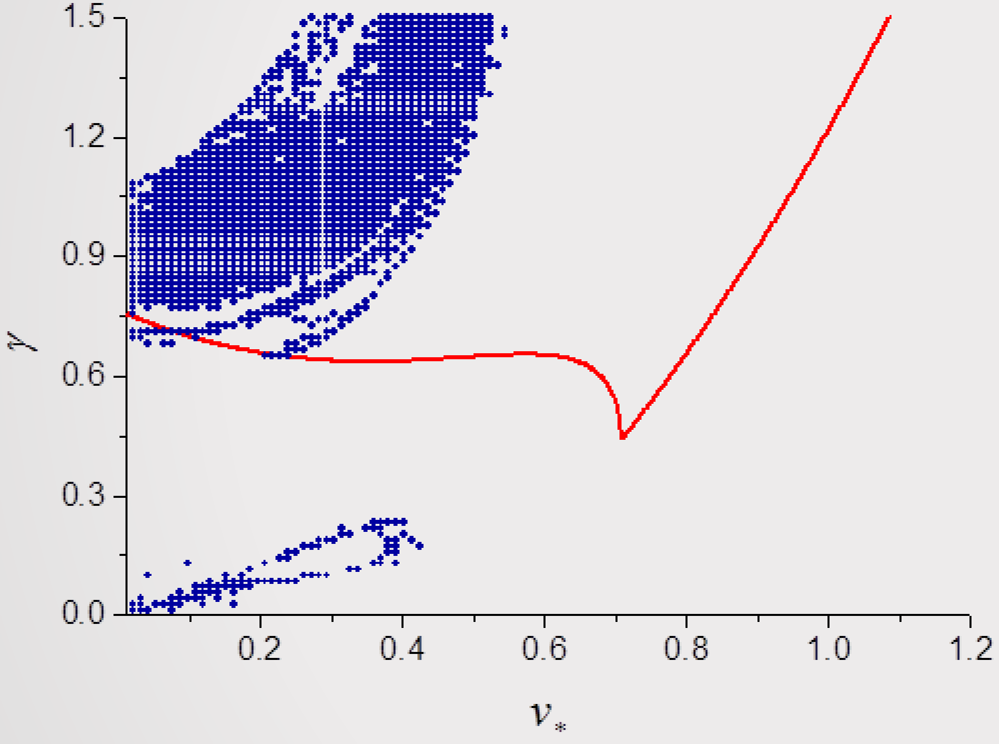

$$\pi\gamma\omega\,\mathrm{sech}\left(\frac{\pi\omega}{2}\right) > \frac{16}{35}\beta\frac{a^4}{b\sqrt{2ab}} - \frac{4}{3}\left(\alpha - 3\beta v_*^2\right)\frac{a^2}{\sqrt{2ab}} +$$

$$+\begin{cases} 2T_0 a\left[\sqrt{\dfrac{1}{2}+\sqrt{\dfrac{1}{4}-\dfrac{b}{2a^2}v_*^2}} - \sqrt{\dfrac{1}{2}-\sqrt{\dfrac{1}{4}-\dfrac{b}{2a^2}v_*^2}}\right] & \text{for } v_* < \dfrac{a}{\sqrt{2b}} \\ 0 & \text{for } v_* \geq \dfrac{a}{\sqrt{2b}} \end{cases}$$

Phase portraits and Poincaré maps of chaotic trajectories of the oscillator at $v^*=0.14$, $\gamma=0.98$

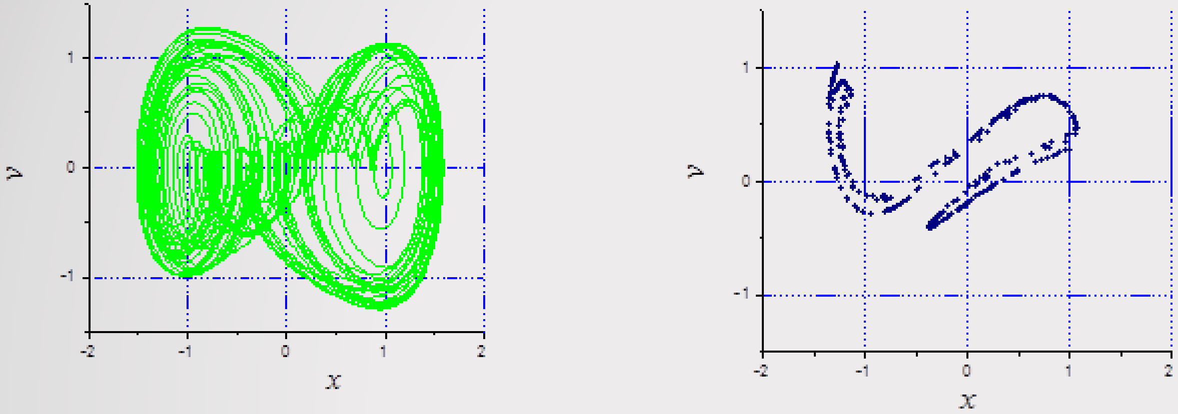

Phase portraits and Poincaré maps of trajectories of the oscillator at $v_*=0.1626$, $\gamma=0.0845$

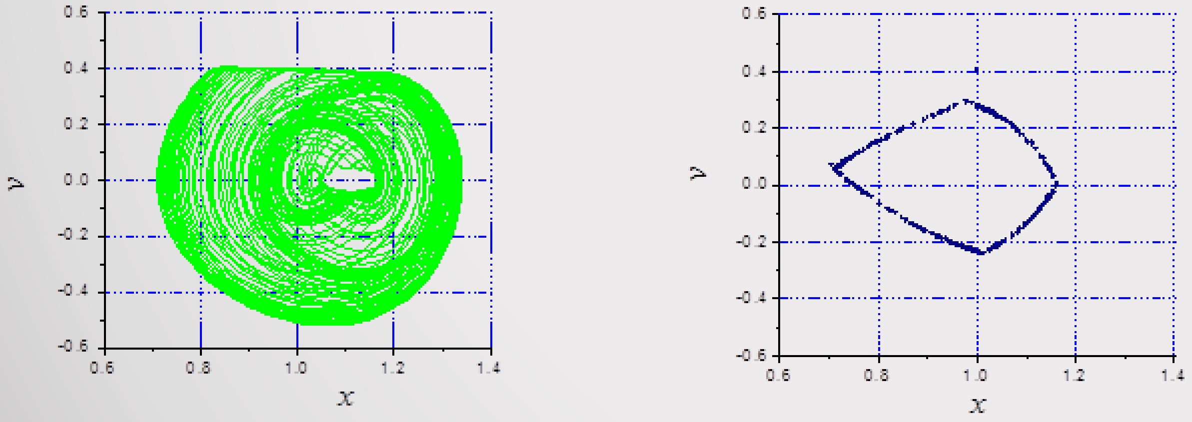

Phase portraits and Poincaré maps of periodic trajectories of the oscillator at $v_*=0.7$, $\gamma=1.0$

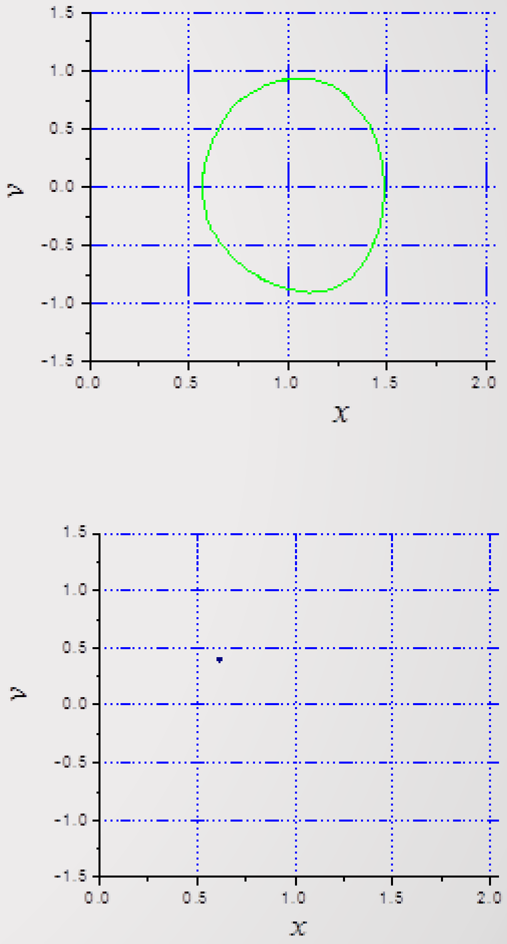

Regular and chaotic behavior exhibited by coupled oscillators with friction

Analyzed 2-DOF model with friction.

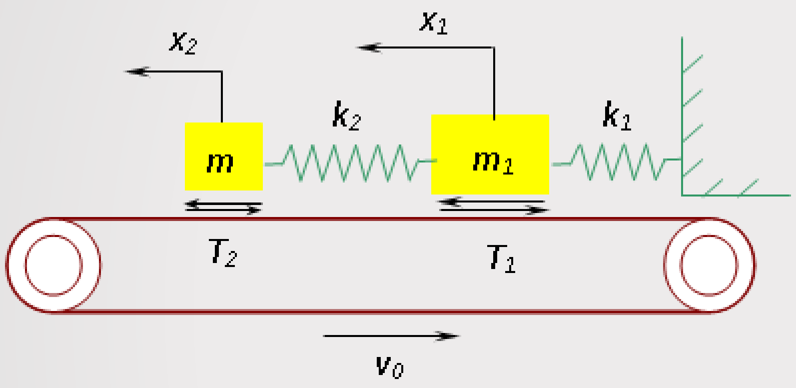

$$\begin{cases} m_1\ddot{x}_1 = -k_1x_1 - k_2x_1 + k_2x_2 + T_1(w_1) \\ m_2\ddot{x}_2 = -k_2x_2 + k_2x_1 + T_2(w_2), \end{cases}$$

$w_i = v_0 - \dot{x}_i$ (*i*=1, 2)

Dry and viscous friction model.

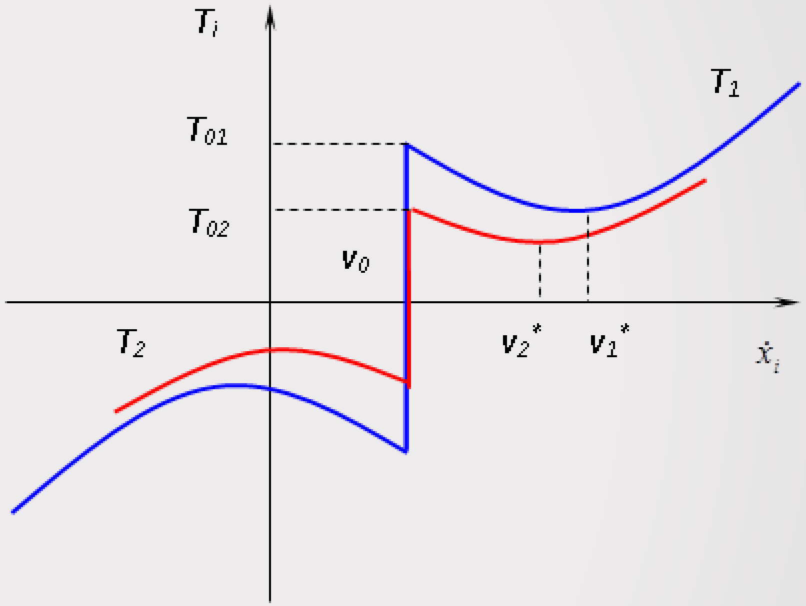

$$T_i(w_i) = T_{0i}\,sign\ w_i - \alpha_i(T_{0i})w_i + \beta_i(T_{0i})w_i^3$$

$$\alpha_i = \frac{3}{4}\frac{T_{0i}}{v_i^*} \qquad \beta_i = \frac{T_{0i}}{4(v_i^*)^3}$$

Domains of chaotic (black) and stick-slip (gray) motion of the first (a), (b) and the second (c), (d) oscillator in sections of space (v_0, T_{01}, T_{02}): (a), (c) T_{02}=5, (b), (d) T_{01}=15.

a)

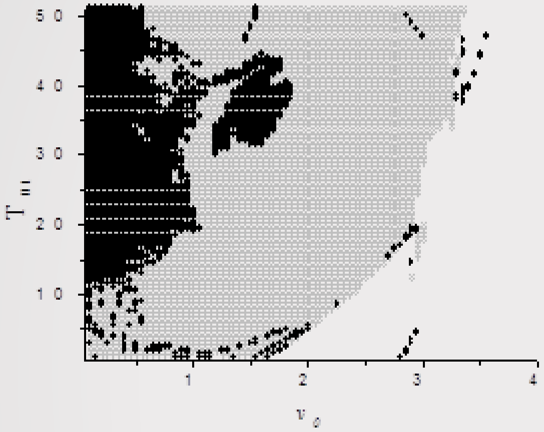

c)

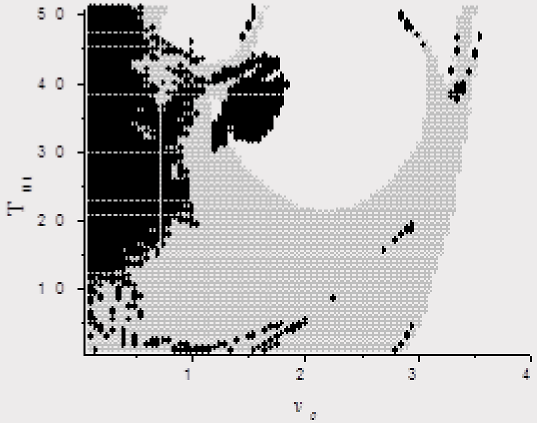

b)

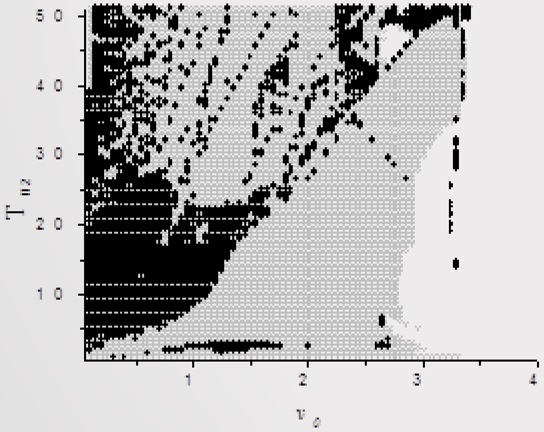

d)

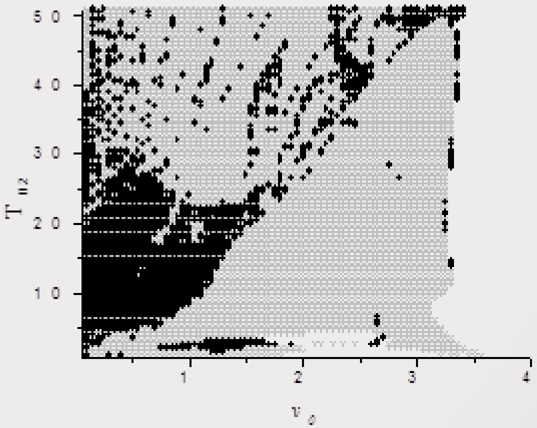

Phase portraits and Poincaré maps of chaotic trajectories of the first and the second oscillator for v_0=0.55, T_{01}=23.5, T_{02}=5.

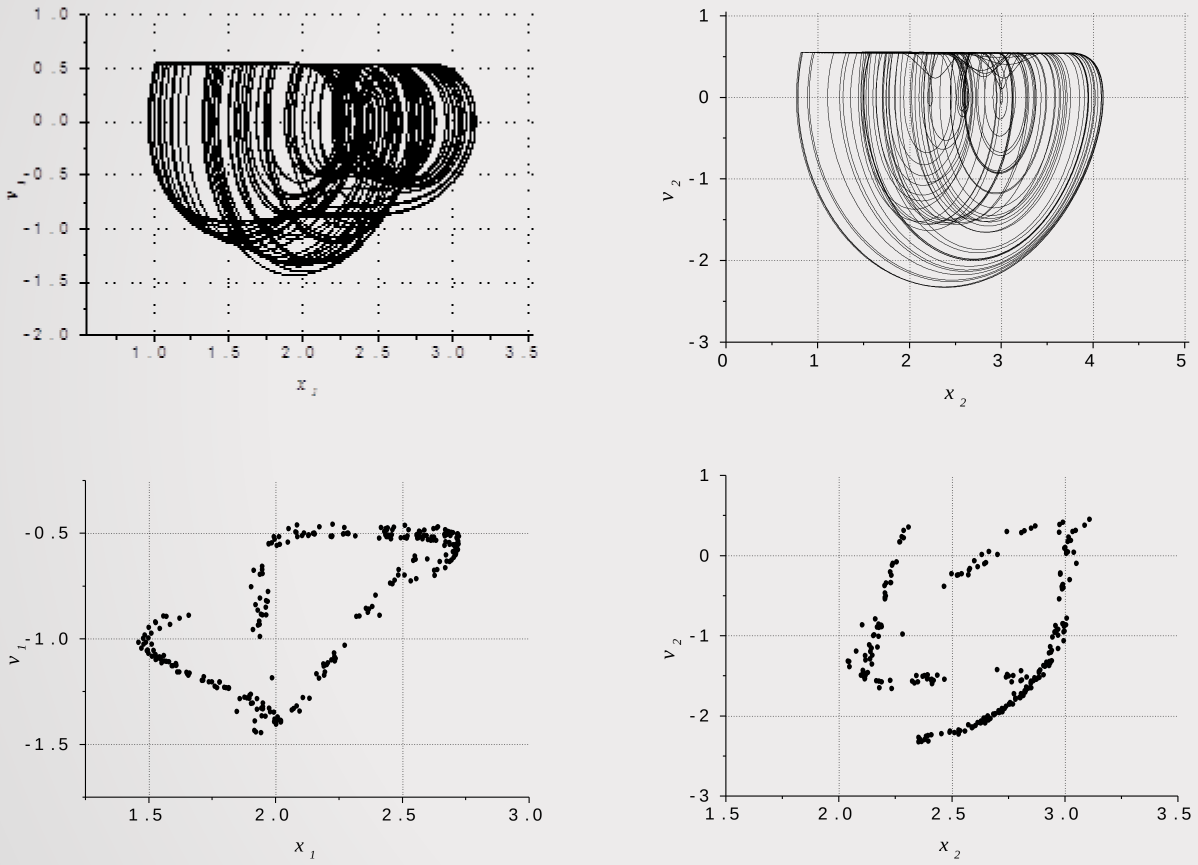

Phase portraits of regular trajectories v_0=2.72, T_{01}=15, T_{02}=46.58.

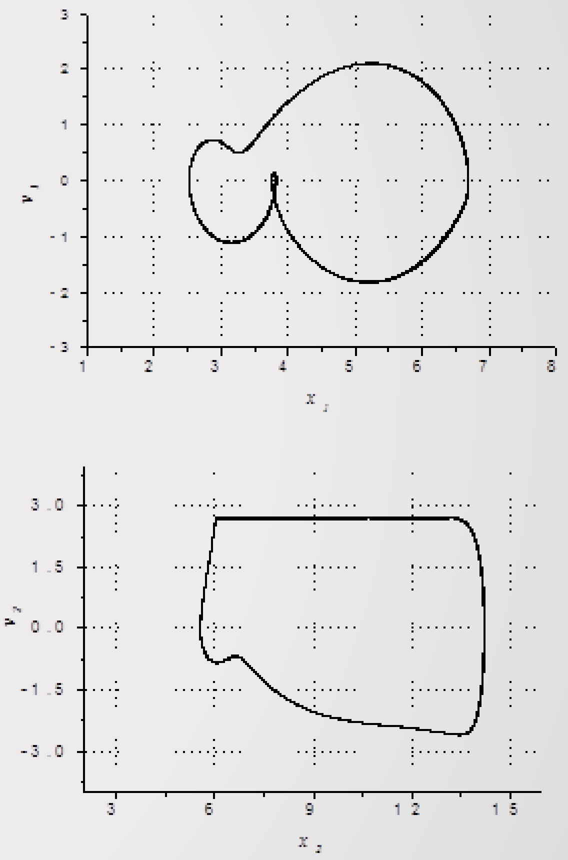

Autonomous coupled hysteretic oscillators under sliding friction.

Coupled Masing hysteretic oscillators under sliding friction

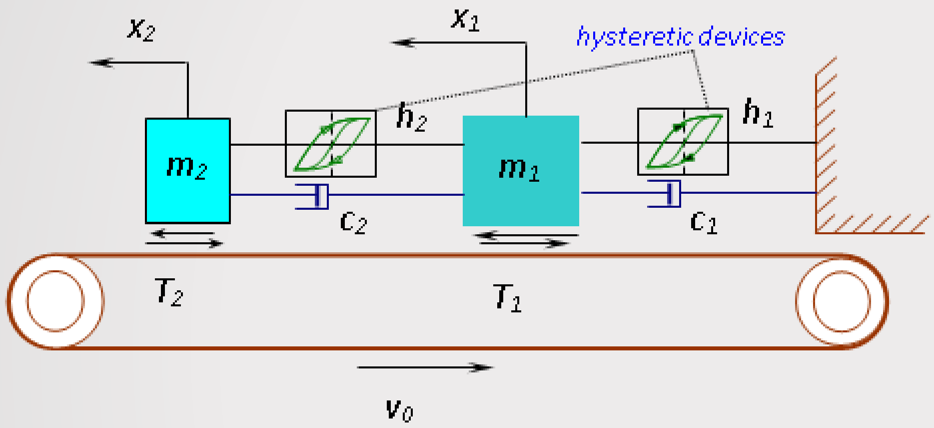

$$\begin{cases} \ddot{x}_1 + \xi_1(\dot{x}_1 - \dot{x}_2) + \xi_2\dot{x}_1 + \eta[(1-\alpha)(2g(x_1) - g(x_2)) + \alpha(2z_1 - z_2)] = \Theta_1(v_0 - \dot{x}_1), \\ \ddot{x}_2 + \mu[\xi_2(\dot{x}_2 - \dot{x}_1) + \eta((1-\alpha)(g(x_2) - g(x_1)) + \alpha(z_2 - z_1))] = \Theta_2(v_0 - \dot{x}_2), \\ \dot{z}_i = g'\left(\dfrac{z_i - z_{ji}}{2}\right)\dot{x}_i, \quad i = 1,2 \end{cases}$$

$$g(x) = \frac{(1-\delta)x}{\left(1+|x|^n\right)^{\frac{1}{n}}} + \delta x$$

Friction model

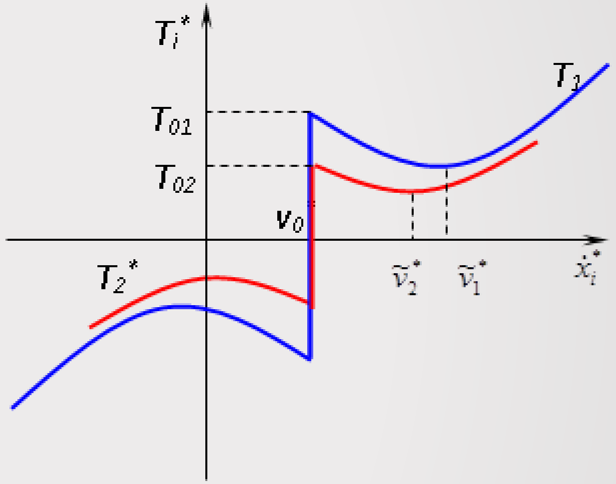

$$\Theta_i(v_0 - \dot{x}_i) = T_{0i}\,sgn\,(v_0 - \dot{x}_i) - \alpha_i(T_{0i})(v_0 - \dot{x}_i) + \beta_i(T_{0i})(v_0 - \dot{x}_i)^3$$

$$\alpha_i = \frac{3}{4}\frac{T_{0i}}{\tilde{v}_i} \qquad \beta_i = \frac{T_{0i}}{4(\tilde{v}_i)^3}$$

Evolution of the stick-slip chaos regions for the coupled Masing hysteretic oscillators in the parametric plane (v_0, T_{01}) on the increase of the hysteretic dissipation α=0.2; α=0.5; α=0.8

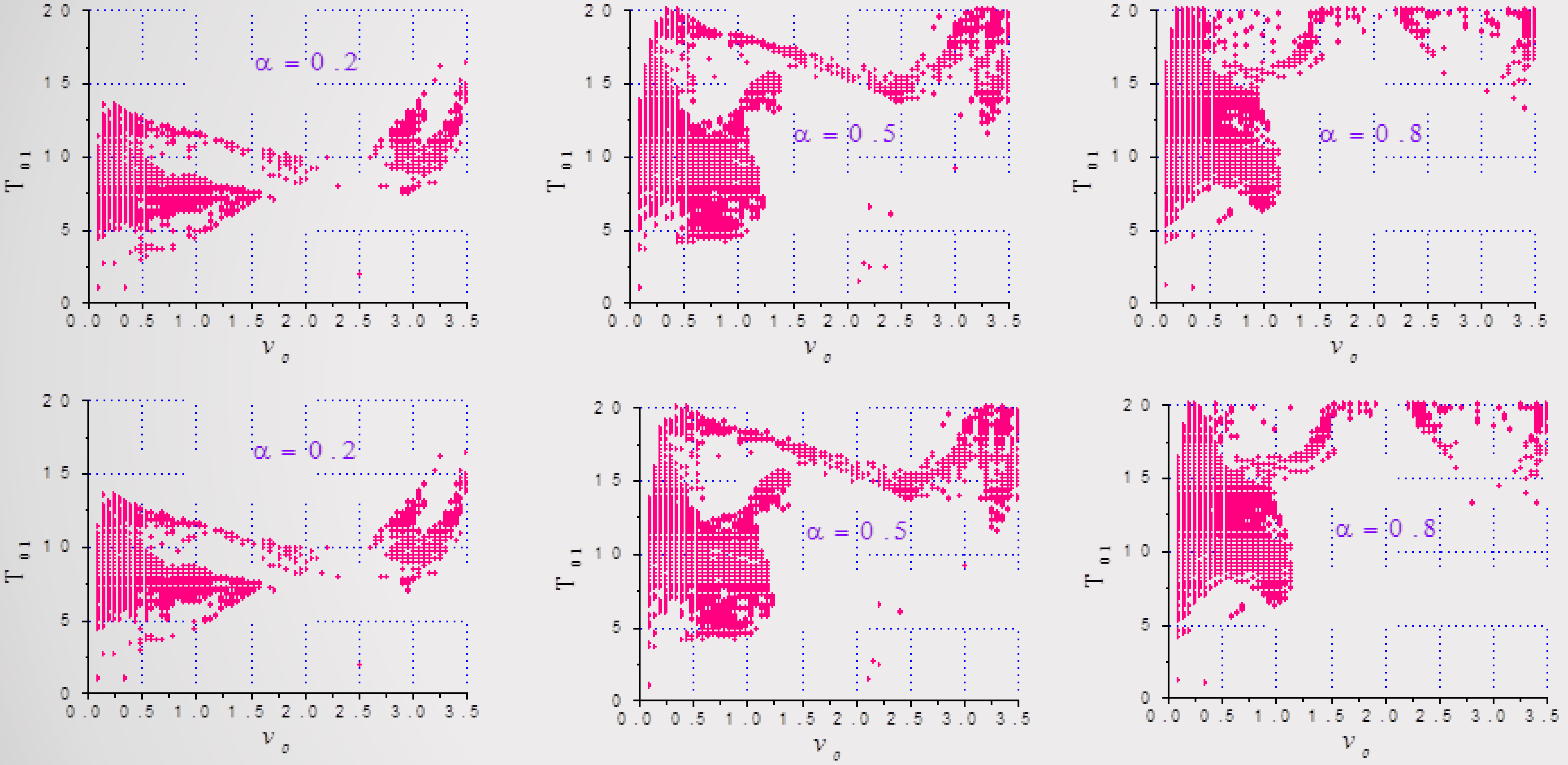

the first Masing oscillator

the second Masing oscillator

Parameters of the system T_{02}=3, ξ_1=0.001, ξ_2=0.0005, η=6, μ=2, $\tilde{v}_1 = 4$, $\tilde{v}_2 = 3$, δ=0.05, n=10.0 are fixed

Phase planes and hysteretic loops of both Masing hysteretic oscillators

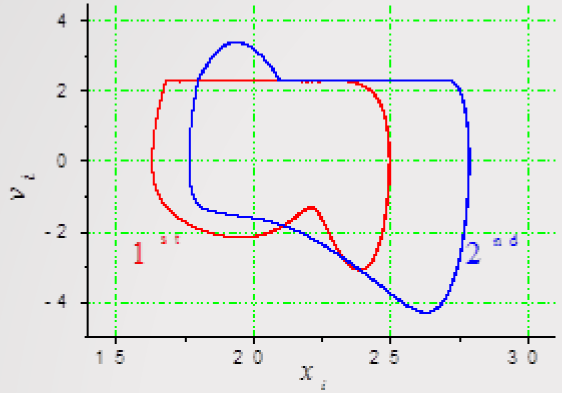

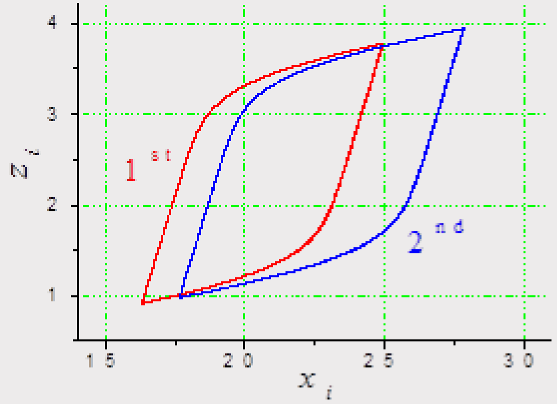

at v_0=2.3, T_{01}=17, T_{02}=3, α=0.5

The parameters correspond to periodic motion of the oscillators in accordance with the regions obtained

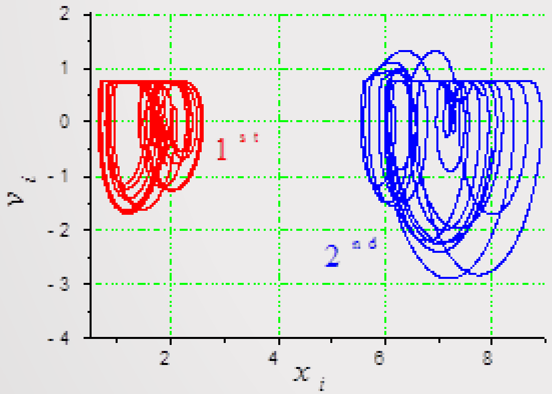

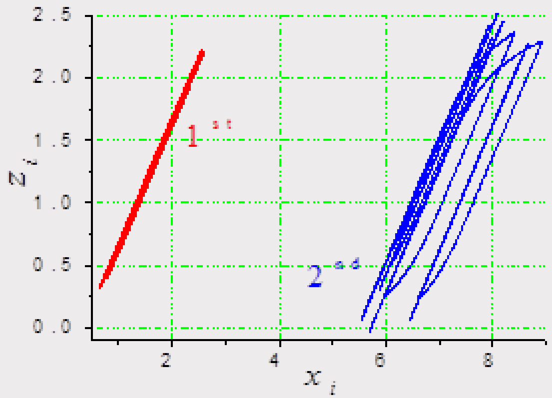

at v_0=0.75, T_{01}=8, T_{02}=3, α=0.5

The parameters correspond to chaotic behavior of the oscillators in accordance with the regions obtained

Evolution of the stick-slip chaos regions for the coupled Masing hysteretic oscillators in the parametric plane (v_0, T_{02}) on the increase of the hysteretic dissipation α=0.2; α=0.5; α=0.8

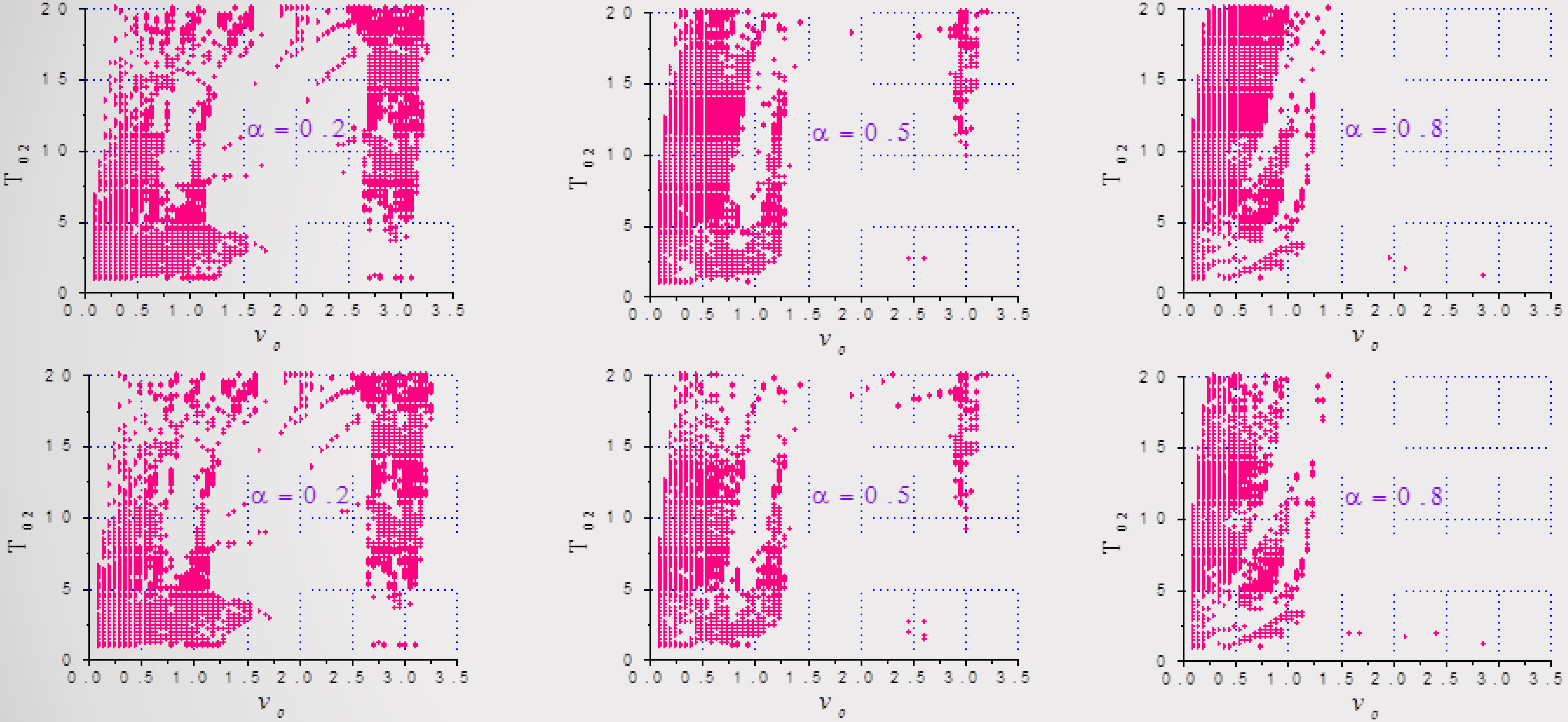

the first Masing oscillator

the second Masing oscillator

parameters of the system T_{01}=7, ξ_1=0.001, ξ_2=0.0005, η=6, μ=2, $\tilde{v}_1 = 4$, $\tilde{v}_2 = 3$, δ=0.05, n=10.0 are fixed

Phase planes and hysteretic loops of both Masing hysteretic oscillators

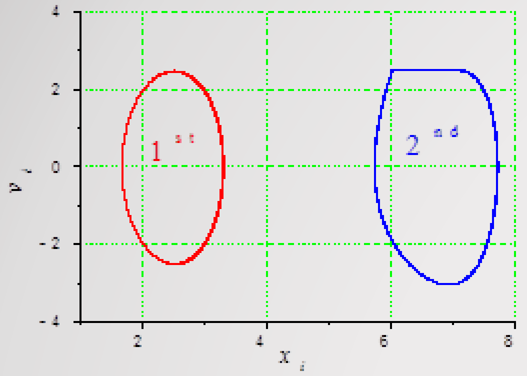

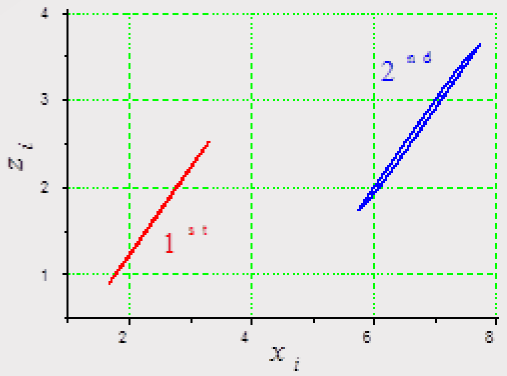

at v_0=2.5, T_{01}=7, T_{02}=10, α=0.5

The parameters correspond
to periodic motion of the oscillators

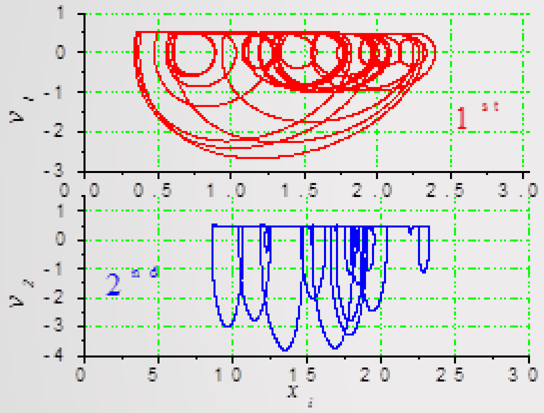

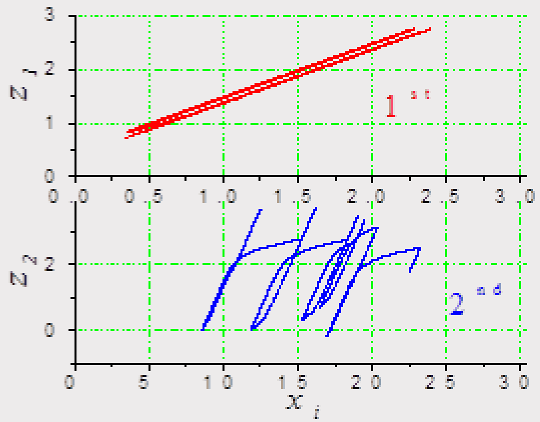

at v_0=0.5, T_{01}=7, T_{02}=10, α=0.5

The parameters correspond
to chaotic behavior of the oscillators

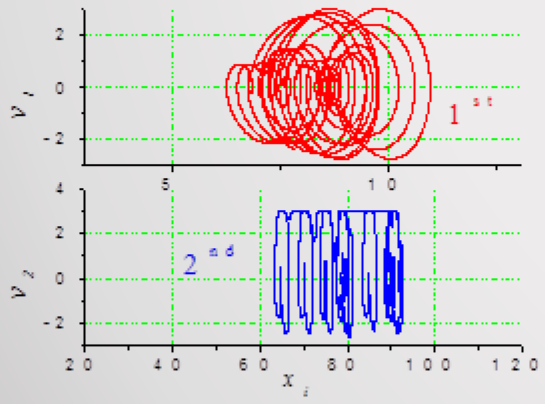

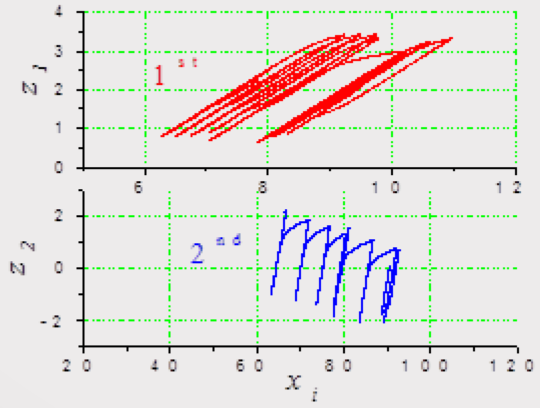

at v_0=3, T_{01}=7, T_{02}=15, α=0.5

The parameters correspond
to chaotic behavior of the oscillators

in accordance with the regions obtained

Autonomous coupled hysteretic oscillators under sliding friction.

Coupled Bouc-Wen hysteretic oscillators under sliding friction

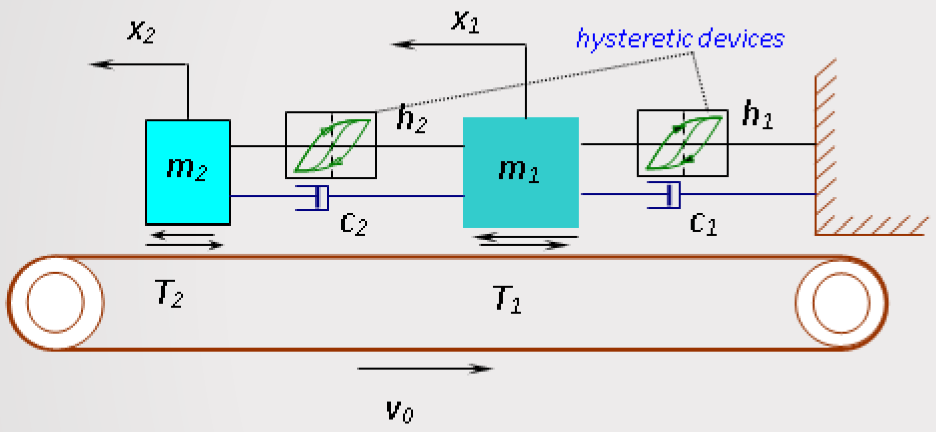

$$\begin{cases} \ddot{x}_1 + \xi_1(\dot{x}_1 - \dot{x}_2) + \xi_2\dot{x}_1 + \delta(2x_1 - x_2) + (1-\delta)(2z_1 - z_2) = \Theta_1(v_0 - \dot{x}_1), \\ \ddot{x}_2 + \mu\left[\xi_2(\dot{x}_2 - \dot{x}_1) + \delta(x_2 - x_1) + (1-\delta)(z_2 - z_1)\right] = \Theta_2(v_0 - \dot{x}_2), \\ \dot{z}_i = \left[k_z - (\gamma + \beta\, sgn(\dot{x}_i)\, sgn(z_i))|z_i|^n\right]\dot{x}_i, \quad i = 1,2 \end{cases}$$

Friction model

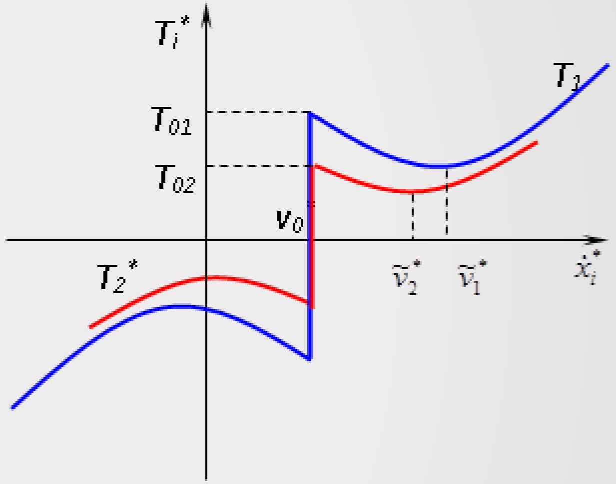

$$\Theta_i(v_0 - \dot{x}_i) = T_{0i}\, sgn\,(v_0 - \dot{x}_i) - \alpha_i(T_{0i})(v_0 - \dot{x}_i) + \beta_i(T_{0i})(v_0 - \dot{x}_i)^3$$

$$\alpha_i = \frac{3}{4}\frac{T_{0i}}{\tilde{v}_i} \qquad \beta_i = \frac{T_{0i}}{4(\tilde{v}_i)^3}$$

Evolution of the stick-slip chaos regions for the coupled Bouc-Wen hysteretic oscillators in the parametric plane (v_0, T_{01}) on the increase of the hysteretic dissipation δ=0.8; δ=0.5; δ=0.2

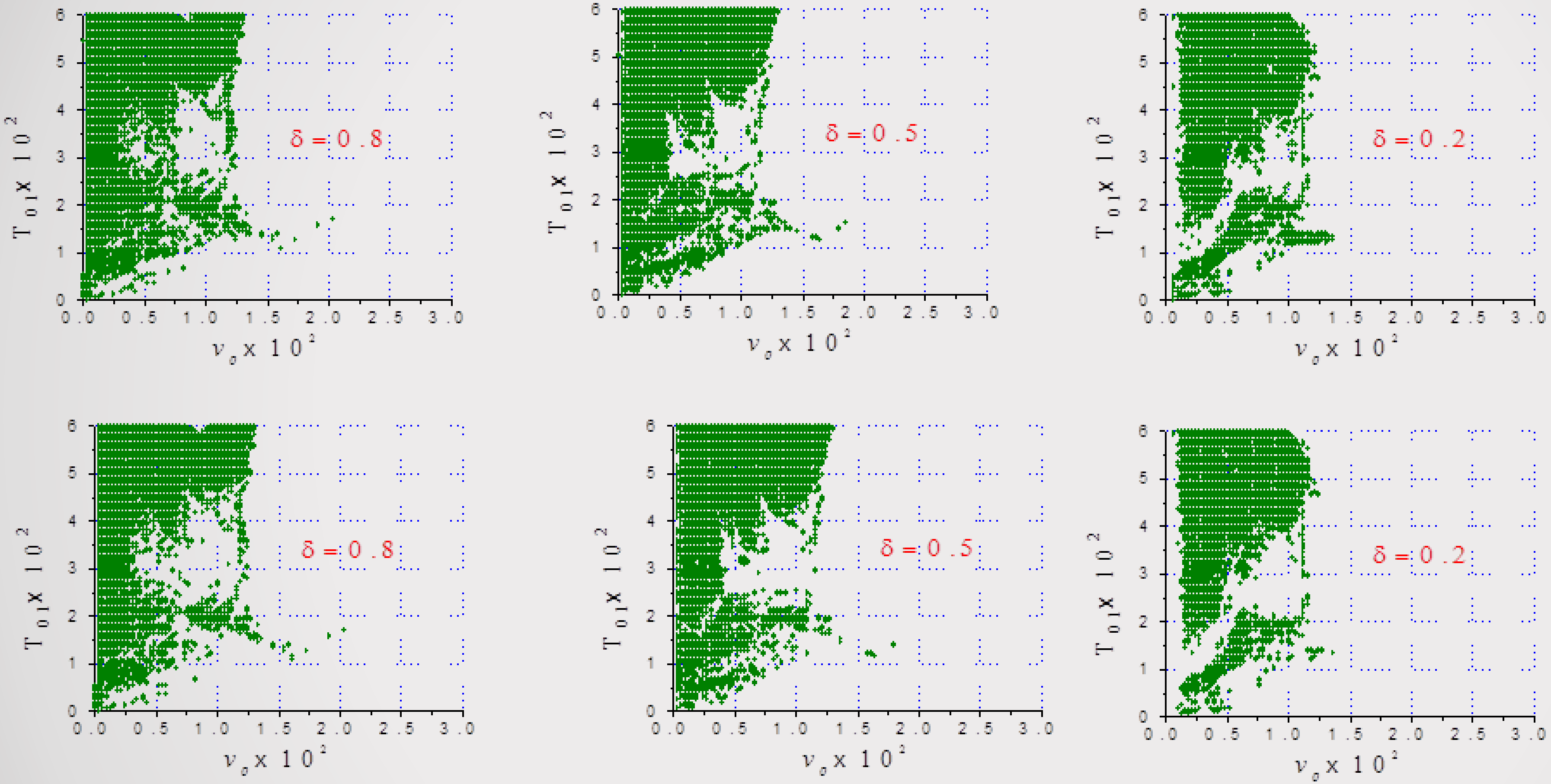

the first Bouc-Wen oscillator

the second Bouc-Wen oscillator

Parameters of the system T_{02}=0.02, ξ_1=0.002, ξ_2=0.001, μ=1.5, $\tilde{v}_1 = 0.04$, $\tilde{v}_2 = 0.03$, k_z=0.5, γ=0.3, β=5, n=1.0 are fixed

Evolution of the stick-slip chaos regions for the coupled Bouc-Wen hysteretic oscillators in the parametric plane (v_0, T_{02}) on the increase of the hysteretic dissipation δ=0.8; δ=0.5; δ=0.2

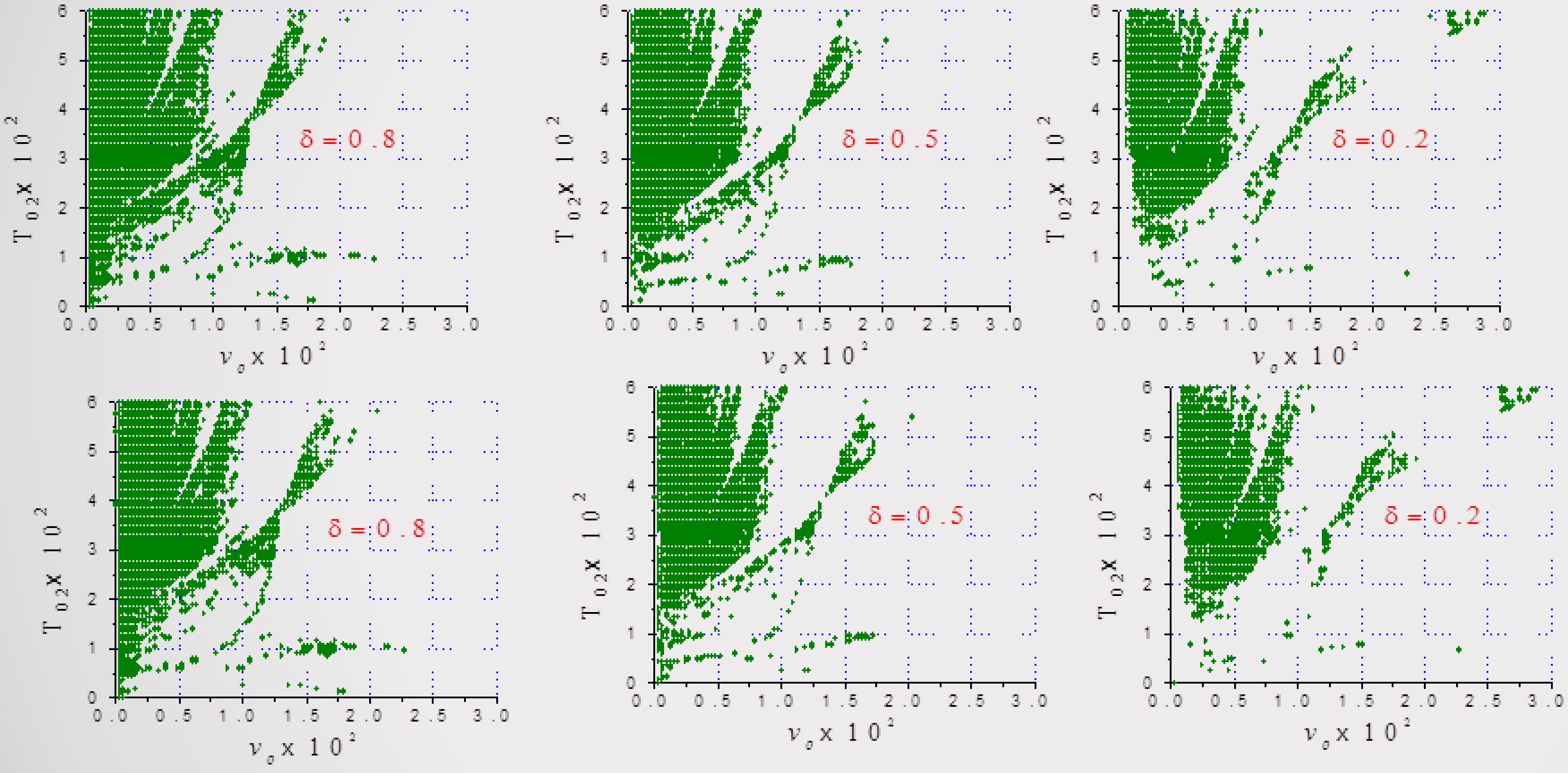

the first
Bouc-Wen oscillator

the second
Bouc-Wen oscillator

Parameters of the system T_{01}=0.025, ξ_1=0.002, ξ_2=0.001, μ=1.5, $\tilde{v}_1 = 0.04$, $\tilde{v}_2 = 0.03$, k_z=0.5, γ=0.3, β=5, n=1 are fixed

Phase planes and hysteretic loops of both Bouc-Wen hysteretic oscillators

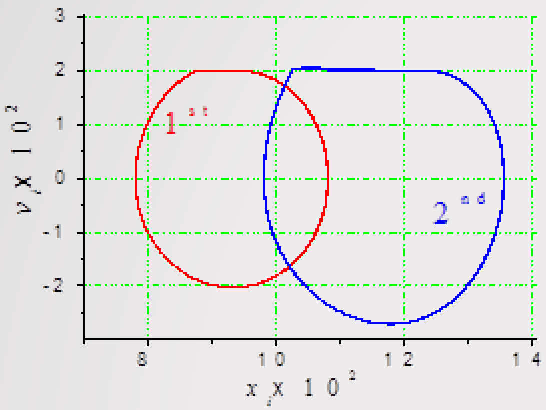

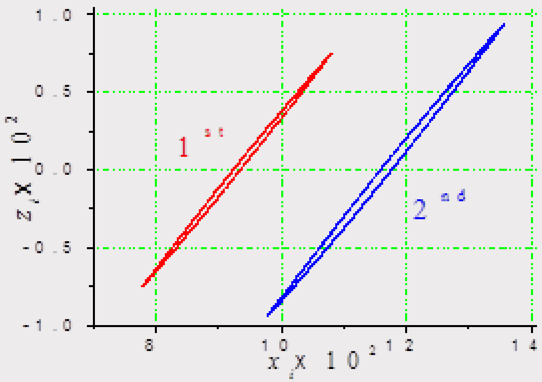

at v_0=0.02, T_{01}=0.02, T_{02}=0.02, δ=0.2

The parameters correspond to periodic motion of the oscillators
in accordance with the regions obtained

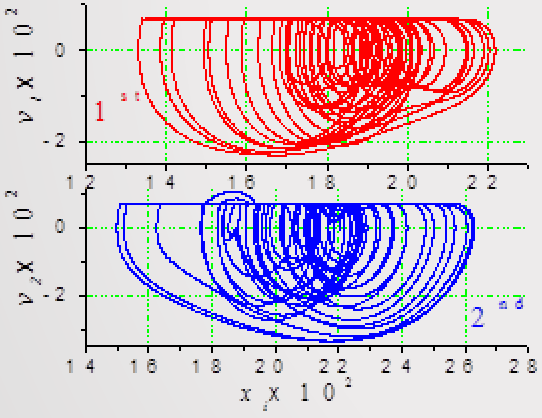

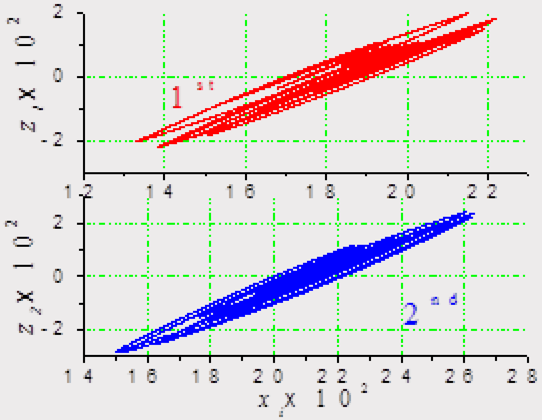

at v_0=0.007, T_{01}=0.045, T_{02}=0.02, δ=0.2

The parameters correspond to chaotic behavior of the oscillators
in accordance with the regions obtained

Autonomous coupled hysteretic oscillators under sliding friction.

Coupled hybrid hysteretic oscillators under sliding friction

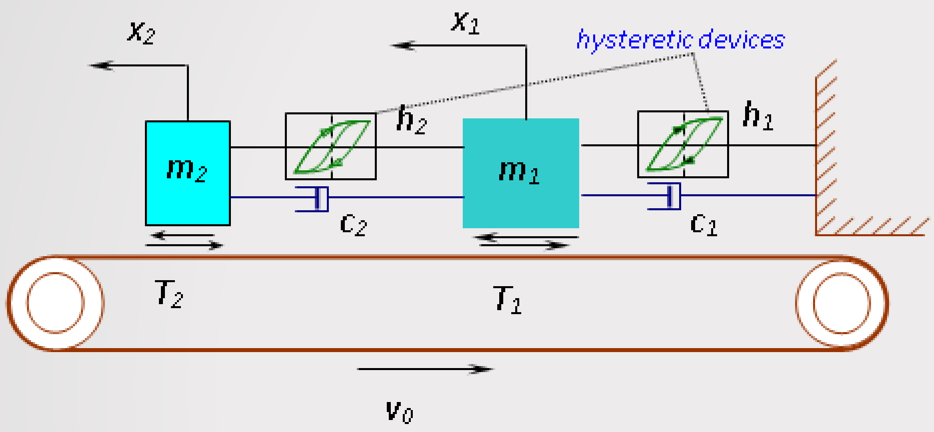

Friction model

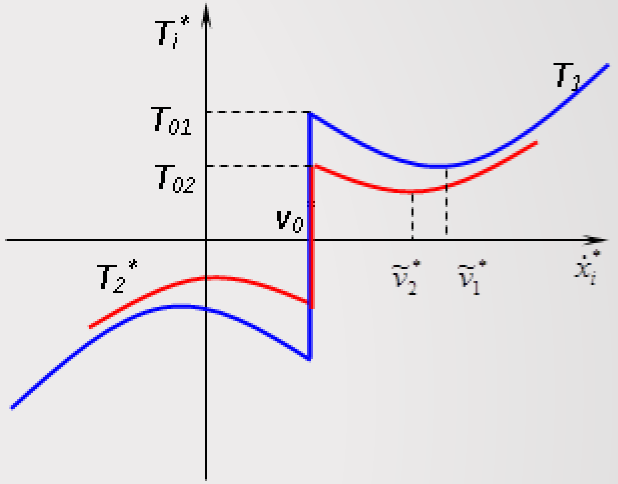

$$\begin{cases} \ddot{x}_1 + \xi_1(\dot{x}_1 - \dot{x}_2) + \xi_2\dot{x}_1 + (1-\alpha)(g(x_1) - g(x_2)) + \alpha(z_{1,M} - z_{2,M}) + \delta x_1 + (1-\delta)z_{1,BW} = \Theta_1(v_0 - \dot{x}_1), \\ \ddot{x}_2 + \mu\left[\xi_2(\dot{x}_2 - \dot{x}_1) + \delta(x_2 - x_1) + (1-\delta)(z_{2,BW} - z_{1,BW})\right] = \Theta_2(v_0 - \dot{x}_2), \\ \dot{z}_{i,BW} = \left[k_z - (\gamma + \beta\, sgn(\dot{x}_i)\, sgn(z_{i,BW}))\left|z_{i,BW}\right|^n\right]\dot{x}_i, \quad i = 1,2 \\ \dot{z}_{i,M} = g'\left(\dfrac{z_{i,M} - z_{ij,M}}{2}\right)\dot{x}_i, \quad i = 1,2 \end{cases}$$

$$g(x) = \frac{(1-\delta)x}{\left(1+|x|^n\right)^{\frac{1}{n}}} + \delta x$$

$$\Theta_i(v_0 - \dot{x}_i) = T_{0i}\, sgn\,(v_0 - \dot{x}_i) - \alpha_i(T_{0i})(v_0 - \dot{x}_i) + \beta_i(T_{0i})(v_0 - \dot{x}_i)^3$$

$$\alpha_i = \frac{3}{4}\frac{T_{0i}}{\tilde{v}_i} \qquad \beta_i = \frac{T_{0i}}{4(\tilde{v}_i)^3}$$

hysteretic devices h_1 and h_2 in the Masing's and in the Bouc-Wen's forms are

$$h_M^*(x_i, z_{i,M}) = (1-\alpha)g^*(x_i^*) + \alpha z_{i,M}^*$$

$$h_{BW}^*(x_i, z_{i,BW}) = k_1^* x_i^* + \delta_p z_{i,BW}^*$$

Evolution of the stick-slip chaos regions for the coupled hybrid hysteretic oscillators in the parametric plane (v_0, T_{01}) on the increase of the hysteretic dissipation

α=0.2, δ=0.8; α=0.5, δ=0.5; α=0.8, δ=0.2

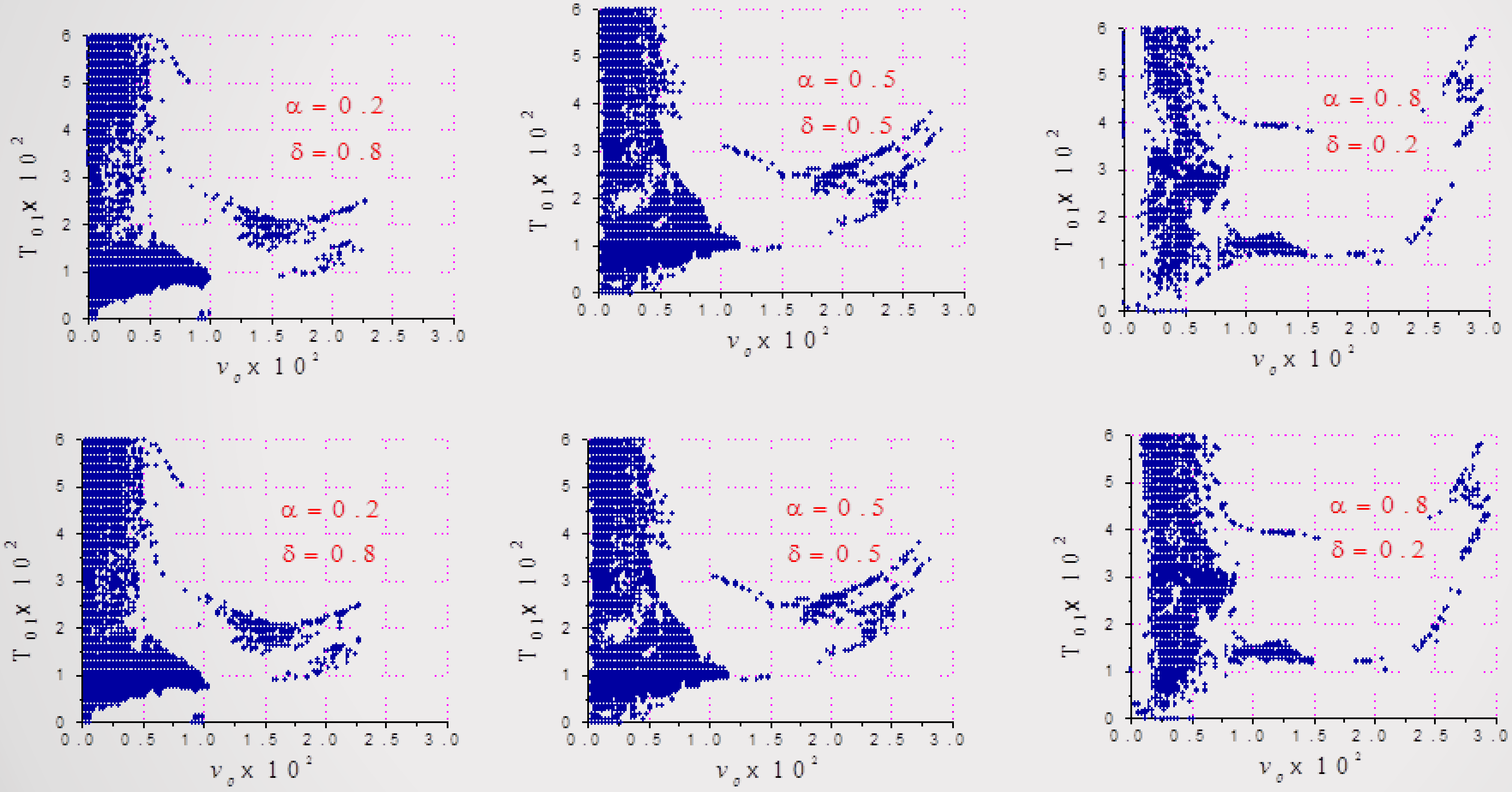

the first hybrid oscillator

the second hybrid oscillator

Parameters of the system T_{02}=0.02, ξ_1=0.002, ξ_2=0.001, μ=1.5, $\tilde{v}_1 = 0.04$, $\tilde{v}_2 = 0.03$, k_z=0.5, γ=0.3, β=5, n=1.0, δ_M=0.05, n_M=0.2 are fixed

Evolution of the stick-slip chaos regions for the coupled hybrid hysteretic oscillators in the parametric plane (v_0, T_{02}) on the increase of the hysteretic dissipation

α=0.2, δ=0.8; α=0.5, δ=0.5; α=0.8, δ=0.2

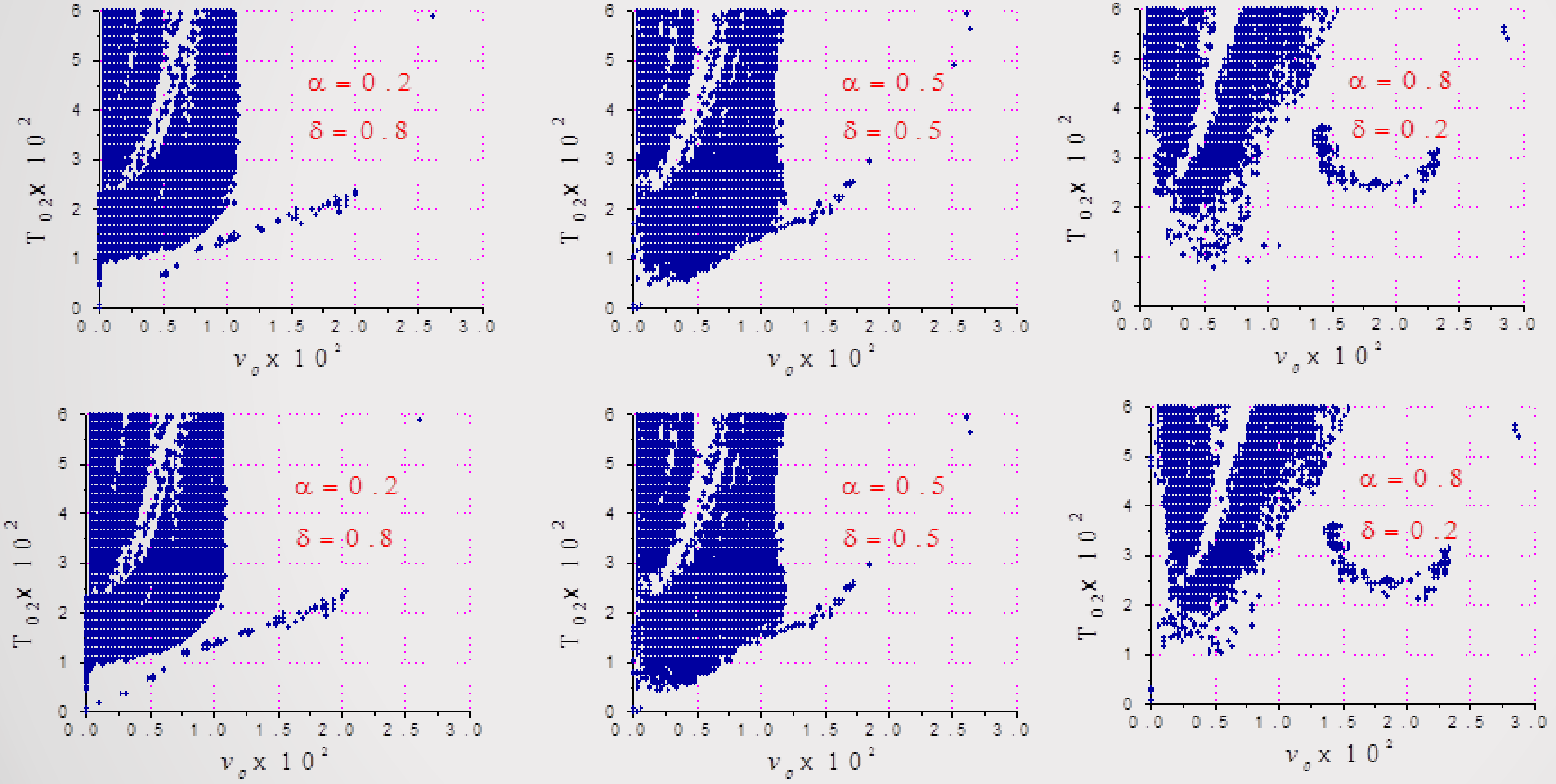

the first hybrid oscillator

the second hybrid oscillator

Parameters of the system T_{01}=0.01, ξ_1=0.002, ξ_2=0.001, μ=1.5, $\tilde{v}_1 = 0.04$, $\tilde{v}_2 = 0.03$, k_z=0.5, γ=0.3, β=5, n=1.0, δ_M=0.05, n_M=0.2 are fixed

Phase planes and hysteretic loops of the hybrid hysteretic oscillators

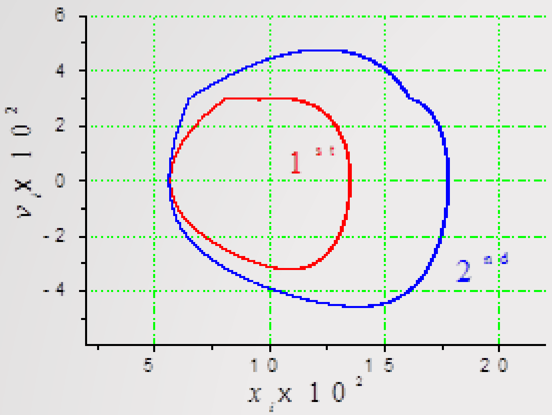

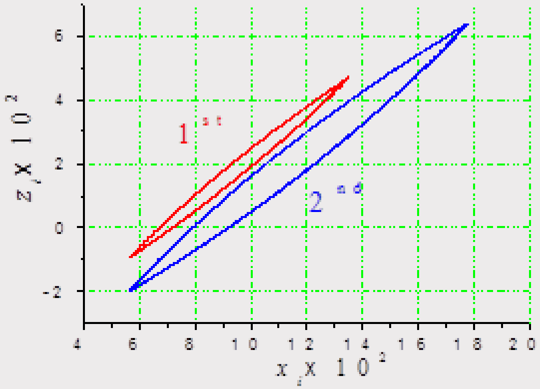

at v_0=0.03, T_{01}=0.06, T_{02}=0.02, α=0.5, δ=0.5

The parameters correspond to periodic motion of the oscillators in accordance with the regions obtained

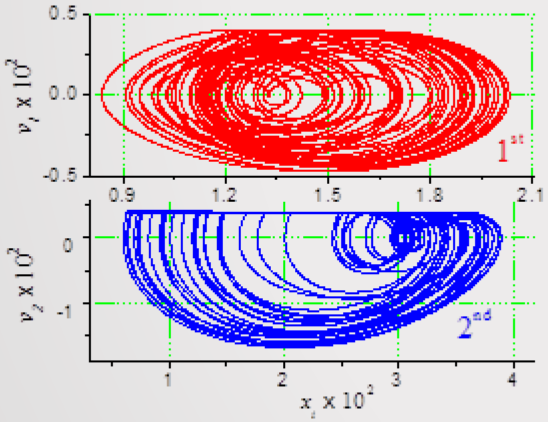

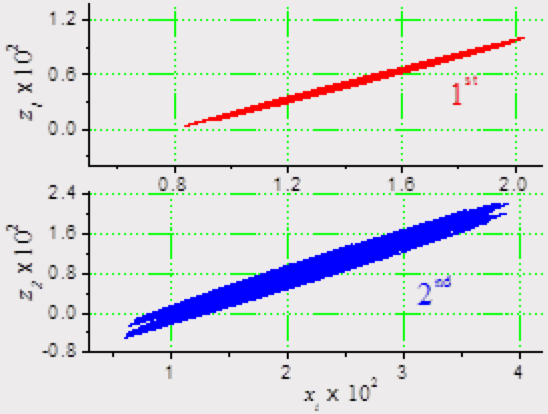

at v_0=0.004, T_{01}=0.01, T_{02}=0.02, α=0.2, δ=0.8

The parameters correspond to chaotic behavior of the oscillators in accordance with the regions obtained

Conclusions III

•A numerical approach for quantifying regular and chaotic dynamics based on the analysis of wandering trajectories is presented. This approach, in contrast to the standard numerical methods (including computations of Lyapunov exponents), is effective, convenient to use, requires much less computational time in comparison with other approaches, and can be applied to the investigation of both “smooth” and “non-smooth” problems. Result’s comparison for the test models with other investigations demonstrates a very good agreement with other groups.

- Chaos in the “smooth” test models
  - Duffing equation. The domains of chaotic behavior agree well with the smooth threshold which corresponds to the homoclinic trajectory criterion [Holmes 1979]. The domains also agree remarkably well with the results of the investigations based on the calculation of the Lyapunov exponents, which was carried out using the Wolf's algorithm [Wolf at al. 1985, Moon 1987]
  - Lorenz system. The results obtained conform well to the investigations and diagrams presented in [Moon, 1987]
  - three-well potential oscillator. The domains of chaotic vibrations obtained are conforming to domains with positive Lyapunov exponents presented by Li and Moon [1990]. Both in the case of two- and three-well potential systems the thresholds, which are corresponding to the homoclinic and heteroclinic bifurcation curves, are undervalued.
- Chaos in the “non-smooth” models
  - Conditions for stick-slip chaotic oscillations in a quasi-autonomous mechanical system with Coulomb and viscous friction have been found. The results obtained show a good agreement between the analytical chaotic threshold constructed by means Melnikov's technique and numerical simulation.
  - Regular and chaotic behavior exhibited by coupled oscillators with friction were quantified.
  - Conditions for chaos occurring in self-excited 2-DOF Masing/Bouc-Wen/hybrid hysteretic systems with friction were found.

References

- [1] J. Awrejcewicz, L. Dzyubak, Stick-slip chaotic oscillations in a quasi-autonomous mechanical system, *International Journal of Nonlinear Sciences and Numerical Simulation*, 4(2), 2003, 155-160.
- [2] J. Awrejcewicz, L. Dzyubak, C. Grebogi, A direct numerical method for quantifying regular and chaotic orbits, *Chaos, Solitons and Fractals* 19, 2004, 503-507.
- [3] J. Awrejcewicz, L. Dzyubak, Stick-slip chaos prediction in self-excited two-dof hysteretic systems with friction, *International Review of Mechanical Engineering*. Vol. 1, n. 1, 2007, pp. 1-17.
- [4] F. Moon, Chaotic Vibrations, Wiley & Sons, New York, 1987.
- [5] Wolf, A., Jack, B., Swinney, H.L., Vastano, J.A., 1985. Determining Lyapunov exponents from a time series. *Physica D* 16, 285–317.

Outline

IV

- **Dynamics of two impacting beams with clearance nonlinearity**

- Governing equations of motion of two Euler-Bernoulli impacting beams
- Impact phase
- Out-of-contact phase
- Switching between phases
- Characterizing beams collisions
- Graphical representation of the analytical solutions obtained
- Conclusions
- References

Dynamics of two impacting beams with clearance nonlinearity

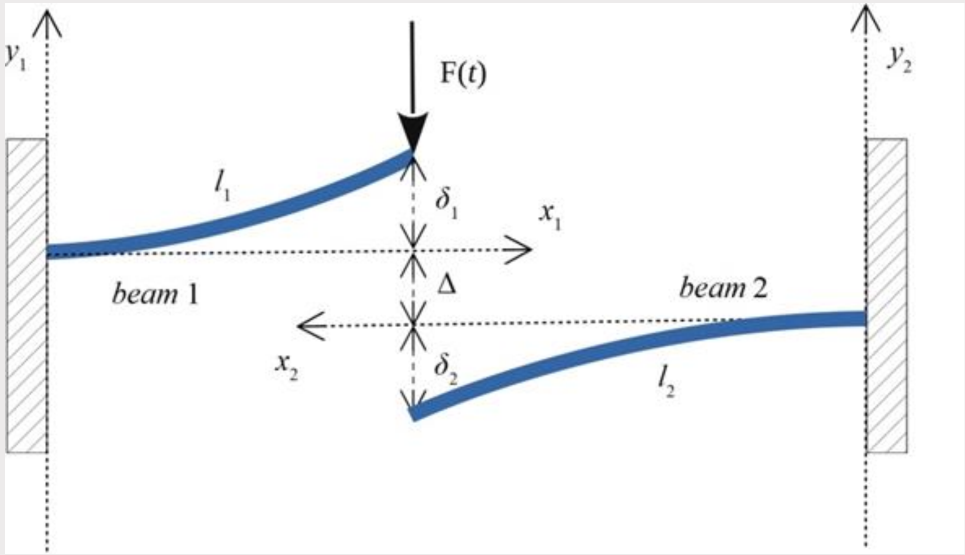

Impacting beams under harmonic excitation

Governing equations of motion of two Euler-Bernoulli impacting beams

$$a_1^2 \frac{\partial^4 y_1(x_1,t)}{\partial {x_1}^4} + \frac{\partial^2 y_1(x_1,t)}{\partial t^2} = 0, \qquad a_2^2 \frac{\partial^4 y_2(x_2,t)}{\partial {x_2}^4} + \frac{\partial^2 y_2(x_2,t)}{\partial t^2} = 0;$$

boundary conditions:

$$y_1(0,t) = 0, \qquad y_2(0,t) = 0, \qquad \frac{\partial y_1(0,t)}{\partial x_1} = 0, \qquad \frac{\partial y_2(0,t)}{\partial x_2} = 0,$$

$$M_1(l_1,t) = E_1 I_1 \frac{\partial^2 y_1(l_1,t)}{\partial {x_1}^2} = 0, \qquad M_2(l_2,t) = E_2 I_2 \frac{\partial^2 y_2(l_2,t)}{\partial {x_2}^2} = 0,$$

impact phase
(inhomogeneous boundary conditions):

$$Q_1(l_1,t) = E_1 I_1 \frac{\partial^3 y_1(l_1,t)}{\partial {x_1}^3} = E_2 I_2 \frac{\partial^3 y_2(l_2,t)}{\partial {x_2}^3} + F(t),$$

$$y_1(l_1,t) = y_2(l_2,t) - \Delta.$$

out-of-contact phase
(inhomogeneous boundary conditions):

$$Q_1(l_1,t) = E_1 I_1 \frac{\partial^3 y_1(l_1,t)}{\partial {x_1}^3} = F(t),$$

$$Q_2(l_2,t) = E_2 I_2 \frac{\partial^3 y_2(l_2,t)}{\partial {x_2}^3} = 0.$$

Impact phase

$$y_1(x_1,t) = y_{1s}(x_1,t) + \sum_{m=1}^{\infty} Y_{1m}(x_1) q_m(t)\,,$$

solution that satisfy inhomogeneous BCs

mode shapes

time dependent coefficients

$$y_2(x_2,t) = y_{2s}(x_2,t) + \sum_{m=1}^{\infty} Y_{2m}(x_2) q_m(t)\,,$$

$$y_{1s}(x_1,t) = \frac{1}{6}\frac{3E_2I_2\Delta - l_2^3F(t)}{E_2I_2l_1^3 - E_1I_1l_2^3}(x_1^3 - 3l_1x_1^2), \qquad y_{2s}(x_2,t) = \frac{1}{6}\frac{3E_1I_1\Delta - l_1^3F(t)}{E_2I_2l_1^3 - E_1I_1l_2^3}(x_2^3 - 3l_2x_2^2);$$

$$E_1I_1k_{1m}^3(1 + cosk_{1m}l_1coshk_{1m}l_1)(coshk_{2m}l_2sink_{2m}l_2 - cosk_{2m}l_2sinhk_{2m}l_2) \quad +$$

$$E_1I_2k_{2m}^3(1 + cosk_{2m}l_2coshk_{2m}l_2)(coshk_{1m}l_1sink_{1m}l_1 - cosk_{1m}l_1sinhk_{1m}l_1) = 0;$$

$$\omega_{1m} = \omega_{2m}, \qquad \omega_{1m} = a_1k_{1m}^2, \qquad \omega_{2m} = a_2k_{2m}^2.$$

Impact phase. Expressions for mode shapes and time dependent coefficients

$$Y_{1m} = A_m \left[sink_{1m}x_1 - sinhk_{1m}x_1 + \frac{sink_{1m}l_1 + sinhk_{1m}l_1}{cosk_{1m}l_1 + coshk_{1m}l_1}(coshk_{1m}x_1 - cosk_{1m}x_1) \right],$$

$$Y_{2m} = A_m \frac{E_1 I_1 k_{1m}^3 (1 + cosk_{1m}l_1 coshk_{1m}l_1)}{E_2 I_2 k_{2m}^3 (cosk_{1m}l_1 + coshk_{1m}l_1)(1 + cosk_{2m}l_2 coshk_{2m}l_2)} \times$$
$$[(cosk_{2m}l_2 + coshk_{2m}l_2)(sink_{2m}x_2 - sinhk_{2m}x_2) + (sink_{2m}l_2 + sinhk_{2m}l_2)(coshk_{2m}x_2 - cosk_{2m}x_2)];$$

$$q_m(t) = q_m(0)cos\omega_m t + \frac{1}{\omega_m}\dot{q}_m(0)sin\omega_m t + \frac{1}{\omega_m}\int_0^t \ddot{\psi}_m(\tau)sin(t-\tau)d\tau.$$

$$q_m(0) = \int_0^{l_1} \rho_1 A_1 y_{01}(x_1) Y_{1m}(x_1) dx_1 - \int_0^{l_2} \rho_2 A_2 y_{02}(x_2) Y_{2m}(x_2) dx_2 + \psi_m(0)$$

$$\dot{q}_m(0) = \int_0^{l_1} \rho_1 A_1 \dot{y}_{01}(x_1) Y_{1m}(x_1) dx_1 - \int_0^{l_2} \rho_2 A_2 \dot{y}_{02}(x_2) Y_{2m}(x_2) dx_2 + \dot{\psi}_m(0)$$

Natural frequencies of the vibrating beams in the in-contact phase $\omega_{1m} = \omega_{2m} = \omega_m$ and in the out-of-contact phase ω_{1n}, ω_{2n} (m=1,2,…,10)

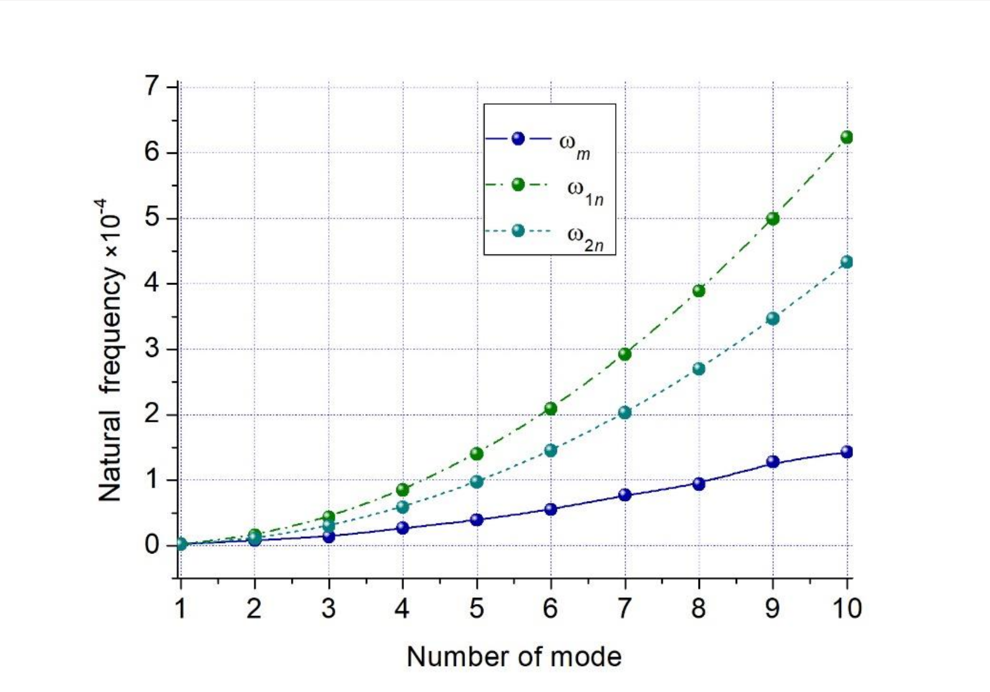

Normalized in-contact mode shapes (a) $Y_{1m}(x_1)$ of the 1st vibrating cantilever beam; (b) $Y_{2m}(x_2)$ of the 2nd vibrating cantilever beam (m=1,2,…,10)

(a)

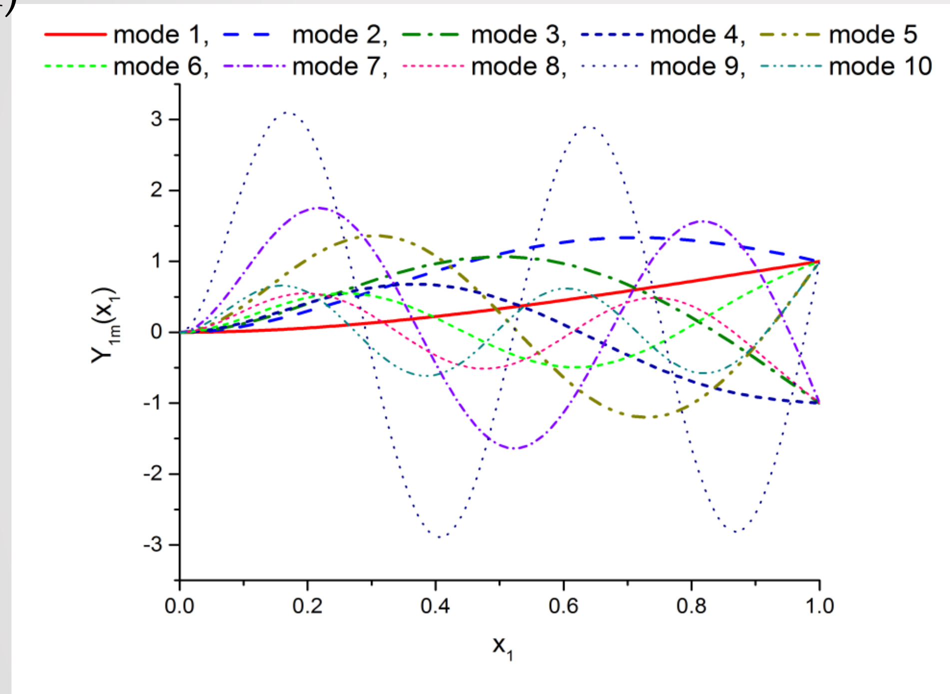

(b)

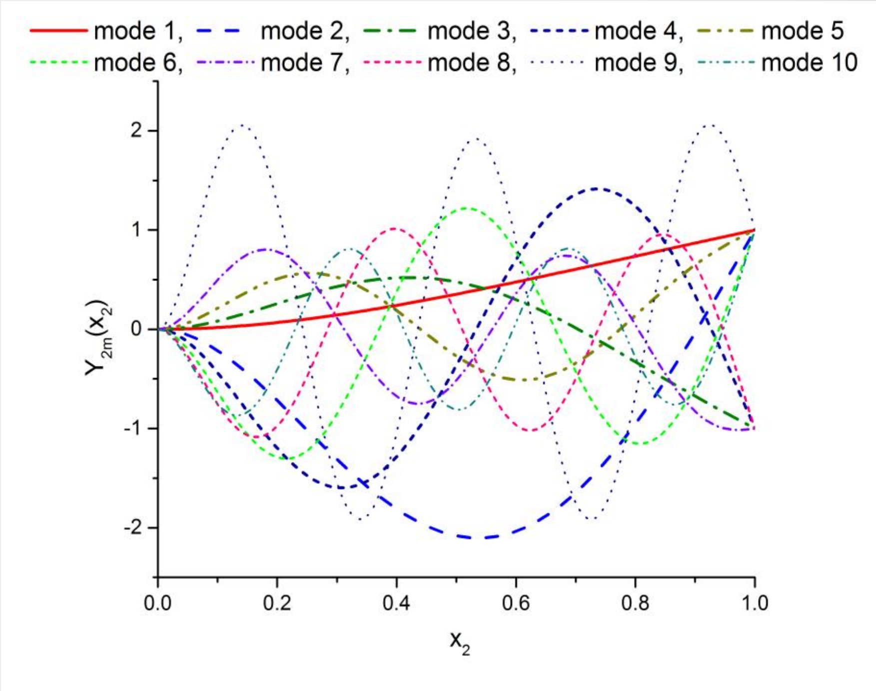

Out-of-contact phase. Expressions for mode shapes and time dependent coefficients

$$cos(k_{in}l_i)cosh(k_{in}l_i) + 1 = 0;\ i = 1,2$$

$$y_1(x_1,t) = y_{1s}(x_1,t) + \sum_{n=1}^{\infty} Y_{1n}(x_1)q_n(t)\,,$$

$$y_2(x_2,t) = \sum_{m=1}^{\infty} Y_{2n}(x_2)q_n(t)\,,$$

$$y_{1s}(x_1,t) = \quad -F(t)\,(3l_1x_1^2 - x_1^3)/6\,E_1I_1,$$

$$y_{2s}(x_2,t)=0;$$

$$Y_{1i} = A_{1i}\left[sink_{in}x_1 - sinhk_{in}x_1 + \frac{sink_{in}l_1 + sinhk_{in}l_1}{cosk_{in}l_1 + coshk_{in}l_1}(coshk_{in}x_1 - cosk_{in}x_1)\right];\ i = 1,2$$

$$q_{1n}(t) = q_{1n}(0)cos\omega_{1n}t + \frac{1}{\omega_{1n}}\dot{q}_{1n}(0)sin\omega_{1n}t + \frac{1}{\omega_{1n}}\int_0^t \ddot{\psi}_{1n}(\tau)sin(t-\tau)d\tau,$$

$$q_{2n}(t) = q_{2n}(0)cos\omega_{2n}t + \frac{1}{\omega_{2n}}\dot{q}_{2n}(0)sin\omega_{2n}t\,.$$

Out-of-contact phase. Initial conditions for time dependent coefficients expressions

$$q_{1n}(0) = \int_0^{l_1} \rho_1 A_1 y_{01}(x_1) Y_{1n}(x_1) dx_1 + \psi_{1n}(0)$$

$$\dot{q}_{1n}(0) = \int_0^{l_1} \rho_1 A_1 \dot{y}_{01}(x_1) Y_{1n}(x_1) dx_1 + \dot{\psi}_{1n}(0)$$

$$q_{2n}(0) = \int_0^{l_2} \rho_2 A_2 y_{02}(x_2) Y_{2n}(x_2) dx_2$$

$$\dot{q}_{2n}(0) = \int_0^{l_2} \rho_2 A_2 \dot{y}_{02}(x_2) Y_{2n}(x_2) dx_2$$

Normalized out-of-contact mode shapes $Y_{1n}(x_1)$, $Y_{2n}(x_2)$ of the 1st and of the 2nd vibrating cantilever beams (m=1,2,…,10)

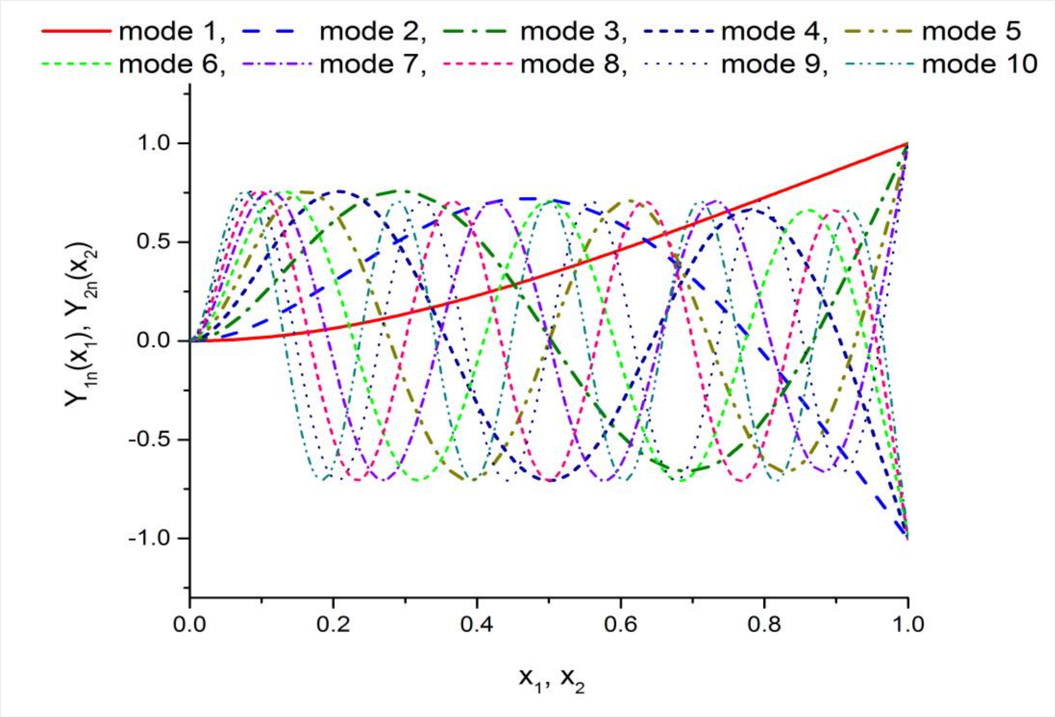

Switching between phases

out-of-contact phase $\longrightarrow$ impact phase transition

$$y_2(l_2,t) - y_1(l_1,t) = \Delta, \qquad \frac{d}{dt}\big(y_2(l_2,t) - y_1(l_1,t)\big) \geq 0;$$

impact phase $\longrightarrow$ out-of-contact phase transition

$$P(t) = 0, \qquad \frac{dP(t)}{dt} \leq 0, \qquad \text{where} \qquad P(t) = E_1 I_1 \frac{\partial^3 y_1(l_1,t)}{\partial {x_1}^3} - F(t).$$

Characterizing beams collisions

$[t_i^+, t_i^-],\ (i = 1,2,\dots,N)$	time spans that correspond to the impact phases during period of simulation $[0, T]$
$t_i^+ \ \ (t_i^-)$	i^{th} impact start (end) time
$C_{Ri} = -\dfrac{v_{2i}^- - v_{1i}^-}{v_{2i}^+ - v_{1i}^+},$ $i = 1,2,\dots,N$	coefficient of restitution calculated for all impact phases $[t_i^+, t_i^-],\ (i = 1,2,\dots,N)$ as the ratio of the relative velocity after collision to the relative velocity before collision
$v_{1i}^+ = \left.\frac{\partial y_1(x_1,t)}{\partial t}\right\vert_{x_1=l_1, t=t_i^+}$ $\left(v_{1i}^- = \left.\frac{\partial y_1(x_1,t)}{\partial t}\right\vert_{x_1=l_1, t=t_i^-}\right)$	velocity of the 1st beam tip at the i^{th} impact start (end) time
$v_{2i}^+ = \left.\frac{\partial y_2(x_2,t)}{\partial t}\right\vert_{x_2=l_2, t=t_i^+}$ $\left(v_{2i}^- = \left.\frac{\partial y_2(x_2,t)}{\partial t}\right\vert_{x_2=l_2, t=t_i^-}\right)$	velocity of the 2nd beam tip at the i^{th} impact start (end) time

Beam deflections surfaces depending on time and the lengths:
(a) $y_1(x_1,t)$ for the first beam; (b) $y_2(x_2,t)$ for the second beam
at A=0.0005, w=40, l_1=0.1, l_2=0.12, δ_1= δ_2=0.0, Δ=0.000011, Δt=0.0001, 0<t<0.07

(a)

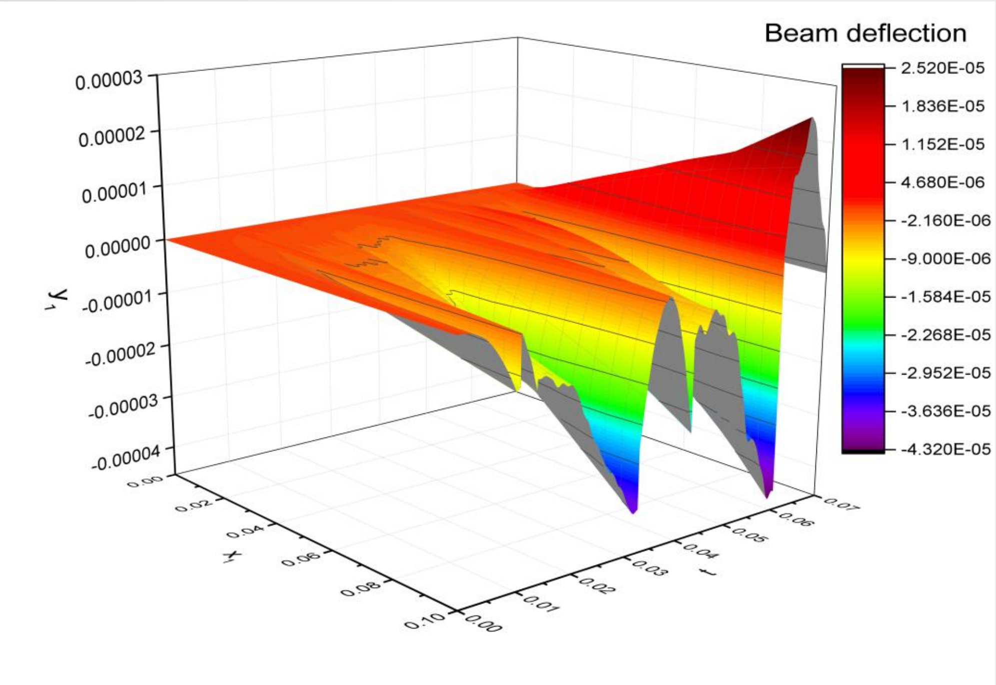

(b)

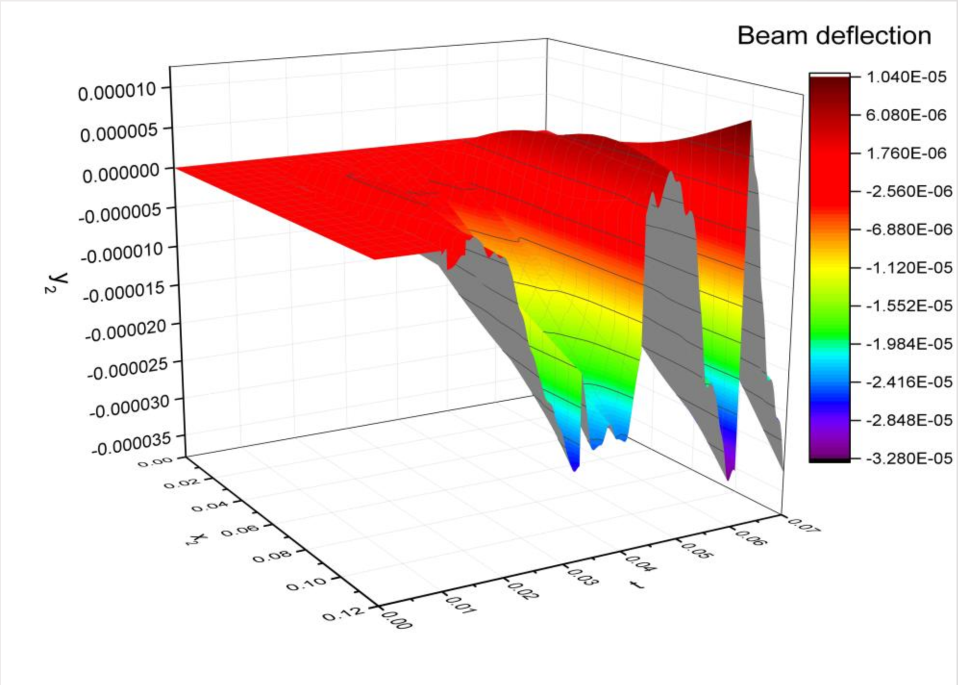

Example 1: Beams deflections $y_1(l_1,t)$, $y_2(l_2,t)$-Δ

at A=0.001, w=50, l_1=0.1, l_2=0.12, δ_1= δ_2=0.0, Δ=0.000011, Δt=0.00001, 0<t<0.6

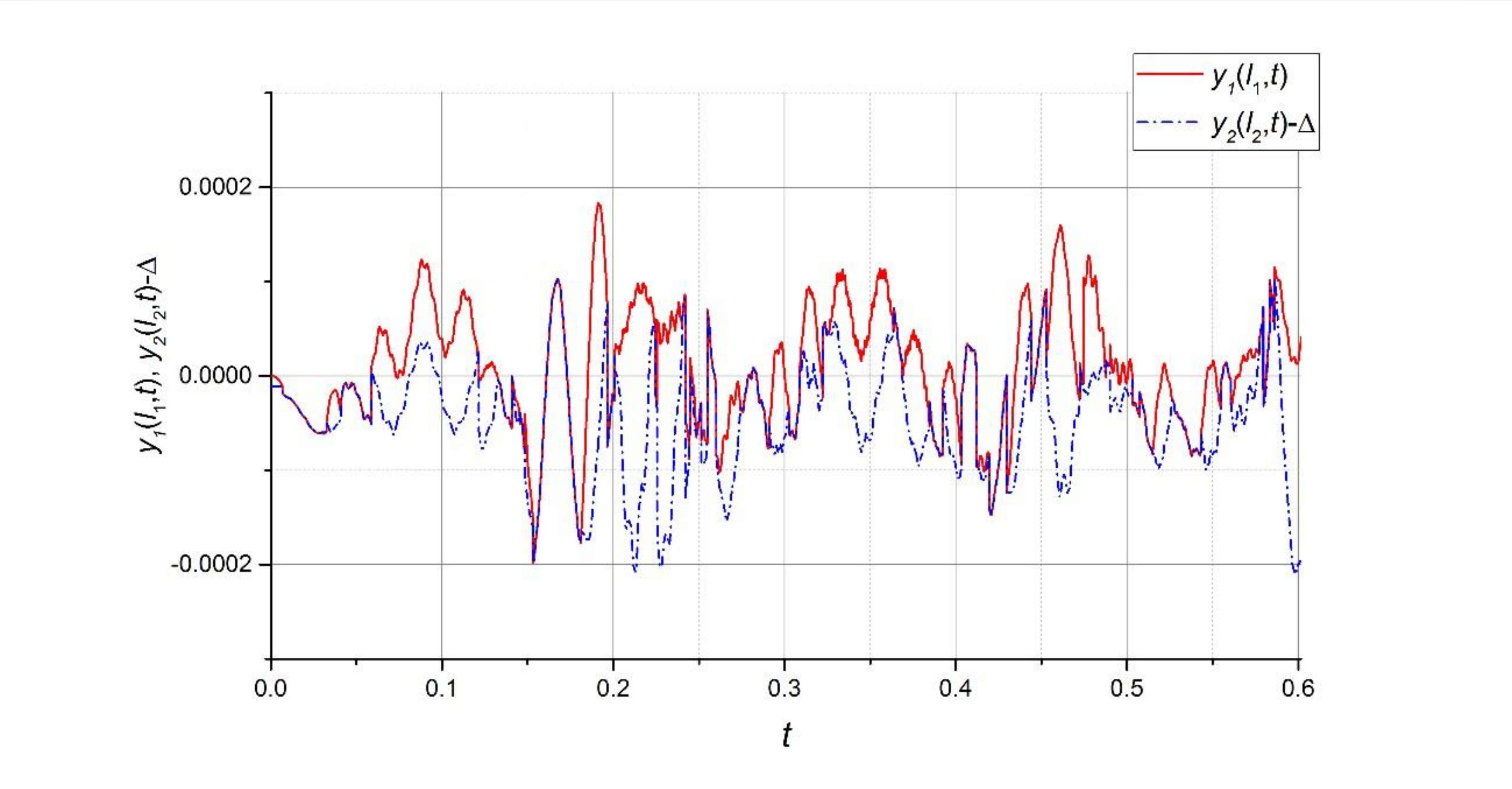

Example 1: (a) Coefficient of restitution C_R of impacting beams; (b) Impact-induced force Q; (c) phase planes

at A=0.001, w=50, l_1=0.1, l_2=0.12, δ_1= δ_2=0.0, Δ=0.000011, Δt=0.00001, 0<t<0.6

(a)

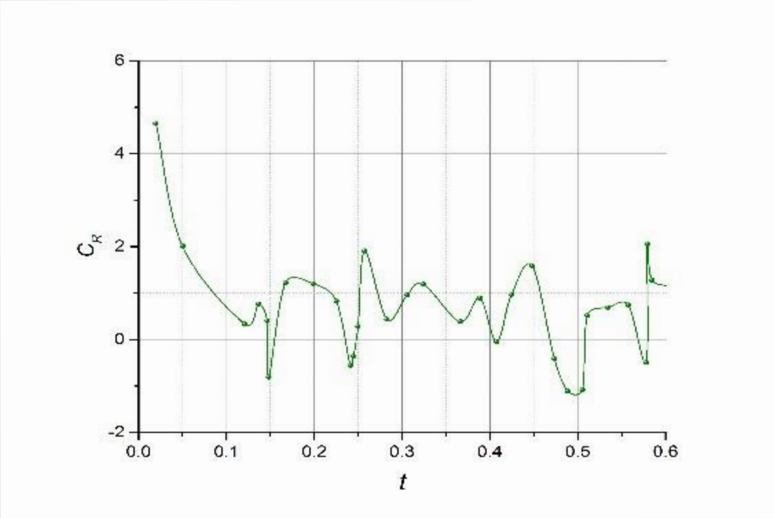

(b)

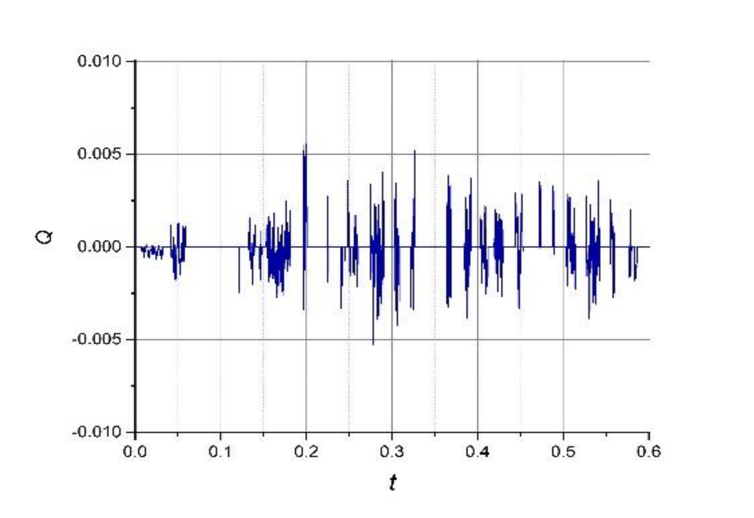

(c)

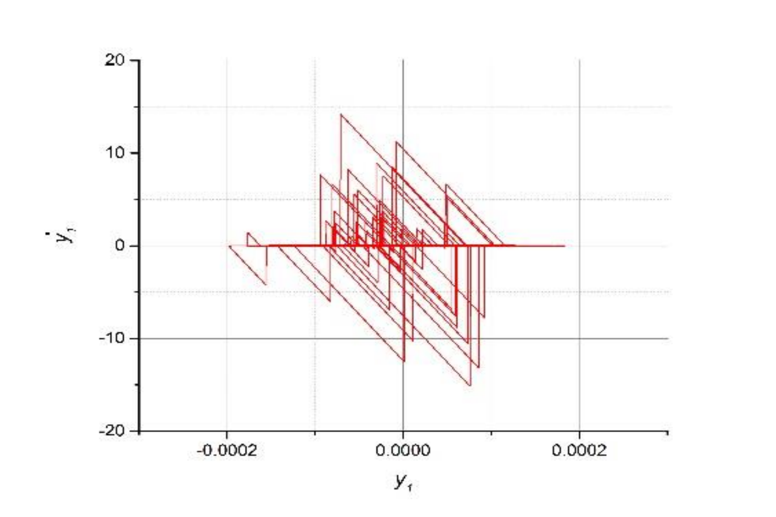

(c)

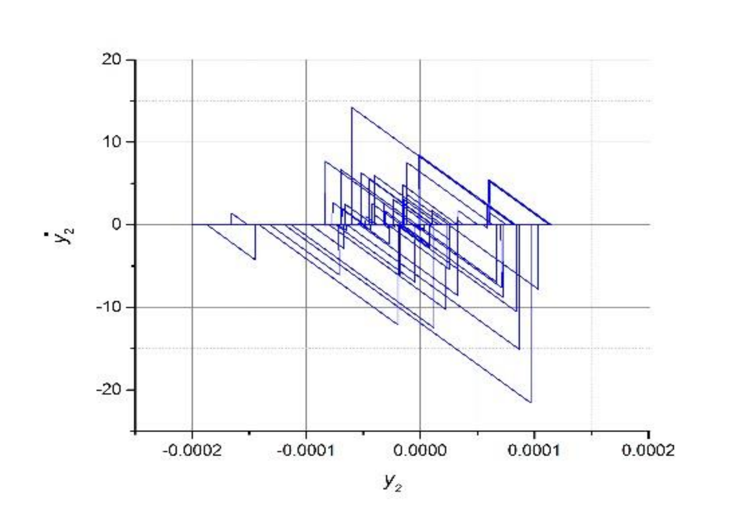

Example 2: No beam impacts during the first period of the external excitation.

Beams deflections $y_1(l_1,t)$, $y_2(l_2,t)$-Δ

at A=0.00013, w=50, l_1=0.1, l_2=0.12, δ_1= δ_2=0.0, Δ=0.000011, Δt=0.00001, 0<t<0.6

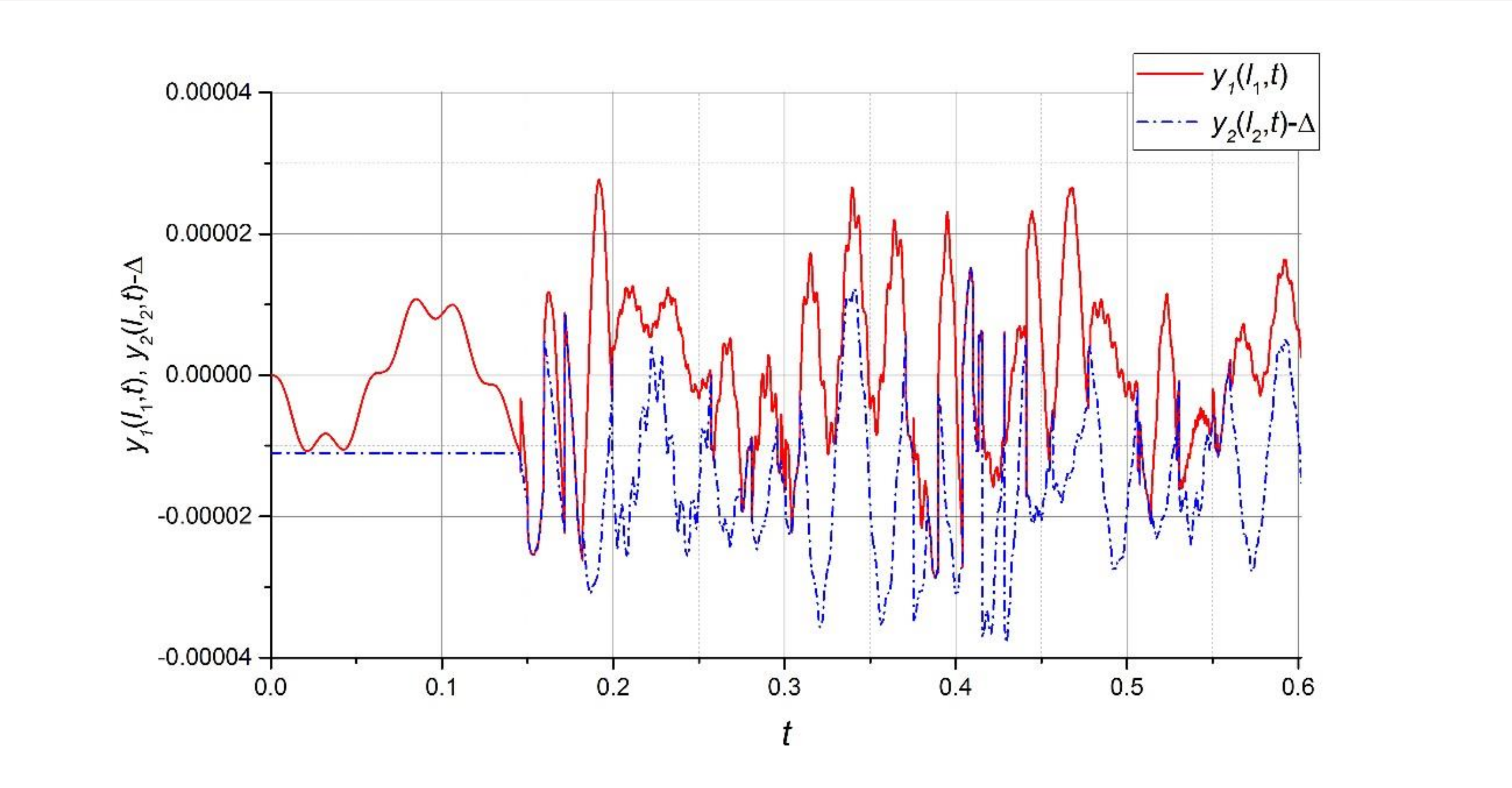

Example 2: (a) Coefficient of restitution C_R of impacting beams; (b) Impact-induced force Q; (c) phase planes

at A=0.00013, w=50, l_1=0.1, l_2=0.12, $\delta_1=\delta_2$=0.0, Δ=0.000011, Δt=0.00001, 0<t<0.6

(a)

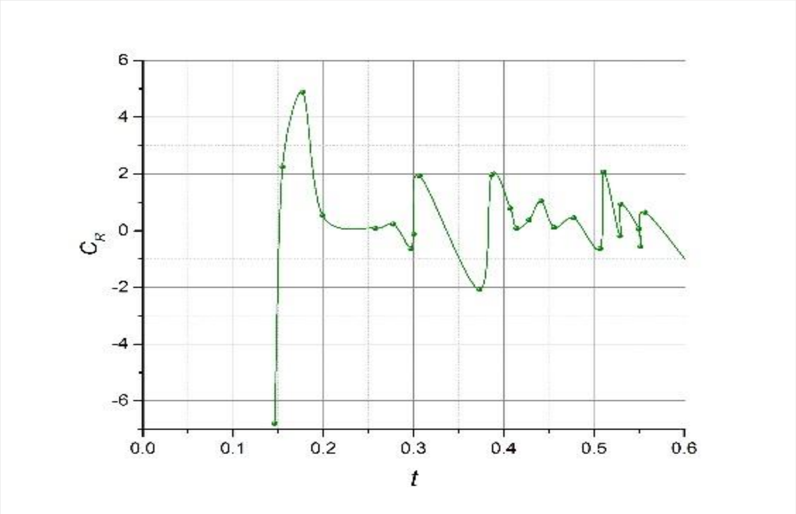

(b)

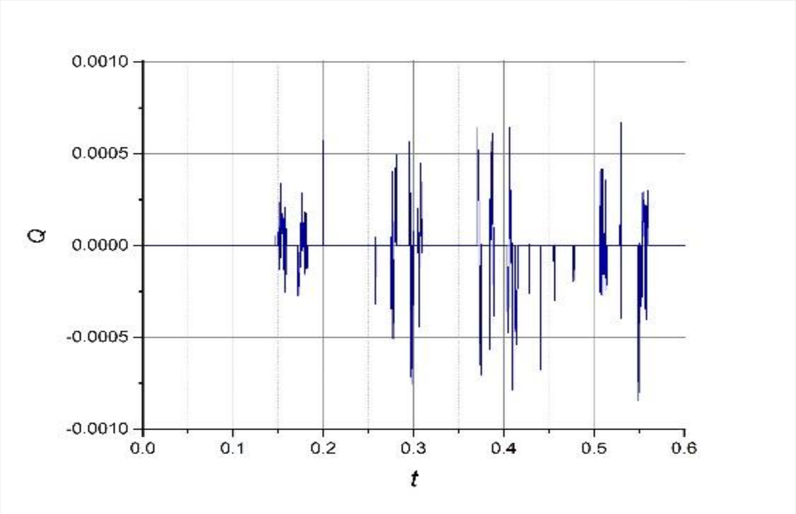

(c)

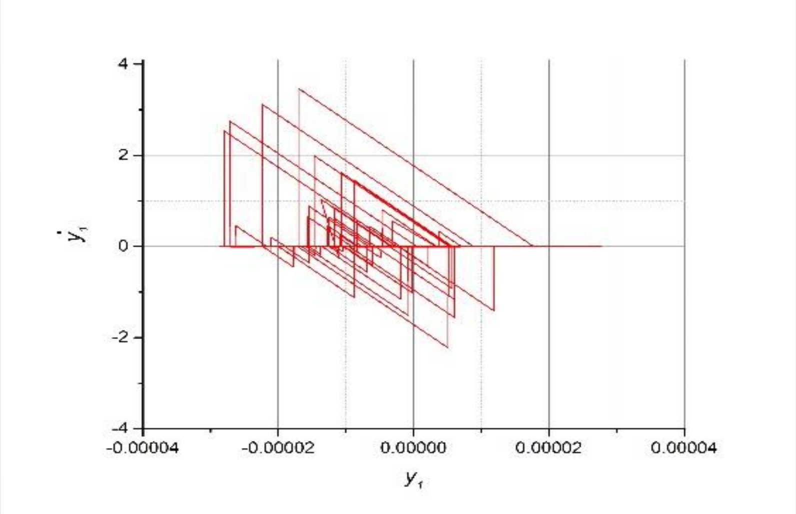

(c)

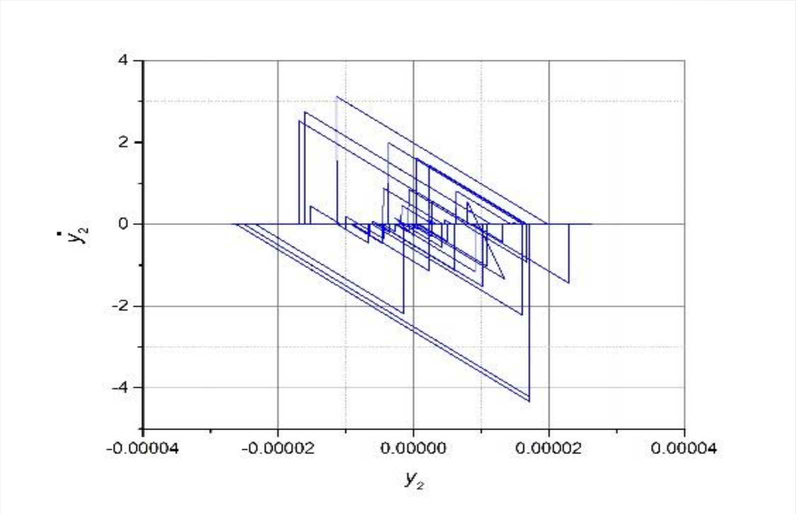

Example 3: Clearance between beams is equal to zero

Beams deflections $y_1(l_1,t)$, $y_2(l_2,t)$-Δ

at A=0.002, w=60, l_1=0.1, l_2=0.12, δ_1= δ_2=0.0, Δ=0.0, Δt=0.00001, 0<t<0.6

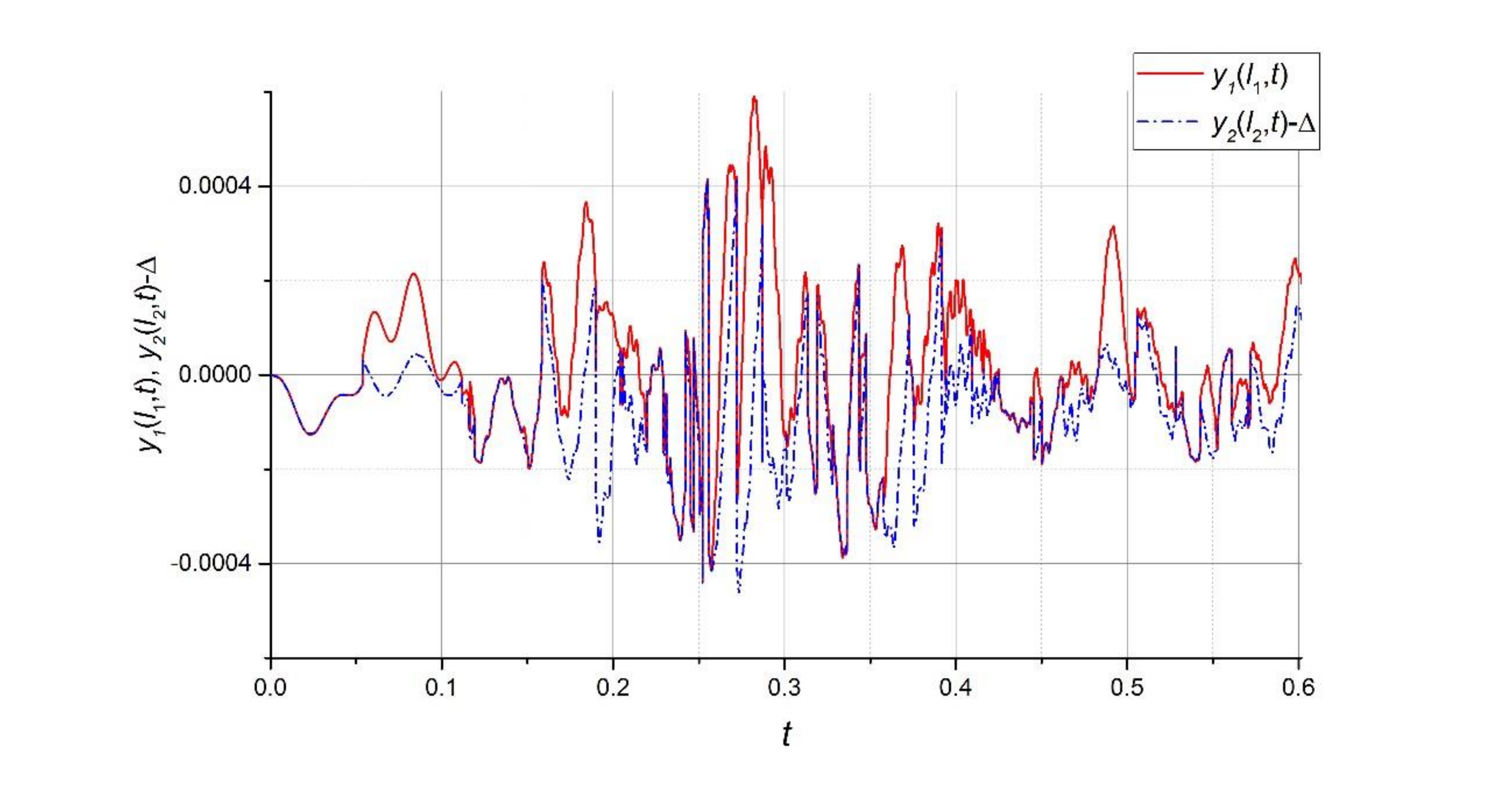

Example 3: (a) Coefficient of restitution C_R of impacting beams; (b) Impact-induced force Q; (c) phase planes

at A=0.002, w=60, l_1=0.1, l_2=0.12, $\delta_1 = \delta_2$=0.0, Δ=0.0, Δt=0.00001, $0<t<0.6$

(a)

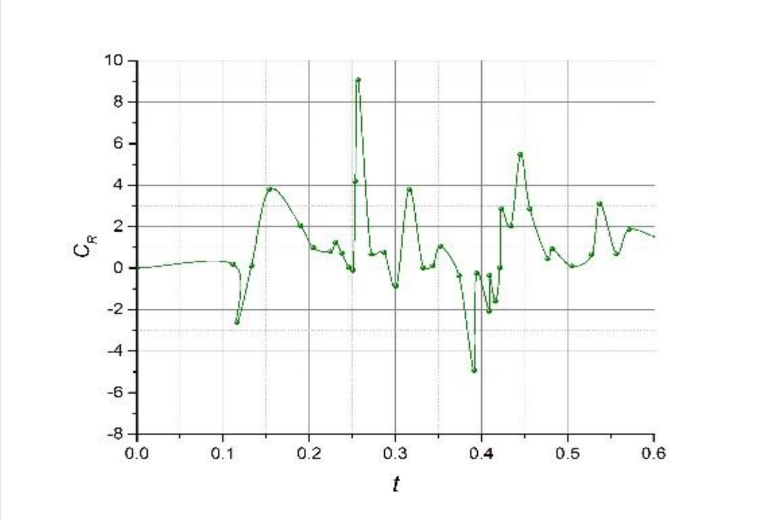

(b)

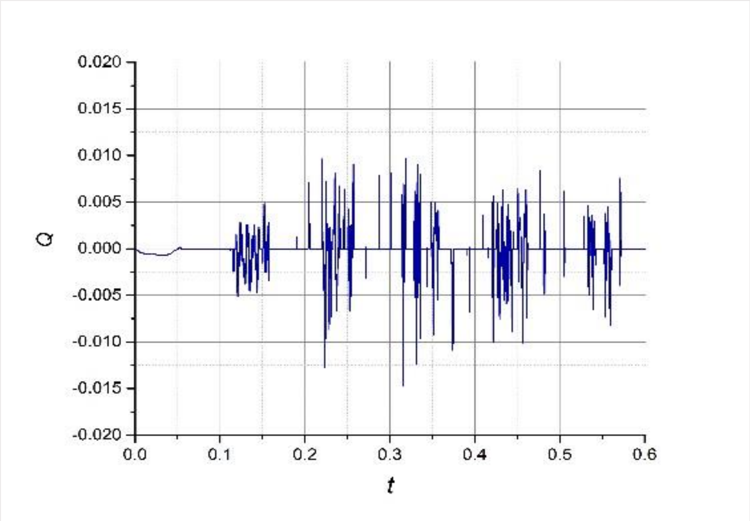

(c)

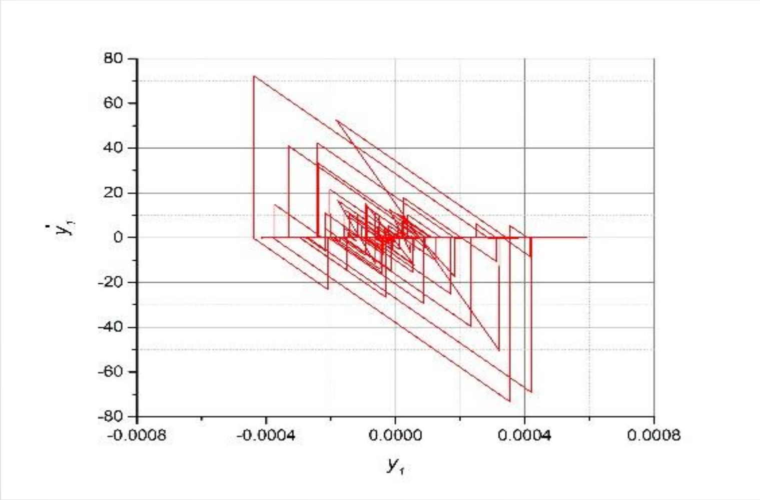

(c)

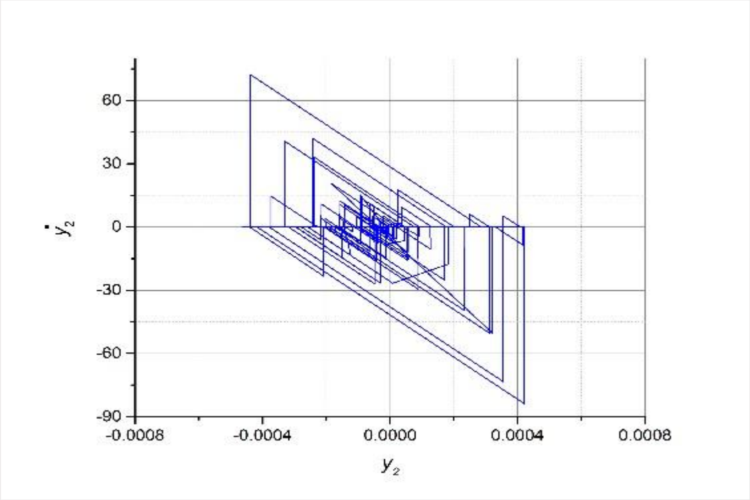

Chaotic motion (a) of the 1st and (b) of the 2nd impacting beam; Nearby trajectories $y_1(l_1,t)$ and $y_2(l_2,t)$ diverge exponentially; δ_0 is the initial uplift at the free end

at A=0.001, ω=50, l_1=0.1, l_2=0.12, δ_1=0 and $\delta_1=10^{-6}$, δ_2=0.0, Δ=0.000011, Δt=0.00001, 0<t<0.8

(a)

(b)

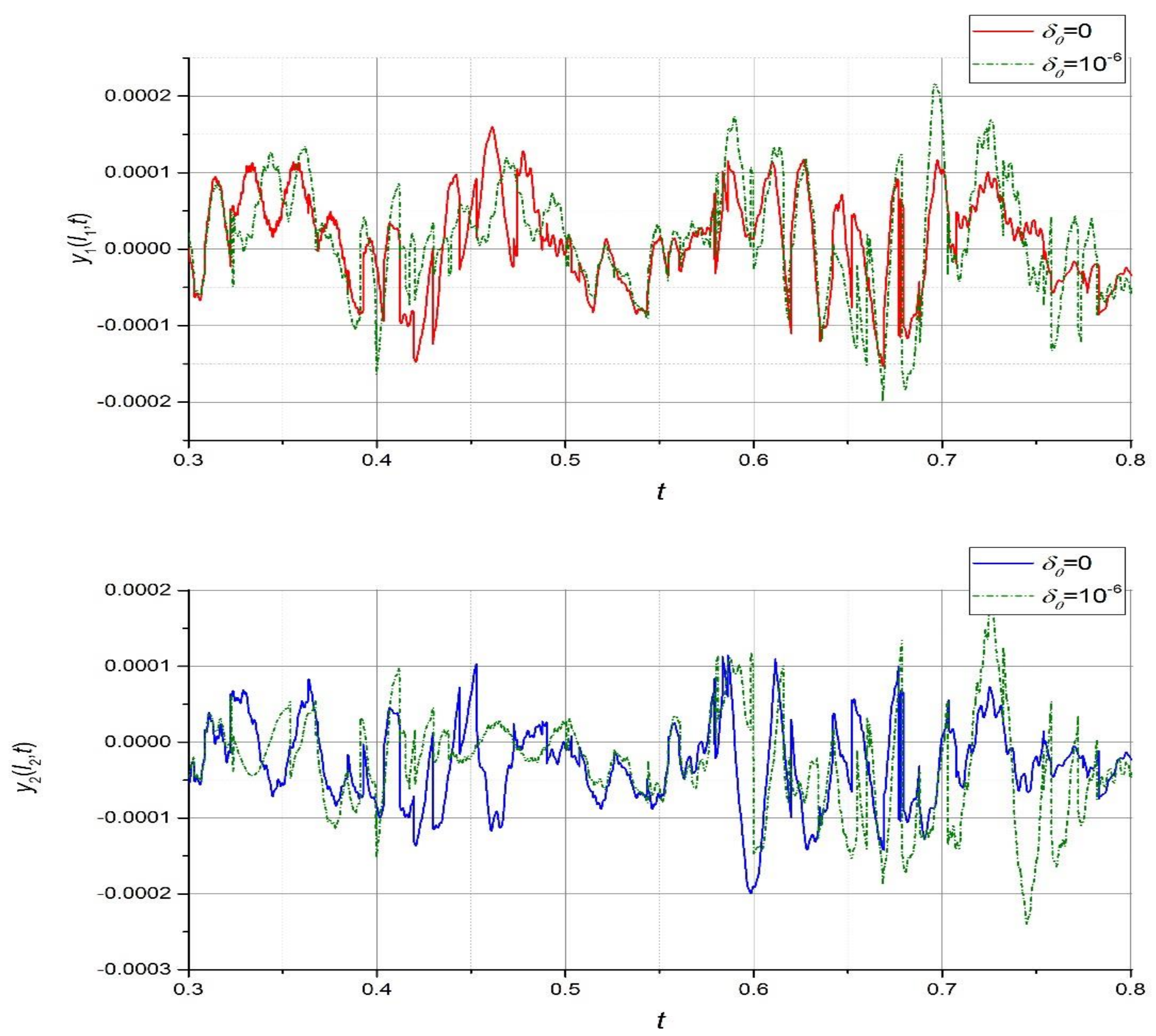

Time before impact start as function of (a) frequency and amplitude of external excitation (ω, F); (b) clearance and amplitude of external excitation (Δ, F); (c) frequency of external excitation and clearance (ω,Δ)

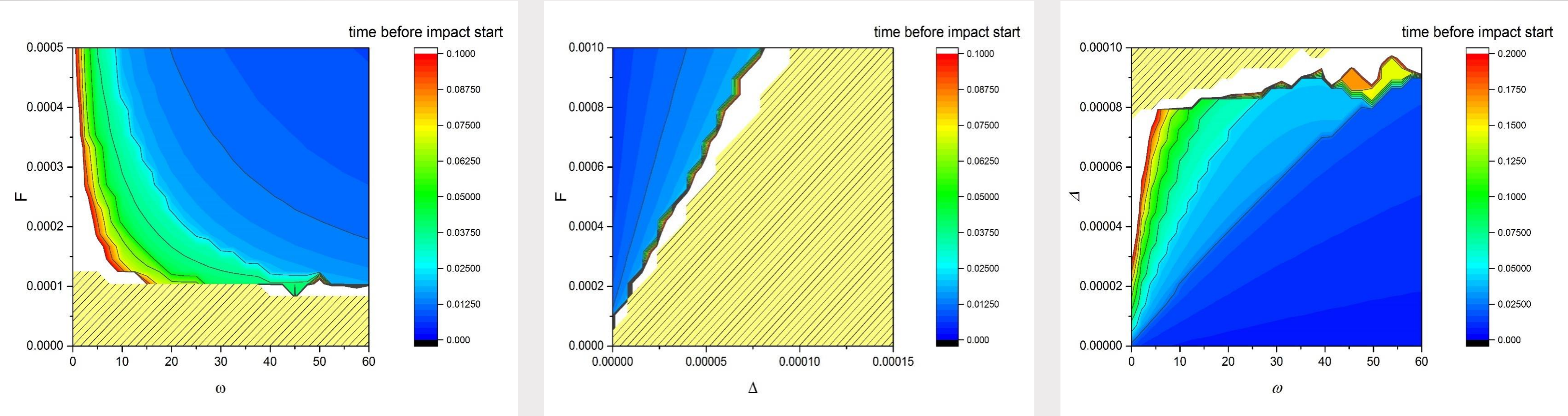

(a) (b) (c)

Conclusions IV

- The analytical solutions, describing the transient dynamics of two impacting beams with clearance nonlinearity, were obtained in the form of eigenfunctions series with time dependent coefficients;
- Several examples were considered for various set of parameters;
- Transient dynamics surfaces, time histories of beams deflections, impact forces, coefficients of restitution as well as phase planes were presented;
- Chaotic behavior of the beams was ascertained on the base of sensitive dependence of the trajectories of motion on the initial conditions;
- Time before impact start level contours were obtained in various control parameter planes (ω, F), (Δ, F) and (ω, Δ);
- Solutions obtained allow to construct long term vibrations of the impacting beams.

References

- J. Awrejcewicz, L.P. Dzyubak, Chaos caused by hysteresis and saturation phenomenon in 2-dof vibrations of the rotor supported by the magneto-hydrodynamic bearing, International Journal of Bifurcation and Chaos. 15(6) (2011) 2041-2055.

- L. Dzyubak, J. Awrejcewicz, A. Bhaskar, Dynamics of two impacting beams with clearance nonlinearity (to be submitted).

- X.C. Yin, Y. Qin, H. Zou, Transient responses of repeated impact of a beam against a stop, International Journal of Solids and Structures. 44 (2007) 7323–7339.

- L.A. Chen, S.E. Semercigil, A beam-like damper for attenuating transient vibrations of light structures, Journal of Sound and Vibration, 164(1) (1993) 53-65.

Thank you for your attention